CORA Cork Open Research Archive
Cartlann Taighde Oscailte Chorcaí

Title	A study of magnesium stearate behaviour in pharmaceutical blends and tablets employing Broadband Acoustic Resonance Dissolution Spectroscopy (BARDS)
Authors	Peddapatla, Raghu V. G.
Publication date	2019
Original Citation	Peddapatla, R. V. G. 2019. A study of magnesium stearate behaviour in pharmaceutical blends and tablets employing Broadband Acoustic Resonance Dissolution Spectroscopy (BARDS). PhD Thesis, University College Cork.
Type of publication	Doctoral thesis
Rights	© 2019, Raghu V. G. Peddapatla. - http://creativecommons.org/licenses/by-nc-nd/3.0/
Download date	2026-11-01 22:25:20
Item downloaded from	https://hdl.handle.net/10468/9699



UCC
University College Cork, Ireland
Coláiste na hOllscoile Corcaigh

Ollscoil na hÉireann, Corcaigh

National University of Ireland, Cork



A Study of Magnesium Stearate Behaviour in Pharmaceutical Blends and Tablets Employing Broadband Acoustic Resonance Dissolution Spectroscopy (BARDS)

Thesis presented by

Raghu Vamshi Goud Peddapatla, B.Pharm, M.Sc.

http://orcid.org/0000-0002-0217-8385

for the degree of

Doctor of Philosophy

University College Cork

School of Pharmacy

Head of School: Prof. Stephen Byrne

Supervisors: Dr. Abina M. Crean, Dr. Maria J. Sousa Gallagher

2019

To,

My beloved parents

Aruna Peddapatla and Praveen Kumar Peddapatla

This thesis is not a work of fiction. If any experiments resemble scientific theories and concepts, then it's purely intentional.

TABLE OF CONTENTS

List of Figures……..vii

List of Tables……...xiv

Declaration……..xvii

Acknowledgements……..xviii

Publications and presentations associated with this thesis……xx

Abstract……xxiii

Abbreviations……xxvi

1. General Introduction 1

1.1 Pharmaceutical Tablets 3

1.1.1 Theory of tablet compression 5

1.1.1.1 Mechanism of tablet compression and/or compact formation 6

1.1.1.2 Bonding or Consolidation 8

1.1.2 Tablet manufacturing method 13

1.1.2.1 Direct compression 13

1.1.2.2 Excipients in direct compressible blend 14

1.2 Tablet lubrication 16

1.2.1 Magnesium stearate 17

1.2.1.1 MgSt variability and its effect on final product quality……..19

1.2.2 Tools to identify MgSt distribution in blends and tablets 20

1.3 Continuous processing 22

1.3.1 Continuous feeding 25

1.4 Broadband Acoustic Resonance Dissolution Spectroscopy (BARDS) 29

1.4.1 Working principles of BARDS 29
1.4.2 Instrumentation and spectral information 31
1.5 Aims and objectives 35

2. Materials and Methods 37
2.1 Materials 38
2.2 Methods 39
2.2.1 Solid state structure analysis 39
2.2.1.1 Powder X-Ray Diffraction 39
2.2.1.2 Differential Scanning Calorimetry (DSC) 39
2.2.1.3 Thermogravimetric Analysis (TGA) 40
2.2.2 Particulate analysis 41
2.2.2.1 Scanning electron microscopy (SEM) 41
2.2.2.2 Particle Size Distribution (PSD) 42
2.2.2.3 Brunauer–Emmett–Teller-Specific Surface Area Analysis (BET) 42
2.2.3 Bulk Properties Analysis 44
2.2.3.1 True density 44
2.2.3.2 Bulk and tapped density 44
2.2.3.3 Flowability – Brookfield Powder Flow Tester 45
2.2.3.4 Dynamic Moisture Sorption-Desorption 46
2.2.3.5 Contact angle 47
2.2.4 Formulation Preparation 48
2.2.4.1 Paracetamol Blends – evaluated in chapter - 4 48
2.2.4.2 Metaclopromide HCl Blends – evaluated in chapter – 5 48
2.2.5 Continuous Feeding 49

2.2.5.1 Continuous feeding – MgSt 50
2.2.5.2 Continuous feeding – Metoclopramide tablet formulations 51
2.2.6 Blend Compaction 52
2.2.6.1 Tablet compaction 52
2.2.6.2 Tablets Characterisation 52
2.2.6.3 Heckel Analysis 53
2.2.6.4 Disintegration Test 53
2.2.6.5 Dissolution Test 53
2.2.6.6 Wetting time of compacted blends 55
2.2.6.7 BARDS 55
2.2.7 Statistical Analysis 56

3. Magnesium stearate variability and its impact on blend compaction 57
3.1 Introduction 58
3.2 Aims and objectives 59
3.3 Results 60
3.3.1 Solid state behaviour 60
3.3.1.1 Powder X-Ray Diffraction (PXRD) 60
3.3.1.2 Thermal Analysis (DSC and TGA) 60
3.3.2 Particulate properties 65
3.3.2.1 Particle morphology (scanning electron microscopy) 65
3.3.2.2 Surface area analysis and Particle size distribution analysis 66
3.3.3 Bulk behaviour 71
3.3.3.1 Flowability 71
3.3.3.2 Moisture sorption characteristics of MgSt samples 74

3.3.4 Impact of MgSt on tablet properties 76
3.3.4.1 Impact on compression 76
3.3.4.2 Impact on dissolution 79
3.4 Discussion 81
3.5 Conclusions 84

4. The behaviour of MgSt during continuous feeding 85
4.1 Introduction 86
4.2 Aim and objectives 88
4.3 Results 89
4.3.1 K-Tron MT12 set-up optimisation using Alfa Aesar 89
4.3.2 Comparison of feeding behaviour of MgSt samples 94
4.3.3 Effect of feeding on MgSt particulate properties 96
4.3.3.1 Effect of Feeding on Particle size distribution 96
4.3.3.2 Effect of feed rate on sample surface area 104
4.3.4 Effect of fed MgSt on tablet properties 104
4.3.4.1 Effect on compression 104
4.3.4.2 Effect of feeding on tablet dissolution 108
4.4 Discussion 112
4.5 Conclusions 115

5. BARDS Analysis of Lubricated Blends 116
5.1 Introduction 117
5.2 Aim and objectives 120
5.3 Results 121

5.3.1 Preliminary BARDS studies – proof of concept 121
5.3.2 Comparison of unlubricated and lubricated formulations by BARDS 125
5.3.2.1 BARDS analysis of blends prior to feeding 125
5.3.2.2 Feeding of blends through K-Tron MT12 feeder 129
5.3.2.3 Tabletability of blends fed through K-Tron MT12 feeder 132
5.3.2.4 BARDS analysis of blends following to feeding 133
5.3.2.5 Contact angle and wetting time of formulations before and after feeding 137
5.4 Discussion 140
5.5 Conclusions 143

6. BARDS analysis of Lubricated Tablets 144
6.1 Introduction 145
6.2 Aim and objectives 148
6.3 Results 149
6.3.1 Tablet characterisation 149
6.3.2 Interpretation of BARDS results 152
6.3.3 Frequency-time profiles of tablets 155
6.3.4 Gas volume - time profile 159
6.4 Discussion 165
6.5 Conclusions 169

7. General Discussion 170
7.1 Magnesium stearate variability and continuous feeding 171
7.2 Applicability of BARDS to study lubricated blends and tablets 175

7.3 Strengths and Limitations 177

7.3.1 Strengths 177

7.3.2 Limitations 177

7.4 Recommendations for future work 178

7.5 Conclusions 179

8. Bibliography 180

Supplementary Information 198

LIST OF FIGURES

Figure 1.1 Different types of tablets and their site of action (Annotated diagram, Tortora and Derrickson, 2011). 4

Figure 1.2 Steps involved in compaction process 5

Figure 1.3 Elastic, plastic and brittle deformation mechanisms of powder under applied compression force 6

Figure 1.4 Relationships between compaction pressure, solid fraction and tensile strength for a given powder (Tye et al., 2005). 9

Figure 1.5 Schematic representation of Heckel Plot (Patel et al., 2006) 12

Figure 1.6. Schematic representation of different manufacturing routes for tablets; (a) Direct compression (b) Dry granulation and (c) Wet granulation (Leane et al., 2015). 14

Figure 1.7 Magnesium stearate chemical structure 18

Figure 1.8 PCMM for continuous manufacturing of oral solid dosage forms (Blackwood, 2017) 23

Figure 1.9 Components of loss-in-weight feeder (Blackshields and Crean, 2018). ... 26

Figure 1.10 Guide to screw selection based on material flow properties (Blackshields and Crean, 2018) 28

Figure 1.11 (A) Schematic diagram (top view) of the prototype BARDS spectrometer (Fitzpatrick et al., 2012). (B) Representative BARDS raw spectrum of 250 mg MCC in 25 mL water at room temperature. 32

Figure 3.1 PXRD diffractograms of magnesium stearate samples. (A) Alfa Aesar (B) Ligamed MF-2-V (C) Ligamed MF-2-V-BI (D) Ligamed MF-3-V 61

Figure 3.2 DSC and TGA thermograms of magnesium stearate samples. (A) Alfa Aesar (B) Ligamed MF-2-V (C) Ligamed MF-2-V-BI (D) Ligamed MF-3-V.....62

Figure 3.3 Scanning electron microscopy micrographs of MgSt samples**.** (A) Alfa Aesar (B) Ligamed MF2V (C) Ligamed MF2VBI (D) Ligamed MF3V 66

Figure 3.4 Particle size analysis of magnesium stearate samples by dry powder laser diffraction. Average values shown n=5, Y error bars indicates standard deviation. .68

Figure 3.5 Particle size analysis of magnesium stearate by pressure titration. (a) D10, (b) D50 and (c) D90. Where * represents $p \leq 0.05$, ** represents $p \leq 0.01$, *** represents $p \leq 0.001$, **** represents $p \leq 0.0001$. 69

Figure 3.6 Flowability of MgSt samples analysed by Brookfield Powder Flow Tester. Plot shows the unconfined failure strength versus major principal consolidating stress for MgSt samples. Average values shown n=2, y error bars indicate max and min values. 73

Figure 3.7 Moisture adsorption isotherms of MgSt samples at 25^0C. (A) Alfa Aesar (B) Ligamed MF-2-V (C) Ligamed MF-2-V-BI (D) Ligamed MF-3-V.....75

Figure 3.8 Tabletability profiles of paracetamol tablets unlubricated and lubricated, prepared with MgSt samples. Average values shown n=20, y error bars indicates standard deviation. 76

Figure 3.9 Compactibility profiles of paracetamol tablets unlubricated and lubricated, prepared with MgSt samples. Average values shown n=20, y error bars indicates standard deviation.....77

Figure 3.10 Compressibility profiles of paracetamol tablets unlubricated and lubricated, prepared with MgSt samples. Average values shown n=20, y error bars indicates standard deviation.....78

Figure 3.11 Dissolution profiles of paracetamol tablets unlubricated and lubricated, prepared with one of the 4 samples of magnesium stearate, produced at 2 MPa and

tested in water at 37°C. Average values shown n=3, y error bars indicates standard deviation.....79

Figure 4.1 Pictures showing (A) build-up of material on hopper walls in non-agitated zones, (B) coating of MgSt on coarse concave screw and (C) coating of MgSt on fine concave screws, during continuous feeding. 90

Figure 4.2 Pictures of MgSt build up near discharge outlet (A) no screen, (B) CCS (C) FSqS 91

Figure 4.3 Feed rate data as function of time during feeding of Alfa Aesar fed from MT12 with CCS and FSqS displayed (A and B) using different moving averages. (C) The effect of sampling interval on RSD. 92

Figure 4.4 Feeding performance of Alfa Aesar (% RSD) with CCS and FCS with three different screen combinations: no screen, CSqS and FSqS at two different feed rate set points.....93

Figure 4.5 Effect of MgSt bulk density on samples feed factor 95

Figure 4.6 Feeding behaviour of four different grades of MgSt using CCS with FSqS at two feed rates. RSD is shown as function of feed rate for K-Tron MT12 feeder. .95

Figure 4.7 Effect of continuous feeding on particle size analysed by laser diffraction at 1.5 bar air pressure for four grades of MgSt. (A) D10, (B) D50 and (C) D90. Average values shown, n=5. ± indicates standard deviation. 98

Figure 4.8 Particle size pressure titration analysis of four grades of MgSt unfed and fed at different feed rates. Average values, n=5. ± shows standard deviation.....101

Figure 4.9 Tabletability profiles of tablets with four grades of MgSt (A) Alfa Aesar (B) Ligamed MF-2-V (C) Ligamed MF-2-V-BI and (D) Ligamed MF-3-V. Average values shown n = 20, y error bars indicate standard deviation. 105

Figure 4.10 Compactibility profiles of tablets with four grades of MgSt (A) Alfa Aesar (B) Ligamed MF-2-V (C) Ligamed MF-2-V-BI and (D) Ligamed MF-3-V. Average values shown n = 20, y error bars indicate standard deviation. 107

Figure 4.11 Compressibility profiles of tablets with four grades of magnesium stearate (A) Alfa Aesar (B) Ligamed MF-2-V (C) Ligamed MF-2-V-BI and (D) Ligamed MF-3-V. Average values shown n = 20, y error bars indicate standard deviation...109

Figure 4.12 Effect of fed MgSt samples on dissolution profiles of Paracetamol tablets produced at 2 MPa and tested in water at 37^{o}C. (A) Alfa Aesar (B) Ligamed MF-2-V (C) Ligamed MF-2-V-BI and (D) Ligamed MF-3-V. Average values shown n = 3, y error bars indicate standard.....110

Figure 5.1 Representative BARDS raw spectrum of 250 mg MCC in 25 mL water ..118

Figure 5.2 BARDS acoustic response of Metoclopramide (25mg), MCC (225 mg) and blend of metoclopramide (10% w/w) and MCC (90% w/w) (250 mg) in 25 mL deionised water (DI). Average values shown, n =3, y error bars indicate standard deviation.....122

Figure 5.3 BARDS acoustic response for blends manually blended in 25 mL deionised water. Metoclopramide 10% w/w and MCC 90% w/w (250mg) after 5 rotations, metoclopramide 10% w/w, MCC 89.5% w/w and 0.5% w/w MgSt (250mg) after 5 rotations and after 100 rotations. Average values shown, n =3, y error bars indicate standard deviation. 124

Figure 5.4 BARDS acoustic response for blends prepared using lab scale blender in 25 mL deionised water. Unlubricated blend (metoclopramide 10% w/w and MCC 90% w/w) (250mg) and lubricated blend (metoclopramide 10% w/w, MCC 89.5% w/w and 0.5% w/w MgSt) (250mg). Samples analysed were collected from 6 different locations in the blender and analysed in duplicate. Average values shown, n =12, y error bars indicate standard deviation.....126

Figure 5.5 Gas volume plots for blends prepared using lab scale blender in 25 mL deionised water. (A) Plot of calculated gas volume versus time and (B) Plot of log of

calculated gas volume versus time for unlubricated (API/MCC) and lubricated blends (API/MCC/MgSt). Samples analysed were collected from 6 different locations in the blender and analysed in duplicate. Average values shown, n =12, y error bars indicate standard deviation. 127

Figure 5.6 Feeding of unlubricated and lubricated blend (A) Image of blends during feeding at three different feed rates and (B) Post feeding assessment of screws..130

Figure 5.7 Feeding performance of unlubricated blend (API/MCC) and lubricated blends (API/MCC/MgSt) at different feed rates through K-Tron MT12 feeder.....131

Figure 5.8 Tabletability profiles of unlubricated and lubricated blend fed at different feed rates and compacted at a range of compression pressures. Average values shown, n=20 at each compression pressure, y error bars indicate standard deviation. (Feed rate SP = Set point). 132

Figure 5.9 BARDS acoustic response for blend samples in 25 mL deionised water. Blends were prepared using lab scale blender and fed at different rates through a screw feeder. (A) Unlubricated blend and (B) Lubricated blend. Average values shown, n =2, y error bars indicate max and min values. 134

Figure 5.10 Gas volume plots for blends in 25 mL deionised water. Blends were prepared using lab scale blender- and fed at three different rates through a screw feeder. (A) Unlubricated blend plot of calculated gas volume versus time, (B) Unlubricated blend plot of log of calculated gas volume versus time, (C) Lubricated blend plot of calculated gas volume versus time, and (D) Unlubricated blend plot of log of calculated gas volume versus time. Average values shown, n =2, y error bars indicate max and min values.....136

Figure 5.11 Contact angle (^{0}) of deionized water on unlubricated and lubricated blend compacts with similar porosity. Average values shown, n =3, y error bars indicate standard deviation. 138

Figure 5.12 Wetting time of blend compacts with aqueous amaranth solution of unlubricated and lubricated blend compacts with similar porosity. Average values shown, n =3, y error bars indicate standard deviation. 139

Figure 6.1 Tensile strength (T.S.) and porosity of unlubricated and lubricated blends compressed at different compression forces. Average values shown n=20, y-error bars indicate standard deviation. 149

Figure 6.2 Heckel plots derived from relative density and compression forces for unlubricated tablets and lubricated tablets. The points between 25 MPa and 150 MPa were used to calculate the yield pressure with R^2 of 0.99 for both unlubricated and lubricated tablets. Average values shown n=20, y-error bars indicate standard deviation.....151

Figure 6.3 BARDS raw spectrum of lubricated tablet compressed at 135 MPa in 25 mL of water at room temperature. Average values shown n=2, y-error bars indicate max and min values.....153

Figure 6.4 Gas-volume plot showing different phases of gas introduction and elimination following addition of a tablet to aqueous media. Tablet compressed from lubricated blend at 135MPa. Average values shown n=2, y-error bars indicate max and min values.....154

Figure 6.5 A log gas-volume showing time range for different phases of gas elimination. Tablet compressed from lubricated blend at 135MPa. Average values shown n=2, y-error bars indicate max and min values. 155

Figure 6.6 Frequency-time profiles of tablets compressed at different compression forces analysed by BARDS in 25 mL of water at room temperature. (A) Unlubricated tablets, (B) Lubricated tablets. Average values shown n=2, y-error bars indicate max and min values. For lubricated tablets, at higher compression pressures of 178 MPa and 234 MPa, n=1 156

Figure 6.7 Gas volume-time plots derived from BARDS frequency data: (A) Unlubricated tablets (B) Lubricated tablets. Average values shown n=2, y-error bars

indicate max and min values. For lubricated tablets, at higher compression pressures of 178 MPa and 234 MPa, n=1 160

Figure 6.8 Gas volume time plots for tablets showing a second gas release due to tablet delamination in lubricated tablets. (A) 178 MPa and (B) 234 MPa. Photographs in insert show delamination behaviour captured by video recording during disintegration process. 161

Figure 6.9 Area under volume curve for unlubricated and lubricated tablets, compressed at different compression pressures. Dotted lines on graph indicate the respective yield pressures of unlubricated and lubricated blends. 162

LIST OF TABLES

Table 1.1 Definition and relationship between the parameters assessed for compressibility, tabletability and compactibility. 10

Table 1.2 Types of lubricants used in tablet formulations 16

Table 2.1 List of materials used in the study. N/A – Not available 38

Table 2.2 Feeding configurations for Alfa Aesar trial. 51

Table 3.1 Grades and suppliers of magnesium stearate 59

Table 3.2 Temperature ranges for endothermic events detected during DSC analysis of MgSt samples. The table also lists thermal process associated with the endotherms and supporting references. 63

Table 3.3 Enthalpies of dehydration, melting, and moisture content of magnesium stearate samples. ND, not determined. 65

Table 3.4 BET surface area of MgSt samples. Average value shown n=3, ± indicates standard deviation 67

Table 3.5 Particle size and percentage reduction in particle size (relative particle size measured a 1.5 bar titration pressure) for MgSt samples analysed at titration pressures of 1.5 bar, 2 bar and 3 bar. N=5. Average values ± standard deviation. NA indicates not applicable and NC indicates no change. 70

Table 3.6 Bulk density, Tapped density and True density of MgSt samples. Average values shown n=3, ± indicates standard deviation 72

Table 3.7 Carr's Index, Hausner Ratio, Flow properties of MgSt samples. Average values shown n=3, ± indicates standard deviation 72

Table 4.1 Feeding configurations investigated for Alfa Aesar feeder set-up optimisation study and associated feeding performance expressed at feeding rate % RSD 89

Table 4.2 Particle size and percentage reduction in particle size (relative to unfed material) due to feeding of MgSt samples at two feed rates. Average values shown n=5. ± indicates standard deviation. NA indicates not applicable and NC indicates no change. 99

Table 4.3 Particle size and percentage reduction in particle size (relative to material analysed at titration pressures of 1.5 bar) for MgSt samples fed at 0.15 kg/hr analysed at titration pressures of 1.5 bar, 2 bar and 3 bar. Average values shown n=5. ± indicates standard deviation. NA indicates not applicable..... 102

Table 4.4 Particle size and percentage reduction in particle size (relative to material analysed at titration pressures of 1.5 bar) for MgSt samples fed at 0.25 kg/hr analysed at titration pressures of 1.5 bar, 2 bar and 3 bar. Average values shown, n=5. ± indicates standard deviation. NA indicates not applicable..... 103

Table 4.5 Impact of feed rate on surface area of MgSt samples. Average values shown, n=3. ± standard deviation..... 104

Table 4.6 Tukey's multiple comparison tests for dissolution profiles of paracetamol tablets prepared with different MgSt samples..... 111

Table 5.1 BARDS profile lag times and time to return to steady state for metoclopramide, MCC, blend of metoclopramide – MCC, and blend of metoclopramide-MCC-MgSt prepared by manual rotation. 124

Table 5.2 Calculated gas volume elimination rate constant (*k*) and time ranges used for the calculation of the rate constant for samples of unlubricated and lubricated blend formulations. Samples were taken from various locations in the lab scale blender. 129

Table 5.3 Lag time, time to return to steady state, calculated gas volume elimination rate constant (k) and time ranges used for calculation of the constant for samples of unlubricated and lubricated blends. 137

Table 6.1 Properties of tablets compressed from unlubricated and lubricated blends at a range of compression pressures. Average values shown, ± indicate standard deviation.....150

Table 6.2 Time periods associated with time taken to reach frequency minima (f_{min}) Δt, the gas equilibrium phase at f_{min} and time taken to reach steady state (ΔT) for unlubricated and lubricated tablets compressed at different compression forces. Values are calculated from the BARDS frequency-time profiles. (n=2). * indicates gas equilibrium phase time range before tablet lamination in BARDS medium 158

Table 6.3 Gas elimination rate constant (k(s^{-1})) for unlubricated and lubricated tablets compressed at different compression forces. Values are calculated from the BARDS log gas volume-time profiles and the time ranges used for the calculation are also shown. R- Squared indicates the linear fit for the selected time ranges for the gas elimination rate constants. (n=2) 164

DECLARATION

This thesis is submitted to the National University of Ireland, University College Cork by Raghu Peddapatla for examination in the degree of Doctor of Philosophy (Pharmacy – Pharmaceutics). This thesis has not been submitted for any other purpose or degree offered by this or any other university. The material presented in this thesis is entirely the author's own original work, except where duly noted and acknowledged. This thesis was authored by Raghu Peddapatla with supervision and editorial advice from my PhD supervisor, Dr. Abina Crean.

Magnesium stearate continuous feeding experiments in chapter 4 were performed with assistance from Dr. Caroline Blackshields and Dr. Michael Cronin, School of Pharmacy, UCC. BARDS analysis of formulations in Chapter 5 and Chapter 6 were performed with assistance from Dr. Rizwan Ahmed and Dr. Dara Fitzpatrick, School of Chemistry, UCC.

Signature: **Date**

ACKNOWLEDGEMENTS

First and foremost, I would like to thank my parents Aruna and Praveen Kumar Peddapatla, for their unconditional love, support and encouragement in every part of my life. I would also like to thank my younger brothers Sai Teja and Sai Prashanth for being my support systems. I would wholeheartedly thank my grandparents for encouraging me to pursue my dreams.

I wish to acknowledge all the help, support and guidance of my supervisors, Dr. Abina Crean and Dr. Maria Gallagher. They taught me how to conduct innovative research from the beginning of my research career here in the school and I appreciate all their contributions of time, ideas, and encouragement to make my PhD experience enriching. I would also like to thank Dr. Caroline Blackshields, for her unconditional support throughout the tenure of my PhD. I would like to thank the PMTC for the funding I received that allowed me to pursue PhD.

I would like to thank all the staff in the School of Pharmacy. In particular, Dr. Brendan Griffin and Dr. Sonja Vucen, for their valuable suggestions. The technical staff of the school – Dr. Michael Cronin, Dr. Ken Devine, Dr. Tom O'Mahony and Ms. Aine Healy for their help, for their help with techniques like the tableting, TGA, DSC, HPLC and BET where necessary. The administrative staff Ms. Noreen Moynihan, Ms. Kathleen Murphy and Ms. Aisha Murphy have also ensured that the paperwork has flowed smoothly throughout my research.

I have been lucky to collaborate with Dr. Dara Fitzpatrick's and Dr. Rizwan Ahmed, which gave me an opportunity to learn extensively about BARDS. I would also like

to thank my former lab mates, Rakesh, Graham, Evin and Mary Ellen for their help during my early days at the lab. I thank all my friends and researchers - Carol, Aoife, Ana Luiza, Waleed, Fatma, Valeria, Ziad, Uday, Laura, Tania, Niklas and Elaine.

I would like to thank my best friends Padmavathi and Rohini for their care, encouragement, and support. I thank my friends, Sai, Rakesh, Narender, Rajesh, Santhosh, and Chandan.

PUBLICATIONS AND PRESENTATIONS ASSOCIATED WITH THIS THESIS

Publications

- Raghu V. G. Peddapatla, M. Rizwan Ahmed, Caroline A. Blackshields, M. J. Sousa-Gallagher, Sean McSweeney, J. Kruse, Abina M. Crean and Dara Fitzpatrick. 'Broadband Acoustic Resonance Dissolution Spectroscopy (BARDS) – A novel approach to investigate the wettability of pharmaceutical powder blends'. Mol Pharm. 2018 Jan 2;15(1):31-39.

Oral presentations

- Raghu V. G. Peddapatla, Rizwan Ahmed, Caroline A. Blackshields, Sean McSweeney, J. Kruse, Maria De Sousa Gallagher, Dara Fitzpatrick, Abina M. Crean., Broadband Acoustic Resonance Dissolution Spectroscopy (BARDS) -a novel at-line Process Analytical Technology (PAT) to accesses uniformity of pharmaceutical blends/tablets. *PMTC Knowledge day* on August 31st 2017 organised by PMTC at University of Limerick, Limerick, Ireland

- Raghu V. G. Peddapatla, Rizwan Ahmed, Caroline A. Blackshields, Sean McSweeney, Maria De Sousa Gallagher, J. Kruse, Dara Fitzpatrick, Abina M. Crean., A novel approach in investigating the hydration behaviour of powder blends and compacts. *All Ireland School of Pharmacy Conference,* on 24th and 25th April, 2017 at University College Cork, Ireland.

- Raghu V. G. Peddapatla, Rizwan Ahmed, Caroline A. Blackshields, Sean McSweeney, Maria De Sousa Gallagher, Dara Fitzpatrick, Abina M. Crean., Broadband Acoustic Resonance Dissolution Spectroscopy (BARDS) -a novel at-line Process Analytical Technology (PAT) to accesses uniformity of pharmaceutical blends/tablets. *EUPAT 8*, on 3rd and 4th October 2016, Cork, Ireland.

Posters

- Raghu V. G. Peddapatla, Rizwan Ahmed, Caroline A. Blackshields, Sean McSweeney, J. Kruse, Maria De Sousa Gallagher, Dara Fitzpatrick, Abina M. Crean., Broadband Acoustic Resonance Dissolution Spectroscopy (BARDS) -a novel at-line Process Analytical Technology (PAT) to accesses uniformity of pharmaceutical blends/tablets. *PMTC Knowledge day* on August 31st 2017 organised by PMTC at University of Limerick, Limerick, Ireland

- Caroline Blackshields, Raghu Peddapatla, Abina Crean. Magnesium stearate variability and its impact on continuous feeding tablet functionality. *PMTC Knowledge day* on August 31st 2017 organised by PMTC at University of Limerick, Limerick, Ireland

- Raghu V. G. Peddapatla, Rizwan Ahmed, Caroline A. Blackshields, Sean McSweeney, Maria De Sousa Gallagher, Dara Fitzpatrick, Abina M. Crean., (2016) Broadband Acoustic Resonance Dissolution Spectroscopy (BARDS) -a novel at-line Process Analytical Technology (PAT) to accesses uniformity of pharmaceutical blends/tablets. *EUPAT 8*, on 3rd and 4th October 2016, Cork, Ireland.

- Raghu V. G. Peddapatla, Caroline A. Blackshields, Michael F. Cronin and Abina Crean (2016) Behaviour of Magnesium Stearate in Continuous Feeding *American Institute of Chemical Engineers Annual Meeting*, from 13th – 18th November, 2016, San Francisco, USA

- Raghu V. G. Peddapatla, Caroline A. Blackshields, Michael F. Cronin, Maria De Sousa Gallagher, Abina M. Crean., (2016) Characterising magnesium stearate variability-understanding its impact on continuous feeding at *10th World meeting on pharmaceutics, biopharmaceutics, and pharmaceutical technology* on April 7th 2016 organised by APV, Germany at SECC, Glasgow, UK

- Raghu V. G. Peddapatla, Graham E. O'Mahony, Maria De Sousa Gallagher, Abina M. Crean., (2015) Characterisation of magnesium stearate from different suppliers. *PMTC Knowledge day* on August 28th 2015 organised by PMTC at University of Limerick, Limerick, Ireland.

ABSTRACT

Magnesium Stearate (MgSt) is the most commonly used lubricant in pharmaceutical industries. Effects of MgSt on the final product have been extensively studied in batch processing. In recent times pharmaceutical companies have been increasingly interested in continuous processing, where the relative effects of material properties and process parameters on blend behaviour during continuous processing has gained significant attention. It is important to assess the behaviour of materials and it is a challenging feat to monitor behaviour of very cohesive materials like MgSt in continuous processing. The main aims of this thesis were, to investigate the role of MgSt supplier variability during continuous feeding through a loss in weight feeder (LIW) and to investigate the capability of Broadband Acoustic Resonance Dissolution Spectroscopy (BARDS) to discriminate between blends and tablets with variable MgSt distribution.

Initially, the variability among four different grades of MgSt samples from two different suppliers was studied. The variability among the samples was evident (chapter-3) and the effect of this variability on continuous feeding performance of MgSt samples was studied (Chapter-4). Bulk density of the samples dictated the feed factor achieved for the MgSt samples, when fed through K-Tron MT12 feeder (Chapter-4). Higher variability in the feed rate RSD was noticed for the MgSt samples, when fed at lower feed rate of 0.15 kg/hr and for samples (Ligamed MF-2-V and Ligamed MF-2-V-BI) with similar properties. Post feeding characterisation of MgSt samples was performed to identify any effect of feeding on particulate properties. A reduction in particle size due to feeding of the samples was noted and

these samples when included in tablet blends, showed a delayed drug release, which was more prominent in tablets with fed MgSt of Alfa Aesar and Ligamed MF-2-V samples. Ligamed MF-3-V was least effected by feeding and when fed samples were included in formulations a very slight delay in drug release was noted compared to other tablets with other MgSt samples (Chapter-4).

A novel technology, BARDS was employed for the first time to analyse the excipients, tablet blends and tablets (Chapter-5 and Chapter-6). Analysis of unlubricated and lubricated blends using BARDS, clearly discriminated between the blends, resulting inan extended acoustic response for lubricated blends. K-Tron MT12 feeder, was used to feed the unlubricated and lubricated blends at three different feed rates (0.2238 kg/hr, 0.5594 kg/hr and 1.006 kg/hr), anticipating lubricated blend with varied degrees of blend lubrication. When analysed using BARDS, unlubricated blend fed at increasing feed rates showed similar acoustic response, whereas lubricated blend showed extended acoustic response, which was dependent on the feed rate (Chapter-5). Gas elimination rate constant was used to determine the degree of lubrication within blends. The degree of overlubrication was further confirmed by the standard wetting techniques and tabletability of the blends (Chapter-5).

Tablets were produced from unlubricated and lubricated blends at a compression pressure range of 30 MPa to 234 MPa. The influence of compression pressure and tablet properties, on the BARDS acoustic response was investigated in Chapter-6. The yield pressures calculated from the Heckel analysis was 98 MPa and 102 MPa for unlubricated and lubricated tablets. A significant change in the BARDS acoustic

response was noticed for tablets produced above and below yield pressure for both blends. Lubricated tablets produced at higher compression pressures, showed delamination, which was identified by BARDS. Slow gas elimination rate constant was observed for lubricated tablets compared to unlubricated tablets.

ABBREVIATIONS

API	Active Pharmaceutical Ingredient
BARDS	Broadband Acoustic Resonance Dissolution Spectroscopy
BD	Bulk density
BET	Brunauer, Emmett and Teller
CAS	Coarse auger screw
CCS	Coarse concave screw
CI	Carr’s index
CMA	Critical material attribute
CMT	Continuous mixing technology
CSlS	Coarse slotted screen
CSqS	Coarse square screen
D10	Diameter at which 10% of a sample's mass is comprised of smaller particles
D50	Diameter at which 50% of a sample's mass is comprised of smaller particles (median particle size)
D90	Diameter at which 90% of a sample's mass is comprised of smaller particles
DC	Direct compression
DI	Deionized
DSC	Differential scanning calorimeter
DVS	Dynamic vapour sorption
EDX	Energy dispersive X-ray

f_a	Fractional gas volume
FAS	Fine auger screw
FCS	Fine concave screw
FDA	Food and drug administration
ffc	Flow index
FF	Feed factor
f_{min}	Frequency minima
FPS	Frames per second
FSlS	Fine slotted screen
FSqS	Fine square screen
g	Gram
h	Hour
H	Hausner ratio
ICH	International Conference for Harmonisation
kg	Kilogram
kHz	kilo hertz
kN	Kilo Newton
l	Litre
LIBS	Laser induced breakdown spectroscopy
LIW	Loss in weight
MA	Material attribute
MCC	Microcrystalline cellulose

MgSt	Magnesium stearate
min	Minute
ml	Millilitre
mm	Millimetre
µm	micron/micrometer
MPa	Megapascal
N	Newton
N/A	Not applicable
NIR	Near infrared
PAT	Process analytical technology
PCMM	Portable Continuous Miniature and Modular
PFT	Powder flow tester
PSD	Particle size distribution
PXRD	Powder X-ray diffraction
QbD	Quality by design
RH	Relative humidity
RPM	Revolutions per minute
RSD	Relative standard deviation
s	Second
SP	Set point
SSA	Specific surface area
SD	Standard deviation

SEM	Scanning electron microscopy
SIMS	Secondary ion mass spectrometry
SRS	Strain rate sensitivity
TD	Tapped density g/cm3
TGA	Thermogravimetric analysis
TS	Tensile strength
% w/w	% weight/weight
Δt	Time to reach frequency minima
ΔT	Time to reach steady state from frequency minima

Chapter -1

General Introduction

1. General Introduction

Innovative technological solutions which enable the production of highly engineered drug products are needed in establishing robust pharmaceutical manufacturing (Rantanen and Khinast, 2015). Batch processing has been used for decades in the manufacturing of pharmaceutical dosage forms. In recent times pharmaceutical companies have become increasingly interested in continuous processing and production for pharmaceutical solid dosage forms.

In this transition between batch and continuous processing, Quality by Design (QbD) requires a better understanding the effects of variability of excipients on the performance and processing of drug products. Evaluating critical material attributes (CMAs) is envisioned to help in understanding their impact on the processing parameters and final quality of the product. This thesis mainly focuses on studying (a) the impact of variability of a lubricant, magnesium stearate (MgSt), (b) the behaviour of the lubricant during a continuous feeding process and (c) the capability of Broadband Acoustic Resonance Dissolution Spectroscopy (BARDS) to detect differences in the degree of MgSt lubrication in blends and tablets.

This introductory chapter provides an overview of pharmaceutical tablets, their manufacturing process (direct compression), principles of tablet compression, MgSt variability and its CMAs, continuous processing and BARDS.

1.1 Pharmaceutical Tablets

Pharmaceutical tablets are solid dosage forms containing active pharmaceutical ingredients (API) with excipients. Tablets are most commonly manufactured by a compression method (Guillory, 2009). Tablets are the most widely used oral dosage forms (Haritha, 2017; Shabana, 2016). They vary in size, shape, weight, hardness, thickness, disintegration and dissolution characteristics, depending on their intended use, formulation and manufacturing mode. Conventional tablets are used in oral administration of drugs and other tablets, such as sublingual, buccal, or vaginal tablets, are prepared to have features most applicable to their particular route of administration. Figure 1.1 shows different types of tablets and their site of action. The main advantages and disadvantages of pharmaceutical tablets are listed below.

Advantages

- Easy and convenient to use (relatively good patient compliance)
- Economical to manufacture and distribute (De Villiers, 2004)
- High absorption capability following administration (i.e. due to a large surface area for absorption in small intestine) with different absorption pathways (i.e., passive, carrier mediated)
- Delayed release can be achieved through different types of tablet coatings
- Tablets are highly stable when compared to other dosage forms (De Villiers, 2004).

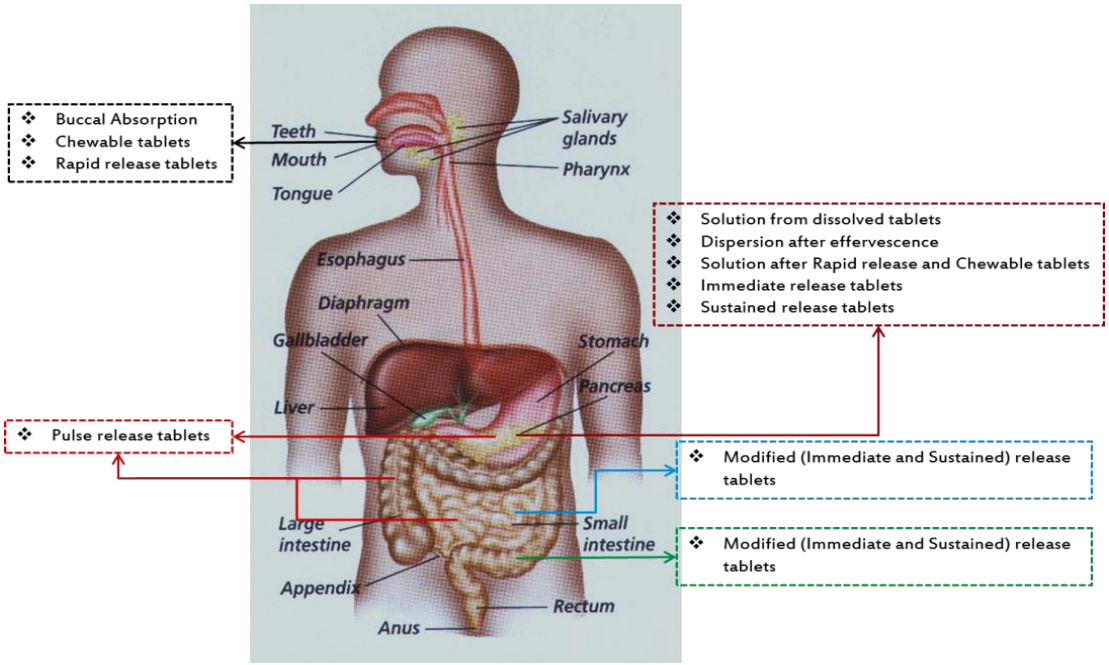


Figure 1.1 Different types of tablets and their site of action (Annotated diagram, Tortora and Derrickson, 2011).

Disadvantages

- Drug absorption from dosage forms in the gastrointestinal tract may be delayed due to presence of food
- Onset of action is slower compared to that of intravenous administration
- Percentage bioavailability can be reduced compared to that of intravenous administration, where it is 100% bioavailability
- Dosage forms with low density and highly amorphous in nature are difficult to compress
- Administration of drugs is not easy in case of children if the drug dose is large
- Chemical and physical properties of the drug make it difficult to overcome compression problems such as capping, lamination, picking and sticking (De Villiers, 2004)

1.1.1 Theory of tablet compression

Consolidation and compression of a solid particulate, solid-gas system, due to applied force is known as compaction (Metin, 1994). Compression involves the reduction in bulk volume as a result of a reduced gaseous phase. As the applied force on the powder increases, the further rearrangement of the particles is inhibited and particle deformation occurs (Patel et al., 2006). During the gaseous phase reduction process, the particles are moved to the closer proximity resulting in bond formation between the particles. At higher compression forces, the mechanical strength of the tablets depends on the consolidation (particle-particle interaction) (Marshall, 1986; Metin, 1994). The various steps involved in powder compaction are shown in Figure 1.2.

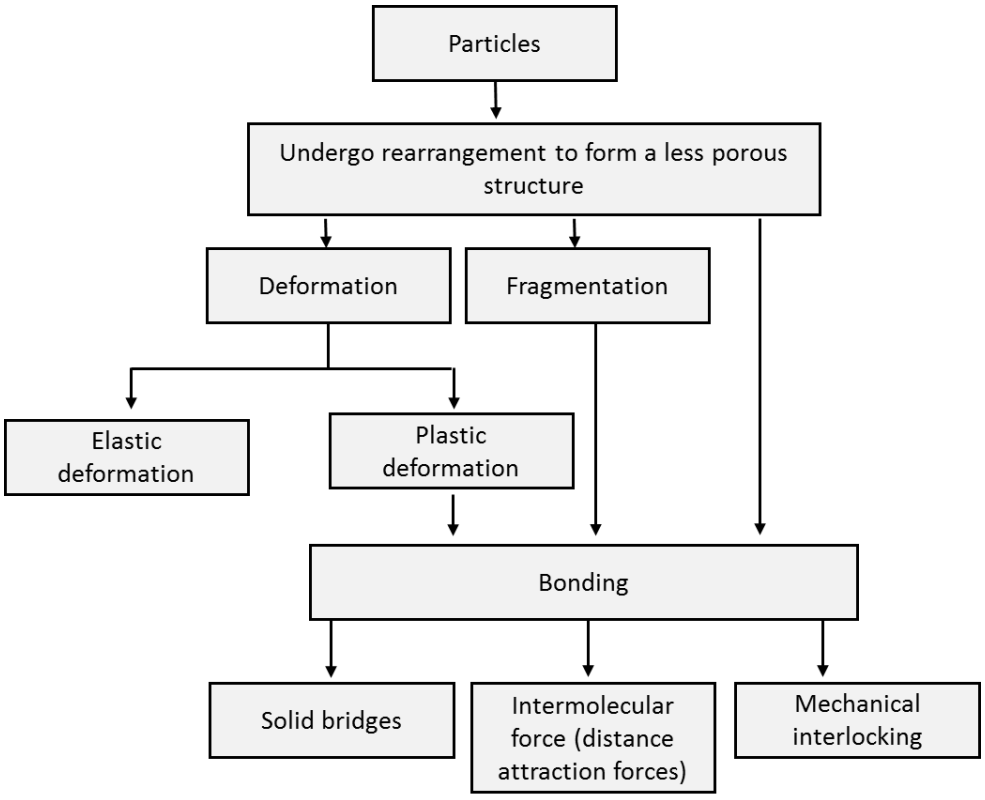


Figure 1.2 Steps involved in compaction process

1.1.1.1 Mechanism of tablet compression and/or compact formation

Upon increase in compression pressure, the further volume reduction of the powder is accomplished by deformation or fragmentation and by forming bonds between the particles (Hiestand et al., 1977; Metin, 1994). Figure 1.3 shows the different deformation mechanisms of powder material under applied compression force.

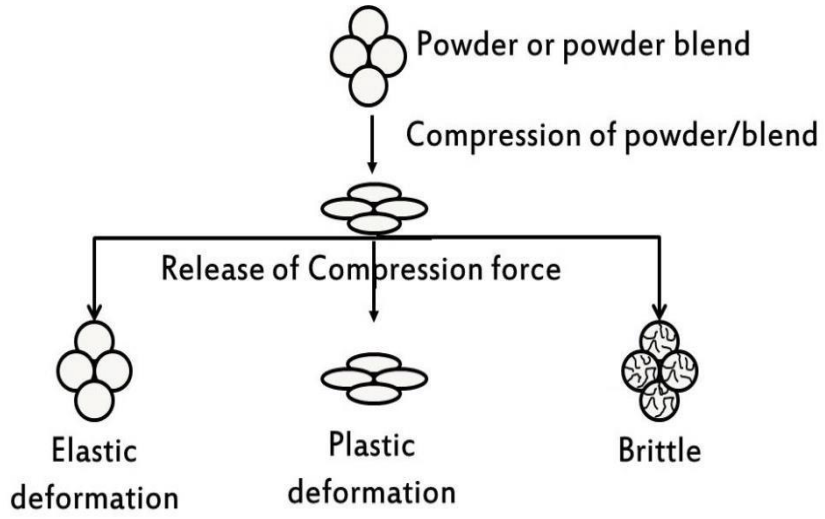


Figure 1.3 Elastic, plastic and brittle deformation mechanisms of powder under applied compression force

Elastic deformation

If the applied pressure (or stress) is released before the deformation reaches the critical value, the particles deform elastically. This type of deformation is reversible and the particles in the compact regain their original shapes when the applied stress is removed as shown in Figure 1.3. An example of such material is starch.

Plastic deformation

If the compression force increased beyond the critical stress value, the particles yield and deform plastically. This type of deformation is irreversible and a permanent change in the shape of the particles will occur (Figure 1.3). An example of such material is microcrystalline cellulose

Many pharmaceutical materials possess a combination of both elastic and plastic properties and are known as viscoelastic materials. Viscoelastic deformation is dependent on both the stress applied and the duration of compression (Aulton and Taylor, 2007). Such materials, whose deformation behaviour is highly dependent on applied stress time and press speed are said to exhibit strain rate sensitivity (SRS) (Katz and Buckner, 2013). Materials such as, maize starch, corn starch, pre-gelatinized corn starch, microcrystalline cellulose and lactose exhibits varying sensitivities to changes in strain rate (Katz and Buckner, 2013; Patel et al., 2006).

Fragmentation

Under the influence of applied stress, after the elastic limit of the material is exceeded, a material will deform plastically or destructively undergo fragmentation forming smaller particles producing newer surfaces for bonding (Figure 1.3) (Patel et al., 2006). The stress value at which the particles start to fragment is called fracture strength. Examples of brittle materials are lactose, sucrose and ascorbic acid.

1.1.1.2 Bonding or Consolidation

Pharmaceutical powders consolidate by reducing the pores or void spaces upon applied compression force, resulting in formation of interparticulate bonds. The type and the intensity of the bonding between the particles during consolidation dictates the mechanical strength of the tablet (Nyström et al., 1993). Consolidation of materials occurs mainly by particle rearrangement, plastic deformation and fragmentation.

Consolidation of materials occurs by different mechanisms such as cold welding, fusion bonding, mechanical bonding, intermolecular force bonding and liquid surface film bonding. When the surface of the particles approaches each other in close proximities, their free surface energies results in strong attractive force leading to formation of bonds by cold welding. During the compression process, there will be a certain amount of frictional heat generated in the powder bed, which results in the melting of the surface area of powder particles. When the melt is solidified, they form a fusion bonding between the particles (Marshall, 1986). During particle deformation, mechanical bonds are formed due to interactions between the particles boundaries. Under compression force, the particles come into close vicinities so that the van der Waal forces interact to consolidate the particles, forming an intermolecular bond (Celik, 2011).

Compaction Triangle

The relationships between compaction pressure, tablet tensile strength and tablet solid fraction are critical to characterise the compaction process of blends. The interaction between these three parameters reflects the relationship between compressibility, tabletability and compactibility as shown in Figure 1.4 and Table 1.1.

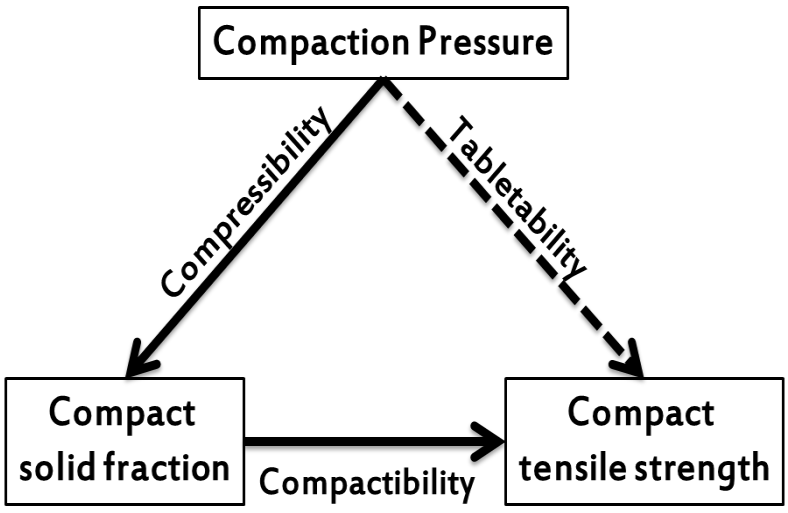


Figure 1.4 Relationships between compaction pressure, solid fraction and tensile strength for a given powder (Tye et al., 2005).

Table 1.1 Definition and relationship between the parameters assessed for compressibility, tabletability and compactibility.

Terminology	Definition	Parameters assessed	References
Compressibility	Ability of powdered material to undergo a reduction in volume upon increase in compression pressure	Tablet porosity or solid fraction Vs. Compression pressure	(Joiris et al., 1998; Patel et al., 2006; Tye et al., 2005)
Tabletability	Ability of a powdered material to be transformed into a tablet of specific strength under applied compression pressure	Tablet tensile strength Vs. Compression pressure	(Joiris et al., 1998; Patel et al., 2006; Tye et al., 2005)
Compactibility	Ability of a powdered material to produce a tablet with sufficient strength under the effect of densification	Tablet tensile strength Vs. Tablet porosity or solid fraction	(Joiris et al., 1998; Patel et al., 2006; Tye et al., 2005)

The relationship between compaction pressure – solid fraction – tensile strength represents the direct cause-effect relationship, whereas the relationship between compression pressure and tablet tensile strength is more indirect (Joiris et al., 1998; Sun and Grant, 2000; Tye et al., 2005). Compactibility is the most important among the three properties, because it reflects the relationship between the two out puts of compression pressure; tablet tensile strength and tablet solid fraction (Tye et al., 2005).

Heckel Model

The Heckel model is used to study the relationship between relative density and applied pressure (Ilkka and Paronen, 1993),

$$\ln[1/1 - D] = KP + A \qquad \text{Equation 1}$$

where D is the relative density of the tablets (g/cm^3), *K* is the slope of a straight line in the Heckel equation, *P* is the compression pressure (MPa), and *A* is a constant. The yield pressure (P_y) is calculated by taking the reciprocal of *K*.

Heckel plots can also be used to differentiate the physical significance of a compression event into three parts as shown in Figure 1.5.

- Region I - Particle rearrangement under low pressures
- Region II - Plastic deformation (or fragmentation or brittle fracture) at medium to high pressure
- Region III – Strain or work hardening at very high pressure.

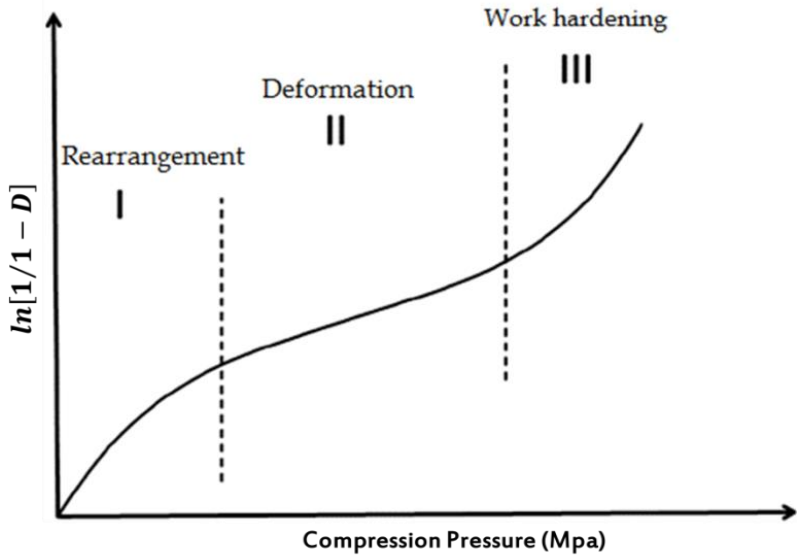


Figure 1.5 Schematic representation of Heckel Plot (Patel et al., 2006)

Compressibility reflects the ability of a material to undergo volume reduction under pressure. A unique feature of the Heckel plot resides in its ability to differentiate between plastic deformation and brittle fracture, by calculating the yield pressure (P_y) from the compaction profile of a specific formulation. If the materials undergo plastic deformation they possess a greater slope than those that undergo brittle fracture, implying the former has a lower yield pressure (Guillory, 2009).

1.1.2 Tablet manufacturing method

The manufacture of tablets is a complex, multi-stage process during which the starting materials change their physical characteristics several times before the final tablet is produced.

1.1.2.1 Direct compression

Direct compression (DC) is the easiest and least complex method to produce tablets, allowing the manufacturer to simply blend the powders in a blender and discharge into the tablet press (hopper) directly followed by compression into tablets (Figure 1.6a). DC is the preferred choice of tablet manufacture in terms of its simplicity, cost and time effectiveness, and elimination of heat and moisture effects (Garg et al., 2015; Jarvinen et al., 2013; Mangal et al., 2015). Excipient selection is critical for DC, as blends should possess excellent flow to ensure a uniform blend and compactibility, which limits its application to only 20% of APIs (Li et al., 2017; Mirani et al., 2011; Vanhoorne et al., 2014). It is the preferred choice of manufacture for tablets containing thermo-labile and moisture sensitive drugs (Jivraj et al., 2000).

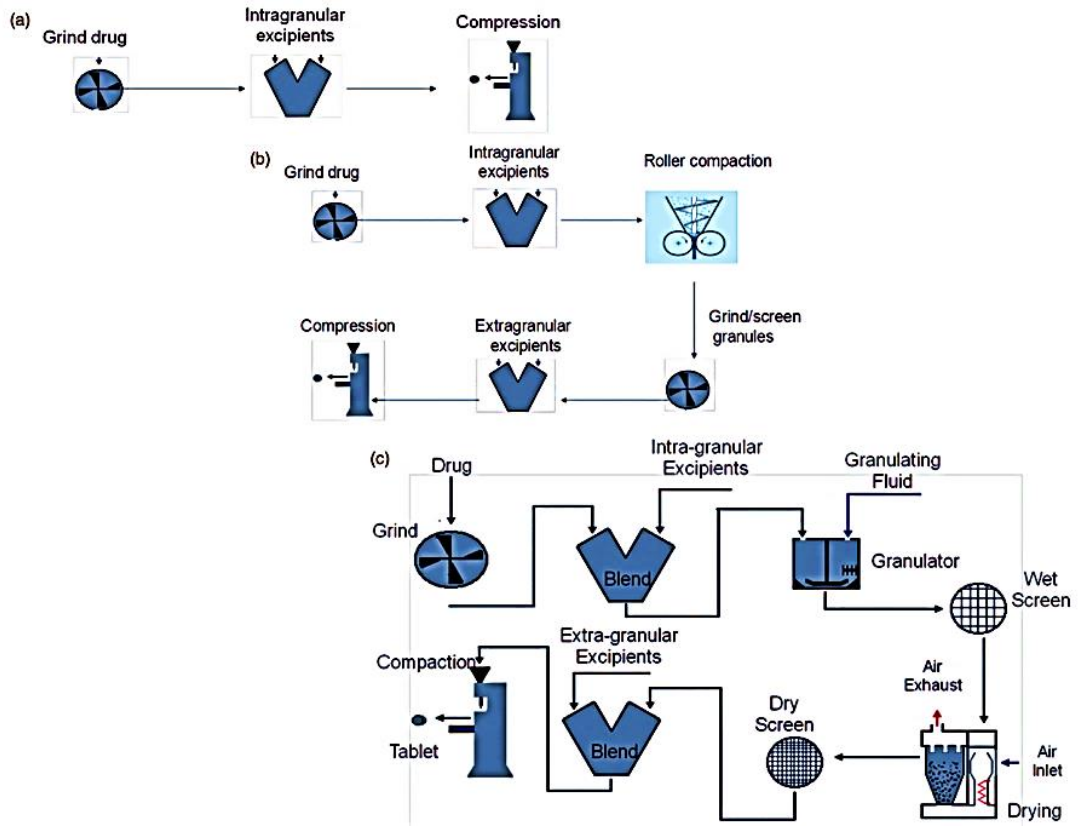


Figure 1.6. Schematic representation of different manufacturing routes for tablets; (a) Direct compression (b) Dry granulation and (c) Wet granulation (Leane et al., 2015).

1.1.2.2 Excipients in direct compressible blend

An excipient is an inert substance that is formulated (blended and compacted) alongside the API (Katdare, 2006). There are a number of reasons why excipients are added to API in dosage forms. Some of these include to increase stability, as bulking agents or fillers or diluents for formulations that have small amounts of API, to facilitate the drug absorption (Borbás et al., 2016), or as solubility enhancers. They may constitute anywhere from 1 to 99% of the total formulation mass (Dave et al., 2015). The international Pharmaceutical Excipients Council (IPEC) has defined a pharmaceutical excipient as follows,

'Any substance other than the active drug or prodrug which has been appropriately evaluated for safety and is included in drug delivery system to either:

- *Aid processing of the system during manufacture, or*
- *Protect, support or enhance stability, bioavailability or patient acceptability, or assist in product identification, or*
- *Enhance any other attribute of the overall safety and effectiveness of the drug product during storage use.'*

Excipients used in DC should possess high bulk density, good flow and good compression properties without affecting the final tablet quality (Jivraj et al., 2000). The PSD of the excipient should be consistent from batch to batch to avoid segregation in blends (Gohel and Jogani, 2005). Particle size of the excipients should be equivalent to the API (Jivraj et al., 2000). Many excipients possess multi-functional properties based on the concentration they are used within the formulation. For example, MCC can be used as anti-adherent at 5-20% w/w, as a disintegrant at 5-15% w/w and as a diluent at 20-90% w/w concentrations (Jivraj et al., 2000).

Some examples of common excipients used in DC are MCC and pregelatinized starch, dibasic calcium phosphate dehydrate, lactose, mannitol and maltose and co-processed excipients such as silicified MCC (98% MCC and 2% colloidal silicon dioxide) (Jivraj et al., 2000).

1.2 Tablet lubrication

Lubrication is one of the key aspects in effective manufacturing of a tablet or capsule dosage form. Lubricants are chemically inert, odourless, and tasteless and act by reducing the friction between the manufacturing equipment and the powder blend to ensure the continuation of pharmaceutical processes such as, blending, roller compaction, tablet manufacturing and capsule filling (Wang et al., 2010). Widely used lubricants in pharmaceutical processes are metallic salts of fatty acids, hydrocarbons & fatty alcohols, fatty acid esters, alkyl sulphate, inorganic materials and polymers. List of commonly used lubricants in pharmaceutical tablet formulations are listed in Table 1.2

Table 1.2 Types of lubricants used in tablet formulations

Category	Examples	Optimum Concentration (%w/w)	References
Metallic salts of fatty acids	MgSt, aluminium stearate, calcium stearate, sodium stearate and zinc stearate	0.25-1	(Wang et al., 2010)
Fatty acids, hydrocarbons and fatty alcohols	Stearic acid	2.5	(Phadke and Collier, 1994)
Fatty acid esters	Sodium stearyl fumerate, sodium lauryl sulphate, dodecanoic acid, sucrose mono laurate	0.12–3	(Wang et al., 2010)
Alkyl sulphate	Magnesium lauryl sulphate, sodium lauryl sulphate	0.5	(Wang et al., 2010)
Inorganic materials	Talc	0.5-5	(Delacourte et al., 1993)

Lubrication efficiency is defined as the capability of lubricant to lubricate the die walls and assist in the ejection of the compressed tablet from the die (Gupta et al., 2009a). It is mainly affected by processing factors such as internal lubrication and external lubrication (Wang et al., 2010). If the lubricant is added and blended with all other ingredients in powder form in a blender, this is called internal lubrication. In internal lubrication, the choice of lubricant is solely dependent on the process. Errors in the lubrication process may affect the tablet properties such as a reduction in breaking force and delay in drug dissolution. To avoid these negative effects on tablet quality, external lubrication systems were developed (Jahn and Steffens, 2005). During external lubrication, only punches and die are lubricated, which is beneficial when the tablet properties are sensitive to lubricant (Jahn and Steffens, 2005; Lindberg, 1970).

1.2.1 Magnesium stearate

MgSt is the most commonly used lubricant, present in more than 2500 pharmaceutical products and a widely used pharmaceutical excipient (Gupta et al., 2009a; Rao et al., 2005). Its chemical name is octadecanoic acid and it exists in form of white powder. It has a chemical formula $Mg(C_{18}H_{35})_2$, which consists of two equivalents of stearate (the anion of stearic acid) and one magnesium cation. The chemical structure of MgSt is shown in Figure 1.7. Commercially available MgSt grades also consists of a large percentage of magnesium palmitate, which may vary from supplier to supplier (Miller et al., 1985).

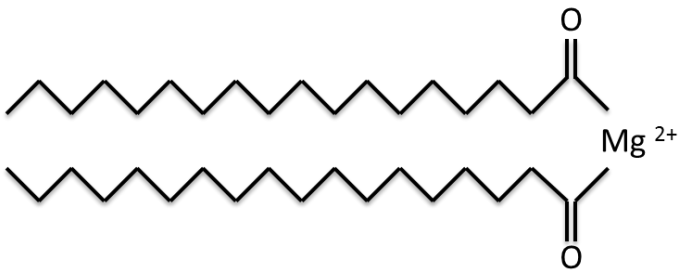


Figure 1.7 Magnesium stearate chemical structure

MgSt is the derivative of bovine or vegetable sources, which constitutes chiefly stearic and palmitic acids (organic fatty acids). Most pharmaceutical companies have transitioned from the use of bovine derived MgSt to vegetable derived MgSt, due to the risks associated with life threatening diseases such as bovine spongiform encephalopathy (BSE) and foot and mouth disease (Gupta et al., 2009a; Hamad et al., 2008). Commonly used sources of MgSt are produced from vegetable sources; palm oil and cotton seed oil after hydrogenation. A fatty acid splitting process takes place in which glycerine and fatty acids are separated. Fatty acids are further refined to yield tallow acid. At this stage, MgSt can be prepared by fusion of tallow acid with magnesium hydroxide or saponification of tallow acid with sodium hydroxide to form sodium tallowate solution. Magnesium sulphate is added to sodium tallowate solution with pH adjustment, dilution with water, wash and dry (Narang et al., 2009). MgSt exists in mono, di and trihydrate forms (Swaminathan and Kildsig, 2001).

The ideal lubricant should be odourless, tasteless, colourless, water soluble, inert and unreactive with other formulation ingredients. MgSt possesses most of these properties with some limitations. Magnesium oxide is a known reactive impurity of

MgSt, which reacts with ibuprofen to form a salt (Kararli et al., 1989). Due to its hydrophobic nature, the negative effects of MgSt on particle bonding, tablet tensile strength, tablet dissolution and disintegration has been widely reported (Li and Wu, 2014; Miller et al., 1985).

1.2.1.1 MgSt variability and its effect on final product quality

Though MgSt is used in low concentrations and inert within a formulation, it plays a major role in dosage form performance. Batch to batch, and source to source variability of MgSt has been reported to impact the tablet quality (Barra and Somma, 1996; Dave et al., 2015). Khan et al., 2008 examined the differences, raw material characteristics and the performance MgSt derived from bovine and vegetable source, in which they reported some minor differences in chemical composition. It was also reported that a dry granulated blend containing MgSt from a bovine source showed higher ejection force than the blend containing MgSt from a vegetable origin (Hamad et al., 2008). Predominately, minute quantities (0.25% to 2-5% w/w) of lubricating agents are added to the pharmaceutical blend to ensure the compression process runs smoothly (Li and Wu, 2014). Concentration and process parameters of the lubricant play a major role in product performance. Many reports show that MgSt when over blended has capacity to form a film over the other excipients of the blend due to its hydrophobic nature (Li and Wu, 2014; Miller et al., 1985). This behaviour affects the product performance by increasing the drug release time (dissolution, disintegration), decreasing tablet hardness and compactibility with MCC, starch and lactose (Lakio et al., 2013; Morin and Briens,

2013; Uzunović and Vranić, 2007). These undesirable effects of MgSt are mainly attributed to its large surface area and hydrophobicity (Rao et al., 2005).

A study by Vezin et al. investigated the effect of lubrication on tablet tensile strength by studying the lubricant mixing time, pre-compression and compression forces when 0.5% w/w MgSt was blended with MCC (Vezin et al., 1983). Tablet properties such as tablet ejection force were reported to be decreased by over blending and tablet hardness was decreased with increase in intensity of blending due to the film formation by the lubricant, which decreased the interparticulate bonding (Johansson and Nicklasson, 1986; Lerk et al., 1977; Mitrevej and Augsburger, 1982; Shah and Mlodozeniec, 1977). Bolhuis et al. determined the effect of MgSt on crushing strength of tablets, when mixed with a MCC/lactose blend, based on the type, size, rotation of the mixer used (Bolhuis et al., 1987). Kikuta et al. proposed the adverse effects of MgSt on tablet hardness, ejection force and disintegration time when over blended (Kikuta and Kitamori, 1994).

1.2.2 Tools to identify MgSt distribution in blends and tablets

Numerous attempts have been made to detect lubricant films in the blends and tablets through indirect techniques. Energy dispersive X-ray microanalysis (EDX) has been applied to detect distribution of MgSt on surfaces (Hussain et al., 1988). Roblot et al. investigated the distribution of MgSt using scanning electron microscopy (SEM) and microanalysis on the surface of lubricated particles. This study results showed the presence of MgSt within the cavities of particles and the surface regularisation due to lubricant (Roblot-Treupel and Puisieux, 1986). The effect of MgSt on potato starch particles was investigated by Abe and Ostuka (Abe

and Otsuka, 2012). They used NIR spectroscopy and identified differences between the distribution of MgSt within a blend, which is blended for 0 and 180 min blending. Hussain et al. used secondary ion mass spectrometry (SIMS) to evaluate the distribution of MgSt and its effect on sodium chloride tablets (Hussain et al., 1990). In this study, they observed that a Na^+/Mg^+ ratio of 521.11 for the uncoated excipient was reduced to 0.94, 1.25 and 13.36 after 2 min. mixing with 0.5% w/w concentration of two commercial and a high purity sample of MgSt. A study by St-Onge et al. quantitatively determined the distribution of MgSt using laser induced breakdown spectroscopy (LIBS), in which when a sample was subjected to laser, a portion of the sample melts producing luminous microplasma (St-Onge et al., 2005). The light emission from the microplasma was analysed through optical emission spectroscopy.

Raman spectroscopy is capable of directly measuring the hydrophobic $–CH_2$ groups present in MgSt, thereby it enables the detection of MgSt concentration of 0.5% w/w in tablet blends and 3% w/w in tablets (Aguirre-Mendez and Romanach, 2007). A study by Henson and Zhang showed that Raman mapping was utilized to analyse the tablets containing low dose (0.5% w/w) API, including the spatial distribution of API and excipients (Henson and Zhang, 2006). Vajna et al.,used Raman imaging (x100 magnification) and captured the distribution of MgSt in imipramine tablets (Vajna et al., 2010). A study by Widjaja and Seah showed that Raman microscopy can be used in combination with band-target entropy minimisation method (advanced multivariate analysis) to map very low concentrations of MgSt in acetaminophen tablets (Widjaja and Seah, 2008). In a study by Zhang et al. no

spectral information of MgSt (2% w/w) in placebo tablets was seen during image analysis following Raman imaging (Zhang et al., 2005).

1.3 Continuous processing

Tablets are the most frequently consumed dosage form, with more than 80% in terms of consumption (Jarvinen et al., 2013). To meet such a high demand pharmaceutical companies are transitioning from batch processing to continuous processing in which pharmaceutical products are manufactured in closed, compact units with a high degree of automation, less manual interference and more operator safety. Continuous processes are highly established in food and chemical industries where the production rates are high (Leuenberger, 2001). Knowledge transfer from those industries to pharmaceutical manufacturing processes would be a major obstacle because in continuous processing the batch size is not well defined and the system is not in equilibrium from the start of the process (Ervasti et al., 2015; Leuenberger, 2001).

A typical continuous process consists of separate feeding systems for API and excipients before the blending step. The blend is then processed into tablets via different modes: dry granulation (blend is roller compacted to form ribbons followed by powdering of ribbons before compression), wet granulation (blend is made into a dump mass by using binder solutions followed by drying and granules milling) and DC (blend is directly compacted into tablets) (Rogers et al., 2013). Figure 1.8 shows a Portable continuous miniature and modular (PCMM) system developed by a consortium of GEA, G-Con and Pfizer for continuous manufacturing of oral solid dosage forms.

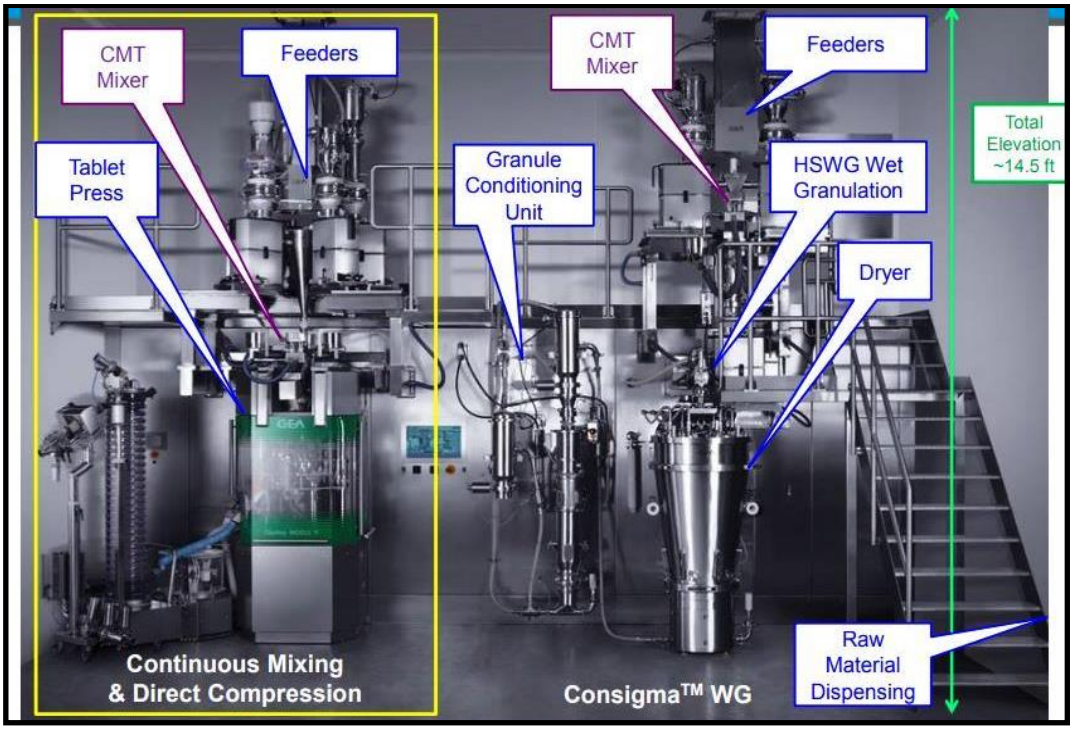


Figure 1.8 PCMM for continuous manufacturing of oral solid dosage forms (Blackwood, 2017)

Handling hydrophobic excipients like MgSt is one of the major challenges in continuous processing, as it could overcoat the powders during blending thereby compromising the tablet quality (Moreton, 2006; Pernenkil and Cooney, 2006). As a result there is a need to understand the lubricant blending behaviour in real time. Process Analytical Technology (PAT) is a system for analysing, designing and controlling manufacturing through timely measurements during the process of manufacturing dosage forms (Hinz, 2006; Järvinen et al., 2013; Vanarase et al., 2010). Pernenkil and Cooney summarised investigations on continuous blenders and feeders. In the publication a range of analytical techniques that can be used in monitoring the continuous blending systems were discussed and the need to design

an efficient feeding system with respect to cohesive powders was highlighted (Pernenkil and Cooney, 2006).

During continuous processing, process and material changes within the manufacturing system should be detected and resolved quickly before it affects the final quality of the finished product. To achieve this level of control during manufacturing, in depth material and process knowledge is essential. Therefore QbD principles are important prerequisite to ensure process control during continuous processing (Crowley and Crean, 2015). Current manufacturing models possess a fixed process were the output is variable. The objective of the continuous process is to transfer to a variable process mode to get a consistent output using QbD principles (Chen et al., 2011).

Currently, there are two approved commercial pharmaceutical products produced via continuous processes on the market. Vertex achieved FDA approval for a continuous process (based on GEA technology) in the manufacture of the cystic fibrosis drug Orkambi in July 2015. In early 2016, Johnson and Johnson in Puerto Rico got the FDA approval, for the first time a change in production method from batch to continuous manufacturing for the production of the protease inhibitor Prezista (Darunavir) used in the treatment of HIV-1 infection (Blackshields and Crean, 2018; Khinast, 2016). GSK built a $50 million continuous manufacturing plant in Singapore involving upstream technology (Palmer, 2015). Hovione entered in an agreement with Vertex to produce continuously in New Jersey as of 2017 (Khinast, 2016). Companies that provide equipment for continuous pharmaceutical drug product manufacturing include GEA, Glatt, Bohle, Continuus.

1.3.1 Continuous feeding

During continuous tablet manufacturing, feeding of raw materials and API into the downstream processing is the foremost important step. Any inconsistencies in powder feeding will be carried forward to the downstream processing resulting in drug products falling outside specification limits and batch failures. Ability to feed powders uninterruptedly, accurately and constantly is regarded as one of the initial critical process parameter in overall tablet manufacturing (Pernenkil and Cooney, 2006; Simonaho et al., 2016). Inconsistencies in feeding of API and other related excipients in a specific formulation at a desired rate will pass inconsistencies onto blending and granulation steps resulting in quality failure of the product (Engisch and Muzzio, 2015; Ervasti et al., 2015). Therefore, continuous manufacturing requires a high degree of process control via in-process testing and improved process understanding to ensure that, the drug products are produced in a controlled manner with reproducible critical quality attributes between batches. To gain an in-depth process understanding, it is essential to identify and understand the physicochemical properties of raw materials involved, which dictate the quality of the final product. During continuous processing, the feeding of powders is accomplished through loss-in-weight (LIW) feeders which control the feedrate gravimetrically (Hopkins, 2006).

Loss-in-weight feeder (LIW)

A LIW feeder consists of three different parts: a volumetric feeder, weighing platform and gravimetric controller (Figure 1.9). The volumetric feeder is located on the top of a weighing platform, which measures the mass of the material that is added into the volumetric feeder. As the material is dispensed through screws, the controller acquires the signal from weighing platform as a function of time. The instantaneous feed rate (-m_{feed}) is determined by equation 2.

$$-m_{feed} = \frac{\Delta w_{feeder}}{\Delta t} \qquad \text{Equation 2}$$

were, Δw_{feeder} is the weight measured by the platform and Δt is the time between two successive measurements.

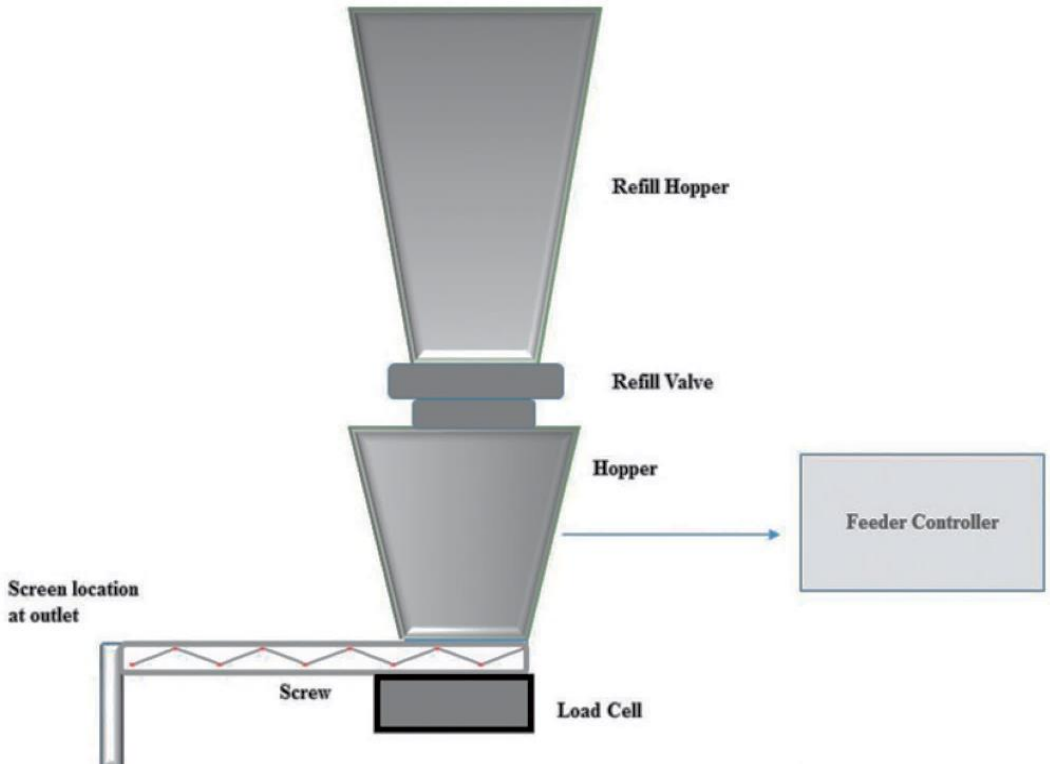


Figure 1.9 Components of loss-in-weight feeder (Blackshields and Crean, 2018).

The LIW feeder can be operated in two different modes: volumetric mode and gravimetric mode. Volumetric feeding is accomplished based on the volumetric parameters of the feeder. For example, a known motor speed is applied to a screw feeder, then theoretically a constant volume of material is discharged through feeder per unit time (Hopkins, 2006). Volumetric feeding consistency is limited due to material density variations, feed rate errors and inconsistencies in material flow (Singh et al., 2015). Whereas the gravimetric feeders have the ability to control the feed rate and optimize the flow variability based on the bulk density changes related to hopper emptying based on loss in weight principle (Engisch and Muzzio, 2012; Hopkins, 2006). The capacity of the feeder is determined by the volumetric study followed by gravimetric analysis to estimate the overall performance (Engisch and Muzzio, 2012).

LIW feeders can be equipped with range of tooling such as screws and screens. Different screws and screens are provided with the feeder to dispense the materials through LIW feeders. Different types of screws are available with different configurations (single or double and spiral or auger), and thread depths. Screens with different designs such as squared screens and slotted screens are also used to dispense cohesive materials. Optimal tooling conditions can be selected based on the powder flow properties (Figure 1.10).

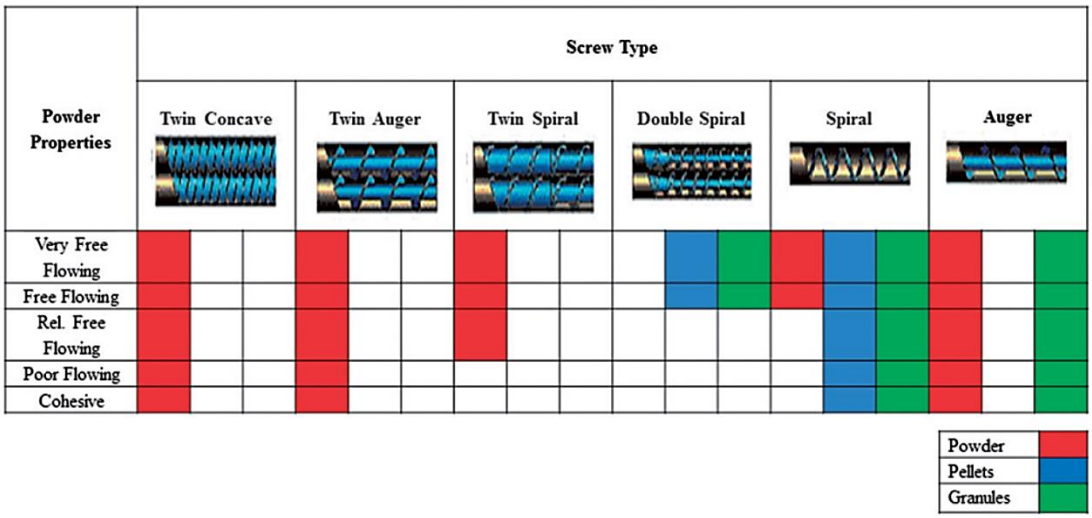


Figure 1.10 Guide to screw selection based on material flow properties (Blackshields and Crean, 2018)

Feeding of cohesive and low density materials such as MgSt is problematic during continuous manufacturing. Due to their high cohesive nature they tend to adhere to the equipment tooling (Engisch and Muzzio, 2015, 2014). The use of concave screws was found to be most suitable for these materials as these possess a 'self-cleaning' function. Cartwright et al. have addressed the importance of accurate powder feeding of low density and poor flowing API, for successful granulation performance in a twin screw extruder by comparing different types of loss in weight feeders (Cartwright et al., 2013). As MgSt is used in very low concentrations in tablet formulations, microfeeders such as K-TRON MT12 or KT20 feeders are used in its feeding. In this thesis we used a KTRON MT12 feeder (detailed in 2.2.5) to assess the feeding behaviour of different grades of MgSt and the effect of the feeding process on tablet blend compression and dissolution.

1.4 Broadband Acoustic Resonance Dissolution Spectroscopy (BARDS)

BARDS is a novel analytical technology developed by Dr. Dara Fitzpatrick in University College Cork, Ireland. BARDS technology is based on the change in acoustic phenomenon observed when material is added into a solvent under resonance (sound). Addition of solid material results in the introduction of gas/air and generation of gas/air bubbles in the solvent, changing the compressibility of the solvent system and reducing the velocity of resonance/sound in the solvent. As the material is wetted and dissolves, the gas/air released is eliminated from the surface of the solvent and the velocity of resonance/sound in the solvent increases. In the BARDS system acoustic resonances are mechanically provoked in the solvent using a stirrer bar and the change in acoustic frequency is monitored after addition of the material (Fitzpatrick et al., 2012a, 2012b).

1.4.1 Working principles of BARDS

The velocity (V) of sound in a medium whether air or liquid medium is determined by equation 3

$$V_{(sound)} = \sqrt{\frac{1}{K.\rho}} \qquad \text{Equation 3}$$

where ρ is mass density (kg m^{-3}) and *K* is compressibility (which is the inverse of bulk modulus) of the medium (Pa^{-1}). The generation of micro bubbles in a liquid decreases the density in a negligible way in comparison to a large increase in compressibility. The net effect is a significant reduction of the sound velocity in the liquid. The following relationship between the fractional bubble volume and the

sound velocity in water was derived by Frank S. Crawford, as given in equation 4 (Crawford, 1982).

$$\frac{v_w}{v} = \sqrt{1 + 1.49 \times 10^4 . f_a} \qquad \text{Equation 4}$$

where v_w and v are velocities of sound (m s^{-1}) in pure and bubble filled water respectively, and f_a is the fractional volume occupied by air bubbles. The factor 1.49×10^4 in the formula was calculated as shown in equation 5.

$$(v_w)^2 \, \rho_w \frac{1}{\gamma p} = 1.49 \times 10^4 \qquad \text{Equation 5}$$

where ρ_w is the density of water, γ is the ratio of specific heats for dry air and p is the atmospheric pressure. Equation 4 is based on the approximation presented originally by Wood *et al*. (Wood, 1955).

BARDS analysis of an induced acoustic excitation of the containing vessel is focused on the lowest variable frequency time course, i.e. fundamental resonance mode of the liquid. The fundamental resonance frequency is determined by the sound velocity in the liquid and the approximate but fixed height of the liquid level, which corresponds to one quarter of its wavelength (Crawford, 1982). The frequency response is described by equation 6.

$$freq = \frac{freq_w}{\sqrt{1+1.49\times10^4 f_a}} \qquad \text{Equation 6}$$

where $freq$ and $freq_w$ are the resonance frequencies of the bubbled filled water and fundamental resonance modes in pure water, respectively. A comprehensive outline of working principles and theory of BARDS was described by Fitzpatrick *et al*., (Fitzpatrick et al., 2012a).

1.4.2 Instrumentation and spectral information

Schematic representation of BARDS spectrometer is shown in Figure 1.11A. The BARDS spectrometer consists of a dissolution vessel equipped with a magnetic stirrer and a micro-phone set above the dissolution vessel, which receives and records the responses from the vessel. There is access at the front of the dissolution vessel and a tripper motor with a weighing boat on it to introduce the sample into the dissolution medium. The glass tumbler containing 25 mL of deionised water is placed on the stirrer plate. The stirrer motor underneath is positioned so as to allow the magnetic stirrer bar to gently tap the inner glass wall, which will act as the source of broadband acoustic excitation. This will induce various acoustic resonances in the glass, liquid and the air column above the liquid. The audio is sampled at a rate of 44.1 kHz. The resonances of the liquid vessel are recorded in a frequency band of 0-20 kHz. A frequency time course is generated as shown in Figure 1.11B.

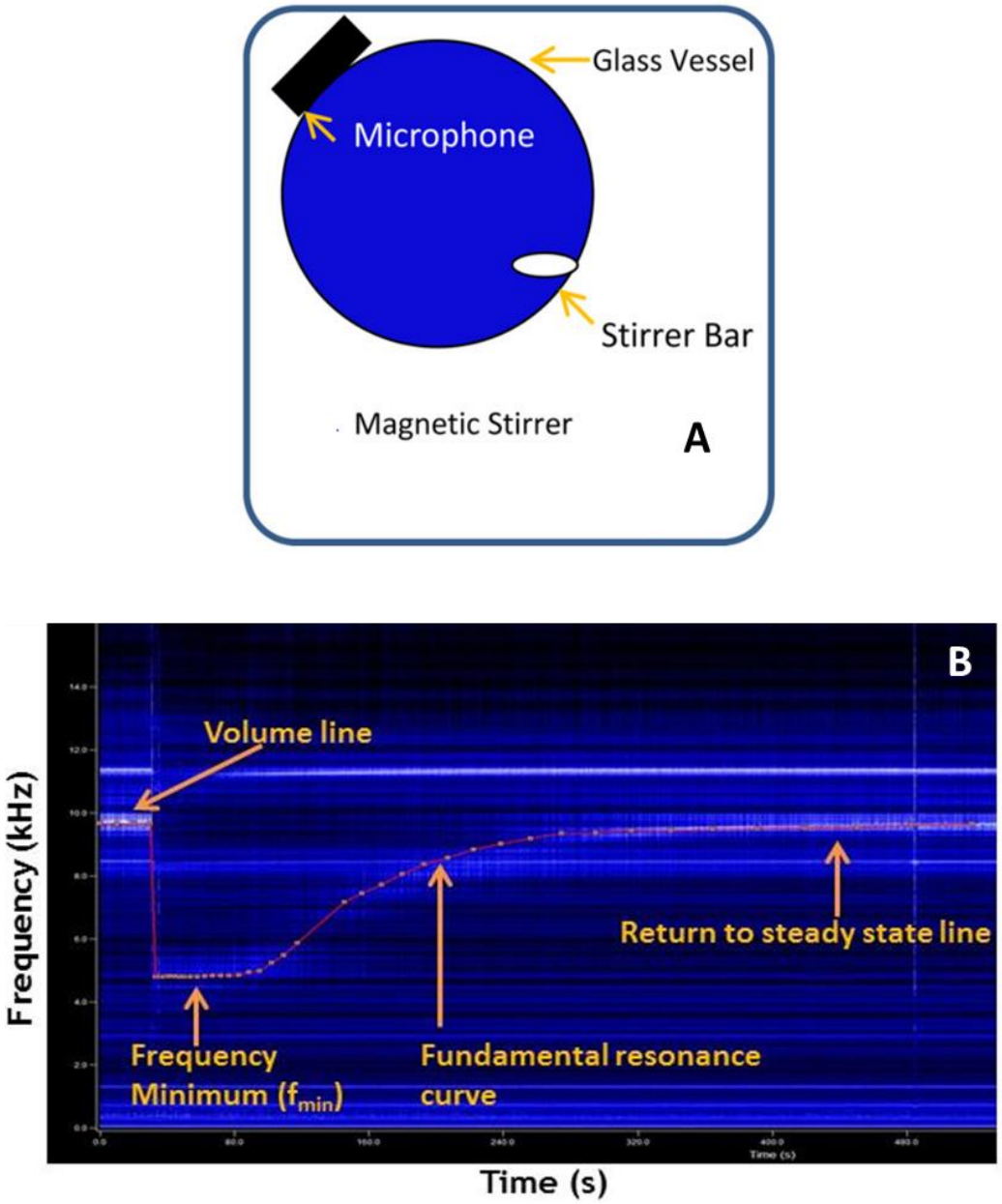


Figure 1.11 (A) Schematic diagram (top view) of the prototype BARDS spectrometer (Fitzpatrick et al., 2012). (B) Representative BARDS raw spectrum of 250 mg MCC in 25 mL water at room temperature.

Acoustic spectra are characterized by specific nomenclature. The first 30 seconds of the spectrum corresponds to steady state resonances of vessel 10 kHz as shown as volume line in Figure 1.11. When the sample is tipped into the deionized water at the 30 second time point, a decrease of resonance frequencies due to a change in the velocity of sound is observed. This resonance line is called the fundamental curve (Fitzpatrick et al., 2012a). The time taken to reach the frequency minimum (f_{min}) is designated as Δt. The time for which the response holds on f_{min} is known as the lag phase. The approximate time taken for the fundamental curve to progress from f_{min} to steady state is designated as ΔT. Lag phase and ΔT are used to identify the degree of wetting of the individual powders, blends and tablets (Evans-Hurson et al., 2016; Fitzpatrick et al., 2014; Peddapatla et al., 2018; Vos et al., 2016).

Fitzpatrick et al., successfully demonstrated the differences between various chemical compounds and commercially available pharmaceutical powder blend products using BARDS (Fitzpatrick et al., 2013, 2012b). Fitzpatrick el al., demonstrated the relationship between gas dissolution, gas oversaturation, outgassing of solutions and BARDS analytical parameters were evaluated for different chemical compounds (sodium chloride, potassium chloride and sodium phosphate) (Fitzpatrick et al., 2013). Another study by Fitzpatrick et al. showed that the BARDS was able to discriminate the distinctive acoustic signature profiles of the enteric coated core spheres of varying size distributions as they dissolved in acoustic media (Fitzpatrick et al., 2014). A study by Evans Hurson et al. showed that the dissolution rate of enteric coated drug spheres depends on pH of the BARDS dissolution media (Evans-Hurson et al., 2016). A recent study by Vos *et al.,* showed

the potential of BARDS to detect the transfer of water into milk protein concentrate (MPC) powder particles with different rehydration characteristics (Vos et al., 2016). Howick et al. recently used BARDS, as a complementary technique to confirm the results seen in USP dissolution studies of a novel ghrelin receptor agonist, FHI-2571 (Howick et al., 2018). BARDS was also used in non-titrimetric determination of acid-base reactions (Ahmed et al., 2018). A study by Alfarsi et al. showed BARDS as a rapid test to determine the enteric coating thickness and integrity of controlled release formulations (Alfarsi et al., 2018).

1.5 Aims and objectives

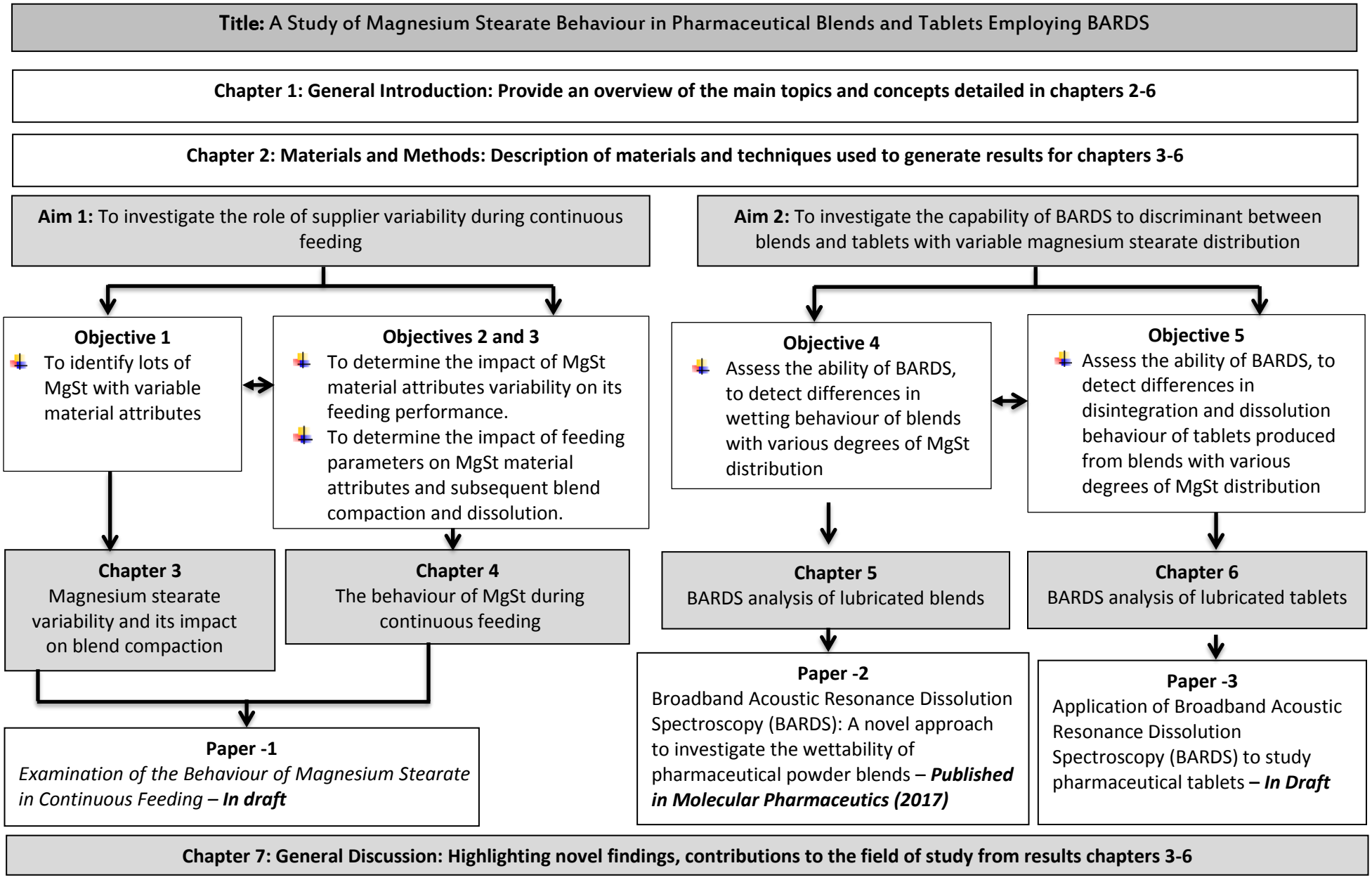
The main aims of this thesis are:

- To investigate the role of MgSt supplier variability during continuous feeding through a loss in weight feeder (LIW)
- To investigate the capability of BARDS to discriminate between blends and tablets with variable MgSt distribution.

To achieve these aims, the following objectives were established, which are further split into four different result chapters

- **Chapter 3**
  - To identify lots of MgSt with variable material attributes (MA).
- **Chapter 4**
  - To determine the impact of MgSt properties on its continuous feeding performance.
  - To determine the impact of feeding parameters on MgSt material attributes and subsequent behaviour during blend compaction and tablet dissolution.
- **Chapter 5**
  - To assess the ability of BARDS, to detect differences in wetting behaviour of blends with variable degrees of MgSt distribution
- **Chapter 6**
  - To assess the ability of BARDS, to detect differences in the behaviour of tablets produced from blends with various degrees of MgSt distribution compressed at different compression pressures.

SCHEMATIC REPRESENTATION OF THESIS



Chapter -2

Materials and Methods

2. Materials and Methods

2.1 Materials

The materials, suppliers and their application in this research are listed in Table 2.1.

Table 2.1 List of materials used in the study. N/A – Not available

Material	Grade	Supplier	Application	Batch number
Metoclopramide Hydrochloride	N/A	Kemprotec Ltd.	Active pharmaceutical ingredient	121119
Paracetamol	N/A	Mallinckrodt	Active pharmaceutical ingredient	6088905V078
MCC	Avicel PH200	FMC Biopolymer	Diluent/Binder	AC60044
MgSt	N/A	Alfa Aesar	Lubricant	10192245
MgSt	MF2V	Peter Greven	Lubricant	C527312
MgSt	MF2VBI	Peter Greven	Lubricant	C307526
MgSt	MF3V	Peter Greven	Lubricant	C526985
Tetramethylamonium hydroxide (25% in Methanol)	N/A	Sigma-Aldrich	HPLC Mobile phase	SHBC0380V
Acetonitrile	Gradient grade	Sigma-Aldrich	HPLC Mobile phase	STBH3004
Water	HPLC grade	Sigma-Aldrich	HPLC Mobile phase	BCBX4373
Glacial acetic acid	Analytical reagent grade	Fisher chemical	pH adjusting agent	1347021
Hydrochloric acid	N/A	Sigma	Dissolution media pH 1.2	N/A

2.2 Methods

2.2.1 Solid state structure analysis

2.2.1.1 Powder X-Ray Diffraction

Principle

When X-rays are diffracted through a sample, crystalline substances act as 3 dimensional diffraction gratings for X-rays with wavelengths similar to the spacing of planes in a crystal lattice. The interaction of the incident rays with sample produces a constructive interference (a diffracted ray) when conditions satisfy Bragg's Law (Ewald, 1962).

Purpose

PXRD was used to analyse the crystallinity of MgSt samples.

Analysis

PXRD patterns for all MgSt samples were obtained using a STOE STADI MP PXRD using a monochromated $K\alpha_1$ ((λ = 1.5406 Å) radiation. Samples were analysed in transmission mode, over 2 theta range 2 to 110 in steps of 0.50 at 1.7 second per step. Analysis was performed in triplicate for each sample.

2.2.1.2 Differential Scanning Calorimetry (DSC)

Principle

In DSC, the energy required to establish a zero-temperature difference between sample and reference material is measured as a function of temperature (Watson and O'Neill, 1962).

Purpose

DSC was performed on MgSt samples to characterise the endothermic transitions, melting behaviour and water present in the samples.

Calibration

Standard samples of sapphire and indium were used in the calibration of the DSC.

Sample preparation

MgSt samples of approximately 2 - 4mg weighed into T_0 aluminium pans and closed.

Analysis

DSC measurements were carried out using a DSC Q1000 (TA instrument). Sample pans were heated from -40^{o}C to 300^{o}C at 10^{o}C/min in a nitrogen atmosphere at a flow rate was 50 ml/min. Data analysis was performed using Universal Analysis 2000 software – V4.5A (TA Instrument). All measurements were performed in triplicate.

2.2.1.3 Thermogravimetric Analysis (TGA)

Principle

During TGA, the mass change of the sample is measured over time in a controlled temperature environment (Gabbott, 2008).

Purpose

TGA was performed on MgSt samples to characterise the type of hydrate and nature of water present in the samples.

Calibration

Calcium oxalate was used in TGA calibration. The resultant thermogram was

matched with the reference thermogram; (1) in the region of water of crystallisation loss at 150^{o}C, (2) carbon monoxide loss as a result of calcium oxalate decomposition at 400^{o}C and (3) further decomposition at 600^{o}C.

Analysis

TGA measurements were carried out using TGA Q500 (TA instrument) with samples of approximately 3 mg weighed into the platinum pan. Samples were heated from ambient temperature to 300^{o}C at a rate of 10^{o}C/min. Nitrogen flow rate was 60 ml/min through the furnace. Data analysis was performed using Universal Analysis 2000 software – V4.5A (TA Instrument). Measurements were performed in triplicate.

2.2.2 Particulate analysis

2.2.2.1 Scanning electron microscopy (SEM)

Principle

High energy beam of electrons are used in a raster scan pattern, which interacts with atoms at various depths within the sample that produces an image (Reimer, 2000).

Purpose

SEM was used to understand the morphology of MgSt samples.

Sample Preparation

Powder was sprinkled on to the carbon tape and excess loose particles were removed with pressurised air. Samples were coated with specific concentration of a

mixture containing gold and palladium (Au:Pd - 80:20) using a sputter coater (Q150T Turbo-Pumped Sputter Coater/Carbon Coater).

Analysis

A Jeol Scanning electron microscope (JSM) – 5510-Jeol Ltd. was used to image the particle morphology at an accelerating voltage of 5kV.

2.2.2.2 Particle Size Distribution (PSD)

Principle

Laser diffraction spectroscopy utilizes diffraction patterns of a laser beam passed through any object (e.g. fluidised powder), to measure the geometrical dimensions of the particles (Lieberman and Schwartz, 1989)**.**

Analysis

Dry powder laser diffraction analysis was performed using Mastersizer, 3000 (Malvern Instruments). Samples were subjected to pressure titrations (increase in air pressure dispersion from 1.5 bar to 3 bar) to study the degree of agglomeration and the ease of de-agglomeration. Samples were placed into the vibratory hopper and the feed rate of the sample was visually monitored until a constant mass flow was achieved. Measurements were taken at 1.5 bar, 2 bar and 3 bar dispersion pressure. The D_{10}, D_{50}, D_{90} are reported for all the samples, n=5.

2.2.2.3 Brunauer–Emmett–Teller-Specific Surface Area Analysis (BET)

Principle

Brunauer–Emmett–Teller theory elucidates the physical adsorption of gas molecules (nitrogen) on solid surface to study the specific surface area (m^2/g) of specific material (Brunauer et al., 1938; Gregg et al., 1967).

Purpose

BET was used to determine the surface area of MgSt samples.

Calibration

The total and external surface areas are measured by evaluating the amount of nitrogen adsorbed, at liquid nitrogen temperature, by carbon black at range of partial pressures of nitrogen. The test results of multipoint and single point surface area of carbon black was found to be 30±0.75 mg^2/g and 29±0.75 mg^2/g, which was in agreement with the calibration standards.

Sample preparation

Samples were degassed at 35^oC for 3 hrs using Micromeritics FlowPrep 060 (Sample Degas System) (Rao et al., 2005).

Analysis

During analysis, liquid nitrogen (N_2) was used to maintain isothermal conditions (-196^{oC}). The specific surface area for MgSt samples was determined from N_2 adsorption isotherms measured using a Micrometrics Gemini VI (Surface Area and Pore Size Analyser). Specific surface area (SSA) was calculated from BET theory (Brunauer et al., 1938). All samples were analysed in triplicates (n=3).

2.2.3 Bulk Properties Analysis

2.2.3.1 True density

Principle

Gas pycnometer work by the employing the Archimedes' principle of fluid (gas) displacement and the technique of gas expansion (Tamari, 2004). True density is measured by purging helium gas into the powder bed.

Purpose

Helium pycnometer was used to determine the true density of MgSt samples and tablet blends.

Analysis

True density of MgSt samples was measured using gas pycnometer (Accu Pyc II 1340 Gas Pycnometer) according to USP <699> Density of Solids. All samples were analysed in triplicates (n=3).

2.2.3.2 Bulk and tapped density

Bulk and tapped density was determined according to USP 35 <616> method using a 100 ml graduated cylinder. The tapped density was measured after tapping with the Tap Density Tester (Erweka). Carr's Index (CI) a measure of the powder bridge strength and stability, was calculated from equation 7. Hausner Ratio (H) a measure of the interparticulate friction, was determined from equation 8. Flowability is rated based on Carr's index and Hausner ratio (Shah et al., 2008).

$$CI = 100 \times \frac{V_B - V_T}{V_B}$$ Equation 7

$$H = \frac{\rho_T}{\rho_B}$$ Equation 8

V_B is bulk volume, V_T is tapped volume, ρ_T is tapped density and ρ_B is bulk density. All measurements were performed in triplicate.

2.2.3.3 Flowability – Brookfield Powder Flow Tester

Principle

The principal of operation of the powder flow tester (PFT) is based on an annular shear cell method, following Jenike silo design principles (Jenike, 1964). A compression lid is driven vertically downward into a powder sample contained in an annular shear cell. The powder sample has a defined volume and the weight of the sample is measured before the start of the test. A calibrated beam load cell is used to control the compaction stress applied to the powder. The annular shear cell is then rotated at a defined speed and the torque resistance of the powder in the shear cell moving against the powder in the stationary lid is measured by a calibrated reaction torque sensor. The geometries of the lid, shear cell, rotational speed of the cell, and the compressive loads applied to the powder all contribute to the calculations which determine the “flowability” of the powder.

Analysis

A Powder Flow Tester (PFT) from Brookfield (Brookfield Engineering Laboratories, Inc.) was used in the analysis of flowability of MgSt powders. The base of the trough was fitted with a perforated screen to prevent powder at the base of the cell from moving during shear. Curved blade was used to level the powder surface in the

trough for flow testing. The mass of the powder was recorded before testing, with the axial distance between the lid and the powder used to calculate changes in the volume of powder during testing. Shear cell kit was attached to the compression plate of the PFT for flow testing. Flow function was a measure of unconfined failure strength versus major principal consolidating stress. Flow index (ffc) for MgSt samples was calculated by inverse slope of flow function. Measurements were performed in triplicate.

2.2.3.4 Dynamic Moisture Sorption-Desorption

Principle

Dynamic vapour sorption (DVS) is a gravimetric technique that measures how quickly and how much of a solvent (water vapour) is absorbed by a sample and measures the change in mass of the sample (Engelund et al., 2010).

Purpose

A DVS Intrinsic (Surface Measurement Systems) was used to study the moisture sorption/desorption behaviour of MgSt samples

Calibration

The calibration was based on the principle that the vapour pressure above a saturated salt solution is constant due to its equilibrium with its surrounding environment at a particular temperature. Calibration was performed individually for the balance, relative humidity generation system and relative humidity probe using lithium chloride.

Analysis

MgSt powder samples were weighed onto a pan and placed in sample chamber. Moisture sorption-desorption studies were carried out using DVS instrument. Initially the sample was dried for 6 hours and equilibrated at 25^{o}C and 10% relative humidity (%RH). Sorption studies were carried out by exposing sample to stepwise humidity change from 0%-90%-0% RH for sorption and desorption cycles. The actual humidity values were controlled to ±0.5% the target and the mass change in samples was recorded every minute.

2.2.3.5 Contact angle

Principle

The contact angle was calculated by fitting the Young equation to the shape of the drop and calculating the slope of the tangent at the liquid–solid–vapour interface line (Pepin et al., 1999).

Calibration

Tensiometer was calibrated for the embedded camera using a metal sphere, to calculate the contact angles of the samples tested.

Sample preparation

For blends: Samples were mounted on double sided adhesive carbon tape adhered to a glass slide and excess powder was removed by tapping the slide.

For tablets: Contact angle measurements were recorded for unlubricated and lubricated tablets with similar porosities to study the wettability.

Analysis

The contact angle of powder samples was measured by the sessile drop method using a Theta-Optical Tensiometer (Biolin Scientific). A water drop of 10 µl volume was dispensed onto the sample surface and video images were captured at a rate of 1.7 frames per second (FPS). Measurements were performed in air under ambient conditions of 22 ± 2°C. All measurements reported are average ± standard deviation, where n = 9.

2.2.4 Formulation Preparation

2.2.4.1 Paracetamol Blends – evaluated in chapter - 4

MCC (50% w/w) and paracetamol (10% w/w) were passed through 450 µm sieve to remove agglomerates and pre-blended in a plastic bag for 1 minute to get an initial blend. To this blend 39.5% w/w MCC is added in a cubic blender with 3.5 litre volume and blended for 30 minutes at 30 rpm using a ERWEKA AR402 drive unit at angle of 90°. Different grades of MgSt were unfed and fed through K-TRON MT12 feeder (described in section 2.2.5) were added separately to the blend at a concentration of 0.5 % w/w and the components were further blended for a further 1 minute. A control formulation without MgSt was also prepared.

2.2.4.2 Metaclopromide HCl Blends – evaluated in chapter – 5

Formulation 1 (unlubricated) and Formulation 2 (lubricated) with a total blend size of 2 kg were blended in a stainless steel double cone blender (DKM) with a 11.9 liter volume operated with ERWEKA AR402 drive unit at angle of 90^0. The blender rotated for 30 minutes at 30 rpm with MCC (90% w/w) and metoclopramide

hydrochloride (10% w/w). MgSt (0.5% w/w) (Alfa Aesar) was added to the formulation 2 and blended for a further 1 minute at 30 rpm. Six blend samples (three samples from the top and three from the bottom of the blender) were collected using a sample thief from each blend and analysed using BARDS (as detailed in section 2.2.6.7).

2.2.5 Continuous Feeding

K-TRON MT12 feeder (Coperion K-TRON) is a loss in weight micro feeder with lower throughputs, which is mainly suitable to feed low amounts of powders. It was supplied with a range of different twin screw designs, for example coarse concave screws (CCS), coarse auger screws (CAS), fine concave screws (FCS), and fine auger screws (FAS). CCS have a self-cleaning function suitable for cohesive materials and the auger screws do not have this self-cleaning ability but have the advantage of higher feeding capacity (Blackshields and Crean, 2018; Engisch and Muzzio, 2014). The feeder was also supplied with different designs of screens, for example coarse square screen (CSqS), fine square screen (FSqS), coarse slotted screen (CSlS) and fine slotted screen (FSlS). In feeder set different screw designs can be paired with different screw designs. The function of the screen is to break up clumps of cohesive powders and can also be used to create back pressure to prevent very free flowing powders from flowing uncontrollably from the feeder (Blackshields and Crean, 2018; Engisch and Muzzio, 2014). An independent catch scale using the K-Sampler Test System was used to collect fed material which was placed directly below the outlet of the feeder to minimise vibrations and was shielded from

external draughts. The material was collected in a stainless steel tray. The feeder and balance was earthed to minimise the formation of electrostatics.

2.2.5.1 Continuous feeding – MgSt

Feeding trials were carried out on a K-Tron MT12 LIW twin screw microfeeder (Coperion K-TRON). CCS and FCS were selected for this study based on the results on a study by Engisch and Muzzio et al., (Engisch and Muzzio, 2015, 2014). For each powder, screw and discharge screen combination, the feed factor (FF) was determined through calibration. The FF is the gravimetric speed equivalent for 100% screw speed with a specific screw and screen setting. It gives an indication of the maximum feed rates that can be achieved for a powder with specific equipment set up. In each case the hopper was filled to approx. 500 g fill weight. Data was recorded every second for 30 minutes with K-Sampler software (COPERION K-TRON).

Establishing feeding conditions for MgSt

The feeding study was conducted in 2 parts. Initially a trial was performed using MgSt from Alfa Aesar as outlined in Table 2.2. The optimum combination of screw and screens (with lowest feed rate %RSD) from the results of this initial study was used in a second experimental trial to compare the feeding behaviour of three other different grades of MgSt.

Table 2.2 Feeding configurations for Alfa Aesar trial.

Exp. No.	Screw Type	Screen Type	Set Point (kg/hr)
1	FCS	FSqS	0.25
2	FCS	FSqS	0.15
3	FCS	CSqS	0.25
4	FCS	CSqS	0.15
5	FCS	No Screen	0.25
6	FCS	No Screen	0.15
7	CCS	FSqS	0.25
8	CCS	FSqS	0.15
9	CCS	CSqS	0.25
10	CCS	CSqS	0.15
11	CCS	No Screen	0.25
12	CCS	No Screen	0.15

2.2.5.2 Continuous feeding – Metoclopramide tablet formulations

This section, part of the feeding studies involved feeding metoclopramide HCl blends. Formulation 1 and formulation 2 (section 2.2.4.2) were each fed with a K-TRON MT-12 twin screw microfeeder to achieve different levels of MgSt distribution within blends in a controlled manner. The feeder set up used in this study comprised of a FCS and FSqS, with the objective of minimizing MgSt build-up on screws. The FF is the theoretical 100% feed rate that can be achieved with a given set of tooling and material and was determined through equipment calibration. The feed rates set points were set at 0.2238 kg/hr, 0.5594 kg/hr and

1.0069 kg/hr for 20%, 50% and 90% of the feed factor for formulation 1. The same feed rates were used for formulation 2 for direct comparison. The hopper was filled to the same level for all feeding runs. The feeder performance was evaluated using an independent catch scale using the K-Sampler Test System. Blend samples were collected and analyzed using BARDS (section 2.2.6.7).

2.2.6 Blend Compaction

2.2.6.1 Tablet compaction

All tablet blend formulations were compressed by DC at target compression forces of 1.5 to 11 kN, which corresponded to compression pressures of 30 to 234 MPa using 8 mm flat faced round punches on a Riva Piccola tablet press (Riva).

2.2.6.2 Tablets Characterisation

Hardness, thickness, diameter and weight of tablets were determined by using SMARTTEST 50 Autotester (Pharmatron). The tablet tensile strength σ (MPa) was calculated using equation 9

$$\sigma = \frac{2H}{\pi t D} \qquad \text{Equation 9}$$

where H is hardness (N), t is tablet overall thickness (mm) and D is tablet diameter (mm). Tablets with and without lubricant were compressed at different compression pressures were analysed using BARDS. Porosity of the tablets was calculated using equation 10

$$Porosity = \frac{Volume\ of\ tablet - Volume\ solid\ fraction\ of\ tablet}{Volume\ of\ tablet} \times 100 \qquad \text{Equation 10}$$

Tablets produced from the unlubricated and lubricated blends are referred to as unlubricated and lubricated tablets respectively.

2.2.6.3 Heckel Analysis

Compressibility of the unlubricated and lubricated blends was examined by fitting the experimental data with Heckel equation 11 (Heckel, 1961) for metoclopramide tablets studied in Chapter 6

$$\ln[1/1-D] = KP + A \qquad \text{Equation 11}$$

where *D* is the relative density of the tablets (g/cm^3), *K* is the slope of straight line in Heckel plot, *P* is the compression pressure (MPa), *A* is the constant. The yield pressure (P_y) was calculated by taking the reciprocal of the Heckel slope *K*.

2.2.6.4 Disintegration Test

The *in vitro* disintegration time was determined for each tablet using a standardised pharmacopoeial disintegration test apparatus, in accordance with USP30 <701> (Hirschfelder, 1930). Disintegration media, water was maintained at 37^{o}C ± 2 ^{o}C. Each tablet was placed in a tube of the apparatus. The tablet was observed for every 1, 3 and 5 minutes until no substantial mass remained in the apparatus. Measurements were performed in triplicate.

2.2.6.5 Dissolution Test

Tablets produced from Paracetamol Blends

The dissolution tests of paracetamol tablets formulated using different MgSt grades (unfed and fed through K-Tron MT12 feeder) was performed using USP paddle apparatus Distek 2100B dissolution tester, at a stirring speed of 50 rpm in deionised

water. Tablets with tensile strength of 2 MPa were chosen across all batches. The dissolution apparatus was maintained at 37°C throughout the experiment. Samples in the amount of 3.5 mL were withdrawn at time points between 1 to 120 min and 24 hours. Dissolution samples were collected for analysis and replaced with an equal volume of fresh dissolution media to maintain a constant total volume. These samples were filtered using a 0.45 µm filter and analysed using UV spectrophotometer at 243 nm. All dissolution tests were performed in triplicate.

Tablets produced from Metoclopramide hydrochloride blends

The dissolution test of metoclopramide hydrochloride tablets was performed using USP paddle apparatus, Distek 2100B dissolution tester, at a stirring speed of 50 rpm in 0.1 N HCl (pH 1.2). Tablets with tensile strength of 2 MPa were chosen across all batches. The dissolution apparatus was maintained at 37°C throughout the experiment. Samples in the amount of 3.5 mL were withdrawn at time points between 1 and 60 min. Dissolution samples were collected for analysis and replaced with an equal volume of fresh dissolution media to maintain a constant total volume. These samples were filtered using a 0.45 µm filter and analysed using HPLC.

Mobile phase for HPLC constituted of 30 parts acetonitrile, 70 parts water and 0.2 part of Tetramethylammoonium hydroxide (TMA) hydroxide. pH of the mobile phase is adjusted to 6.5 with acetic acid. A 10 µl sample is injected through Gemini 5µ C_{18} column (250 x 4.60 mm 5 micron) with a mobile phase pumped at a flow rate of 1 ml/min and the samples were analysed at 215 nm using UV detector. All dissolution tests were performed in triplicate.

2.2.6.6 Wetting time of compacted blends

The wetting time of the blends compacted to a porosity of 23.6% ± 1.3 was measured using the following procedure (Pabari and Ramtoola, 2012; Rajpurohit et al., 2011). Two Whatman filter papers were placed in a petri dish of 10 cm in diameter. A small volume (8 mL) of red amaranth solution was added into the petri dish. A tablet was placed carefully on the surface of the filter paper. The time required for the red solution to reach the upper surface of the tablet was noted as the wetting time. All the measurements were made in triplicate and the average value and standard deviation was determined.

2.2.6.7 BARDS

Principle

BARDS is developed on the basis of the change in acoustic phenomena observed when a solute/tablet is added into a solvent. Addition of a solute results in the introduction of air (gas) into the solvent, which changes the compressibility of the liquid system and reduces the velocity of the sound (resonance) therein. These changes in the compressibility of the liquid are recorded by the BARDS instrument as a frequency-time profile (Fitzpatrick et al., 2012a, 2012b). The BARDS spectrometer records the initial steady state resonances of the vessel containing solvent, deionised water, as a reference for 30 seconds once the stirrer is set in motion. Following addition of the sample (blend or tablet) the pitch of the resonance modes in the deionised water decreased giving rise to a frequency minimum *(f_{min})* by effecting the change in the velocity of the sound, before

gradually returning to steady state over several minutes. Details related to BARDS instrument were provided in section 1.4.2.

Purpose

BARDS was used to study the behaviour of excipients, metoclopramide and metoclopramide tablet blends and tablets in an aqueous environment.

Analysis

The target weight of blend samples and tablets analysed was 250 mg. Samples were added to a glass vial with 25 mL DI water at ambient temperature. Spectra were recorded for a total of 800-1200 seconds which is dictated by the rate of return of the fundamental frequency to steady state. All experiments were performed in duplicate for blends and tablets. An average reading and range of values is presented. The time courses of the observed acoustic profiles were measured under standardized conditions of constant volume, concentration, temperature and stirring rate.

2.2.7 Statistical Analysis

Results are presented as average ± standard deviation (SD) unless otherwise stated. Results were compared using ANOVA (Graphpad, Prism). Drug dissolution profiles were tested by comparing the percentage of drug dissolved at each time point using one-way ANOVA followed by Tukey test. Feeding results are presented as average ± %RSD (%RSD = SD/AVGx100).

Chapter 3

Magnesium stearate variability and its impact on blend compaction

3. Magnesium stearate variability and its impact on blend compaction

3.1 Introduction

Despite lubricants being added in very low concentrations (0.25% to 1% w/w) in pharmaceutical blends they have the ability to influence the properties of blends and subsequent tablets. These effects are mainly due to surface interactions between materials or between material and processing equipment (Lee, 2007). A study by Rao et al., and Wada et al., showed that the physical properties and lubrication efficiency MgSt is variable from manufacturer to manufacturer and from lot to lot (Rao et al., 2005; Wada and Matsubara, 1994). Solid state properties such as PSD, crystal habit, agglomeration, density, porosity and surface area of MgSt can affect the lubrication efficiency of MgSt (Dave et al., 2015; Haware et al., 2014; Rao et al., 2005). Fatty acid composition between different grades of MgSt was not shown to affect lubrication properties, whereas MgSt batches with smaller particle size and larger specific surface area showed better lubricity in a study performed by Leinonen et al. (Leinonen et al., 1992). Negative effects on the physical properties of microcrystalline cellulose tablets were observed in a study by Dansereau and Peck when the MgSt grade used had a smaller particle size and larger surface area (Dansereau and Peck, 1987).

3.2 Aims and objectives

As outlined in the introduction to this chapter, the variability of MgSt within batches and between suppliers is widely reported. The aim of this chapter is focused on characterising the selected lots of commercial MgSt samples investigated in this thesis. The main aim of this chapter was to establish the variability between 4 commercial grades of MgSt from two different suppliers (Table 3.1). This information was used to better understand the impact of MgSt variability on continuous feeding in Chapter – 4.

Table 3.1 Grades and suppliers of magnesium stearate

Sample	Brand Name/Grade	Manufacturer	Batch Number
1	Magnesium Stearate	Alfa Aesar	10192245
2	Ligamed MF-2-V	Peter Greven	C527312
3	Ligamed MF-2V-BI	Peter Greven	C307526
4	Ligamed MF-3V	Peter Greven	C526985

The main objectives of this chapter are:

- To determine differences in material attributes (MAs) of each grade of MgSt in terms of their solid-state behaviour (PXRD and thermal analysis), particulate properties (morphology, particle size and surface area) and bulk behaviour (flowability and moisture sorption).
- To determine the effect of MgSt variability on tablet properties such as compactibility, tabletability, compressibility and dissolution.

3.3 Results

3.3.1 Solid state behaviour

3.3.1.1 Powder X-Ray Diffraction (PXRD)

The PXRD patterns of MgSt samples were studied to determine differences in crystal structure, Figure 3.1. PXRD pattern of all MgSt samples exhibited crystalline peaks indicating samples were crystalline in nature, as previously reported (Haware et al., 2014; Sharpe et al., 1997).

Compared to other samples, Alfa Aesar exhibited broad diffuse peaks in the regions 18^{o} - 26^{o} 2θ, Figure 3.1A. Samples MF-2-V, MF-2-V-BI and MF-3-V exhibited sharper and better resolved peaks (Figure 3.1B-D). PXRD analysis indicated that samples from Peter Greven were more crystalline in nature and that the Alfa Aesar sample was less crystalline nature.

3.3.1.2 Thermal Analysis (DSC and TGA)

DSC and TGA analysis was performed on the MgSt samples to characterise the degree of hydration, the nature of water present and melting temperatures of the samples. As discussed in chapter 1, previous studies reported that the nature of hydration state influences the lubrication efficiency and that dihydrates of MgSt were reported to be more efficient lubricants (Miller et al., 1985; Rajala and Laine, 1995; Rao et al., 2005). Thermal analysis showed several endothermic events and differences thermograms between the samples (Figure 3.2).

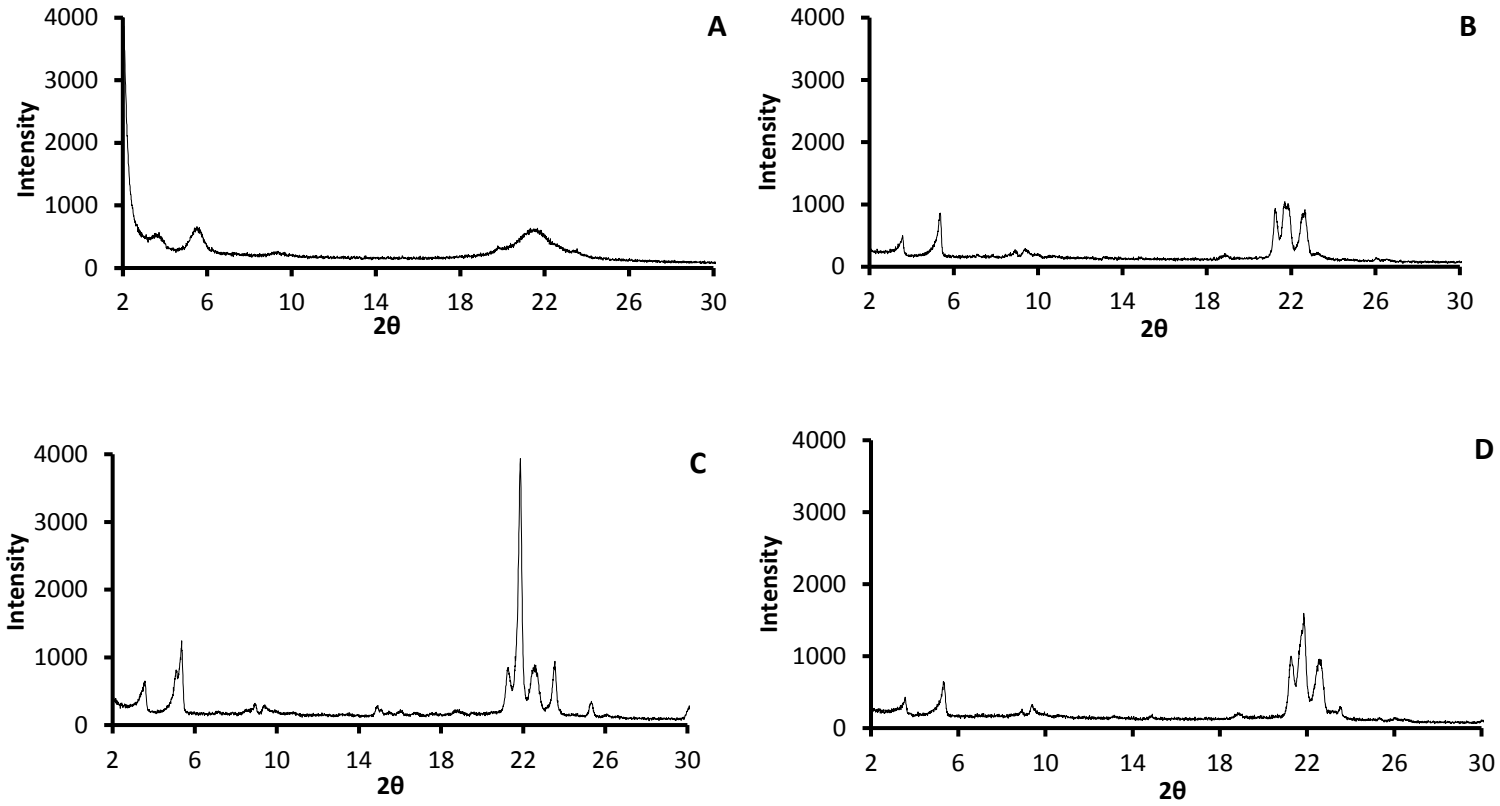


Figure 3.1 PXRD diffractograms of magnesium stearate samples. (A) Alfa Aesar (B) Ligamed MF-2-V (C) Ligamed MF-2-V-BI (D) Ligamed MF-3-V

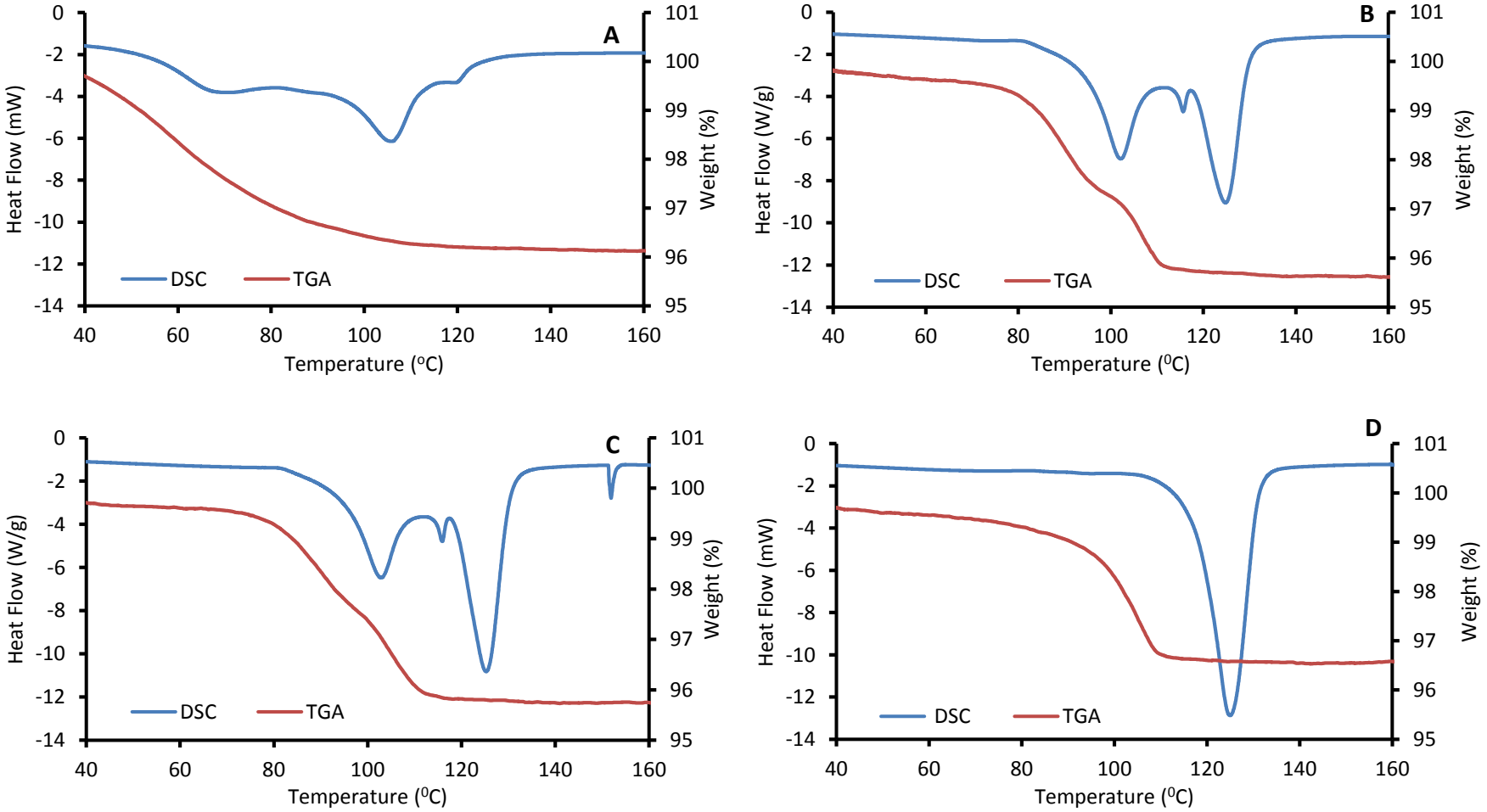


Figure 3.2 DSC and TGA thermograms of magnesium stearate samples. (A) Alfa Aesar (B) Ligamed MF-2-V (C) Ligamed MF-2-V-BI (D) Ligamed MF-3-V

Different endothermic events were observed in DSC thermograms and their respective temperature ranges are shown in Table 3.2. These thermal events were determined by studying the corresponding TGA and with reference to the earlier literature reports.

Table 3.2 Temperature ranges for endothermic events detected during DSC analysis of MgSt samples. The table also lists thermal process associated with the endotherms and supporting references.

Sample	Temperature	Thermal process	References
Alfa Aesar	67^0C – 76^0C	Water desorption	(Haware et al., 2014; Sharpe et al., 1997)
	84^0C – 91^0C	Dehydration	(Sharpe et al., 1997)
	104^0C	Melting	(Rao et al., 2005)
Ligamed MF-2-V	101^0C	Dehydration	(Haware et al., 2014)
	115^0C	Dehydration	(Sharpe et al., 1997)
	125^0C	Melting	(Rao et al., 2005)
Ligamed MF-2-V-BI	101^0C	Dehydration	(Haware et al., 2014)
	115^0C	Dehydration	(Sharpe et al., 1997)
	125^0C	Melting	(Sharpe et al., 1997)
Ligamed MF-3-V	124^0C	Dehydration and melting	(Miller et al., 1985)

The Alfa Aesar sample did not demonstrate any sharp thermal events which is indicative of loosely bound water and lower crystallinity (Rao et al., 2005). The first endotherm for Alfa Aesar sample was observed between 67^oC and 76^oC, which is broad and corresponds to water desorption. A second endotherm was observed between 84^oC – 91^oC, which corresponds to presence of water in a different thermodynamic state, because water loss was observed in more than one step (Rao

et al., 2005; Sharpe et al., 1997). These endotherms were accompanied by weight loss of 3.8% in TGA thermogram (Figure 3.2A). Alfa Aesar showed a melting endotherm at 104^{o}C.

Both samples MF-2-V and MF-2-V-BI exhibited sharp endothermic events at 101^{o}C and 115^{o}C, indicating loss of water in two steps. This was accompanied with a weight loss of 4.26% and 4.04%. Both samples showed a third endotherm at 125^{0}C, which corresponds to melting (Figure 3.2B and C).

The DSC thermogram of sample MF-3-V consists of a single endotherm at 124^{0}C (Figure 3.2D). Since the TGA thermogram shows a weight loss prior to this transition, it appears to indicate merging of dehydration and melting events (Rao et al., 2005; Sharpe et al., 1997). A weight loss of approximately 2% between 85^{0}C and 110^{0}C may be due to presence of hydrated or free water (Sharpe et al., 1997).

All samples showed a moisture loss between 3.30% and 4.26%, which is slightly below the theoretical 1.5 water molecules per mole of MgSt (4.36%) that Wada and Matsubara determined for different combinations of commercial MgSts (Wada and Matsubara, 1994). Enthalpies of dehydration and melting, and moisture content of four samples are shown in Table 3.3.

Table 3.3 Enthalpies of dehydration, melting, and moisture content of magnesium stearate samples. ND, not determined.

Sample	Moisture content (%)	Enthalpy of dehydration ΔH_d (J/g)	Enthalpy of melting ΔH_m (J/g)
Alfa Aesar	3.70±0.07	17.55±1.43	30.23±3.93
Ligamed MF-2-V	4.26±0.06	66.70±9.48	71.60±4.47
Ligamed MF-2-V-BI	4.04±0.06	50.90±3.30	82.82±2.59
Ligamed MF-3-V	3.30±0.04	ND	188.3±4.73

Enthalpy of dehydration of Alfa Aesar was lower (17.55±1.43 J/g) compared to Ligamed samples, indicating strongly bound water within Ligamed samples. Higher enthalpy of melting was observed in Ligamed samples, compared to Alfa Aesar (Table 3.3). Higher enthalpy of melting of melting indicates the greater molecular order or higher crystallinity in Ligamed samples (Haware et al., 2014).

3.3.2 Particulate properties

3.3.2.1 Particle morphology (scanning electron microscopy)

SEM was carried out to identify morphological differences between samples. When viewed under SEM, particles of the Alfa Aesar sample appeared to be plate and needle shaped. All the Ligamed samples are also visualised as plate and needle shaped, but organised as a deck of cards with micro agglomerates (Figure 3.3).

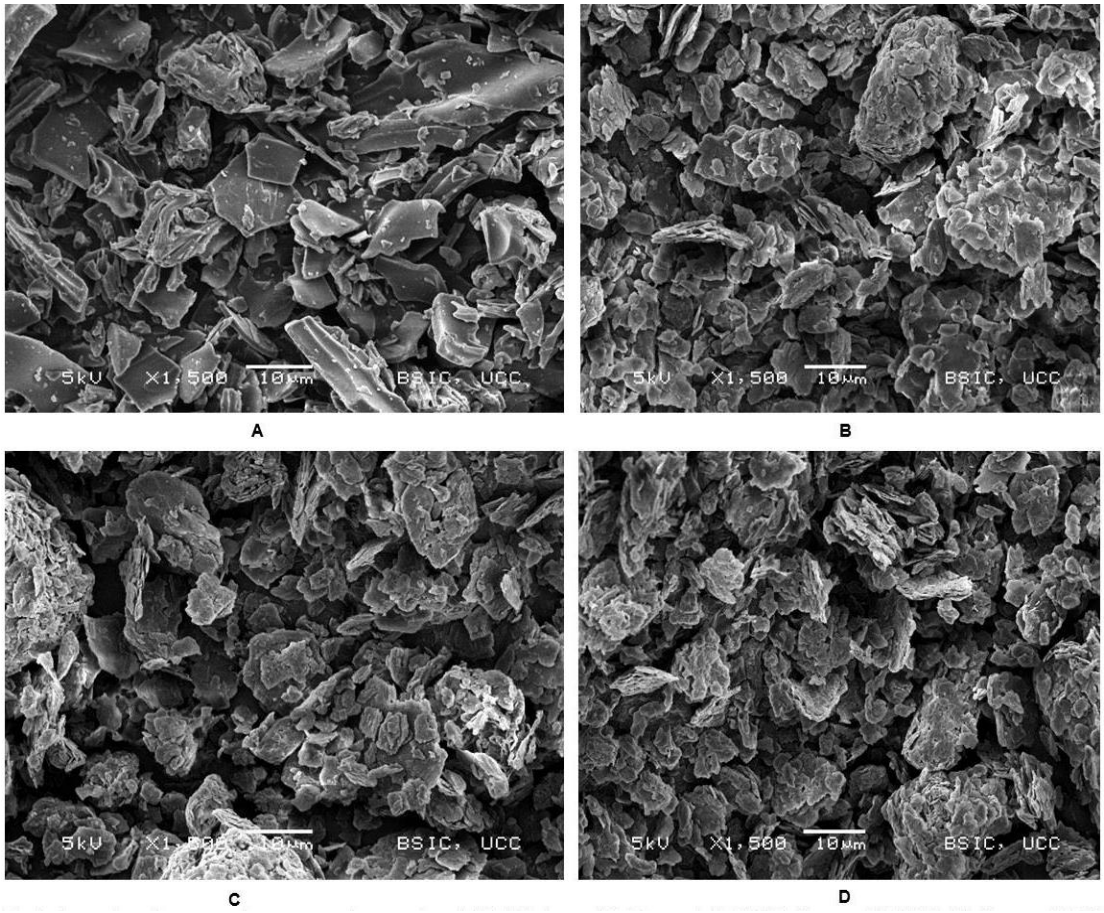


Figure 3.3 Scanning electron microscopy micrographs of MgSt samples**.** (A) Alfa Aesar (B) Ligamed MF2V (C) Ligamed MF2VBI (D) Ligamed MF3V

3.3.2.2 Surface area analysis and Particle size distribution analysis

Surface area and particle size distribution of MgSt has been shown to impact its lubrication efficiency (Kato et al., 2005; Li and Wu, 2014). Lower particle sizes of MgSt result in more lubrication efficiency due to more surface area and providing more surface coverage of the bulk powder. The determined specific surface area of samples is shown in Table 3.4. Ligamed MF-3-V had the largest specific surface area in comparison with other Ligamed samples. In comparison with Ligamed samples, the Alfa Aesar sample had a smaller surface area.

Table 3.4 BET surface area of MgSt samples. Average value shown n=3, ± indicates standard deviation

Sample No.	Grade	Specific surface area (m^2/g)
1	Alfa Aesar	3.08 ± 0.09
2	Ligamed MF-2-V	10.59 ± 0.12
3	Ligamed MF-2-VBI	10.14 ± 0.14
4	Ligamed MF-3-V	15.49 ± 0.12

According to Kato et al. tablet properties and tableting characteristics become more influenced by the effects of MgSt concentration and mixing time when the D50 of MgSt is 10 µm or less, particularly 5 µm or less (Kato et al., 2005). Initially the particle size analysis of MgSt samples was carried out at an air pressure of 1.5 bar, to determine the differences between samples (Figure 3.4). At 1.5 bar dispersive pressure, Ligamed MF-2-V and Ligamed MF-2-V-BI showed similar D10 of 3 µm. D10 of Alfa Aesar and Ligamed MF-3-V was found to be approx. 2.4 µm. The D50 and D90 of all of the samples were significantly different ($p < 0.0001$) with exception of samples Ligamed MF-2-V and MF-3-V (Figure 3.4). Alfa Aesar which had the smallest surface area, showed a D50 and D90 less than that of Ligamed MF-2-V-BI, which had a larger surface area.

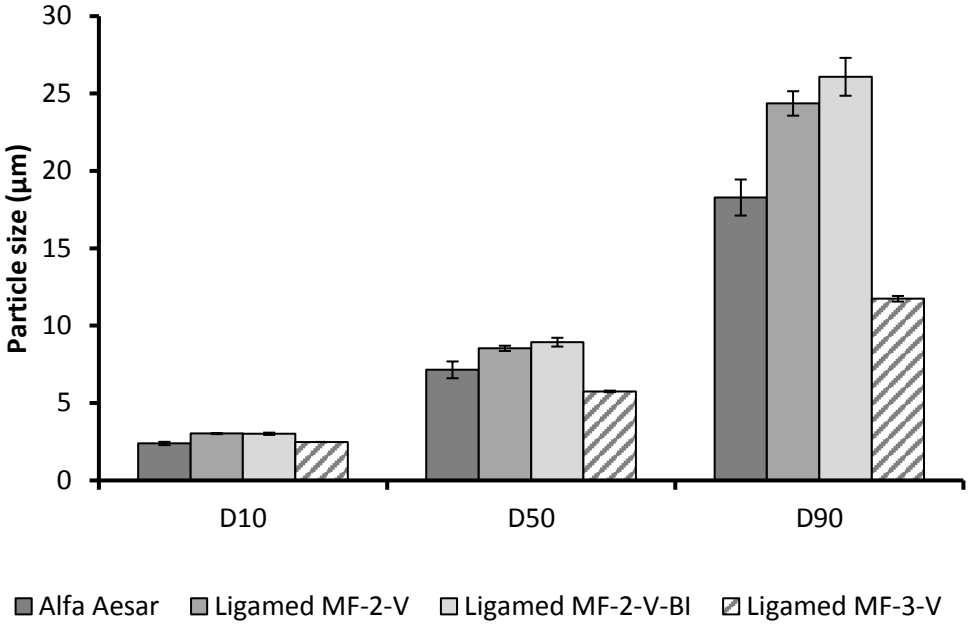


Figure 3.4 Particle size analysis of magnesium stearate samples by dry powder laser diffraction. Average values shown n=5, Y error bars indicates standard deviation.

As shown in SEM, all the MgSt samples existed in agglomerate forms. Therefore, particle size analysis of MgSt samples was further investigated under different air dispersion pressures (2 bar and 3 bar) to study the ease of de-agglomeration. The percentage reduction in particle size is shown in Table 3.5. From Figure 3.5A and B, it is evident that there is a reduction in particle size (D10 and D50) for the samples with increase in air dispersion pressure indicating that the samples were composed of agglomerates, with the exception of the Ligamed MF-2-V-BI sample at 2 bar dispersive pressure.

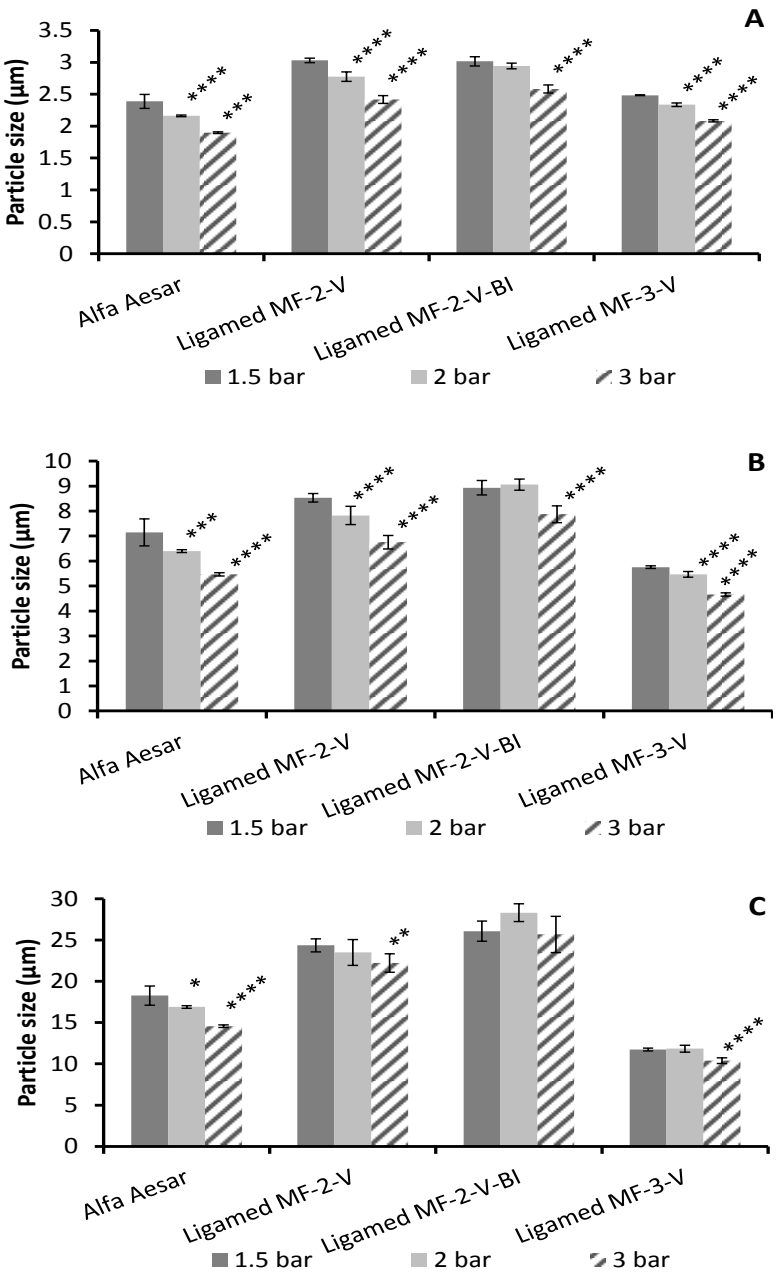


Figure 3.5 Particle size analysis of magnesium stearate by pressure titration. (a) D10, (b) D50 and (c) D90.

Where * represents $p \leq 0.05$, ** represents $p \leq 0.01$, *** represents $p \leq 0.001$, **** represents $p \leq 0.0001$.

Table 3.5 Particle size and percentage reduction in particle size (relative particle size measured a 1.5 bar titration pressure) for MgSt samples analysed at titration pressures of 1.5 bar, 2 bar and 3 bar. N=5. Average values ± standard deviation. NA indicates not applicable and NC indicates no change.

Particle size	Air Pressure (Bar)	Alfa Aesar		Ligamed MF-2-V		Ligamed MF-2-V-BI		Ligamed MF-3-V	
		Particle size (µm)	% reduction	Particle size (µm)	% reduction	Particle size (µm)	% reduction	Particle size (µm)	% reduction
D10	1.5	2.38±0.10	NA	3.03±0.03	NA	3.01±0.07	NA	2.48±0.00	NA
	2	2.16±0.01	9.46	2.77±0.07	8.44	2.94±0.04	2.45	2.33±0.02	5.96
	3	1.89±0.01	20.52	2.41±0.06	20.25	2.58±0.06	14.39	2.08±0.01	16.18
D50	1.5	7.14±0.54	NA	8.53±0.17	NA	8.93±0.28	NA	5.75±0.05	NA
	2	6.39±0.05	10.50	7.82±0.36	8.34	9.05±0.22	NC	5.46±0.11	5.01
	3	5.46±0.06	23.48	6.75±0.27	20.86	7.87±0.33	11.89	4.66±0.06	19.01
D90	1.5	18.28±1.16	NA	24.36±0.78	NA	26.08±1.22	NA	11.74±0.18	NA
	2	16.90±0.15	7.55	23.50±1.56	3.53	28.32±1.06	NC	11.84±0.41	NC
	3	14.56±0.15	20.35	22.22±1.11	8.78	25.68±2.18	1.53	10.37±0.34	11.64

Especially in the case of Alfa Aesar, where it is quite evident the breaking up of these agglomerates took place and approximately 23% reduction in D50 was observed under the increased pressure Figure 3.5B. A significant reduction of 20% in D90 of Alfa Aesar was noticed as the dispersive air pressure increased to 3 bar. D90 of Ligamed MF-2-V and Ligamed MF-3-V showed a significant reduction of approximately 8% and 11% only at higher dispersive pressure of 3 bar. D90 Ligamed MF-2-V-BI did not show any significant reduction in particle size at different titration pressures Figure 3.5C. The order of degree of de-agglomeration with respect to MgSt samples was, Alfa Aesar > Ligamed MF-2-V > Ligamed MF-3-V > Ligamed MF-2-V-BI.

3.3.3 Bulk behaviour

3.3.3.1 Flowability

The bulk density and true density of each MgSt sample are displayed in Figure 3.6. MgSt samples differed in bulk densities ($p \leq 0.005$). The Alfa Aesar sample showed largest and MF-3-V lowest bulk densities. All samples showed similar true density of approximately 1.1 g/cm^3.

Table 3.6 Bulk density, Tapped density and True density of MgSt samples. Average values shown n=3, ± indicates standard deviation

Sample	Bulk Density (g/cm^3)	Tapped Density (g/cm^3)	True density (g/cm^3)
Alfa Aesar	0.21±0.002	0.38±0.00	1.081±0.004
Ligamed MF-2-V	0.17±0.004	0.28±0.01	1.12±0.001
Ligamed MF-2-V-BI	0.19±0.007	0.30±0.00	1.12±0.005
Ligamed MF-3-V	0.14±0.003	0.21±0.01	1.13±0.019

Hausner ratio and Carr's compressibility index, flow function slope and flow index are displayed in Table 3.7

Table 3.7 Carr's Index, Hausner Ratio, Flow properties of MgSt samples. Average values shown n=3, ± indicates standard deviation

Sample	Carr's Index	Hausner Ratio	Flow function slope	Flow Index (ff_c)
Alfa Aesar	43.71±1.37	1.78±0.04	0.37	2.70
Ligamed MF-2-V	38.72±0.86	1.63±0.02	0.44	2.27
Ligamed MF-2-V-BI	36.41±2.18	1.57±0.05	0.48	2.12
Ligamed MF-3-V	30.30±0.87	1.43±0.02	0.47	2.08

Hausner ratio and Carr's compressibility index differed between the samples, except for Ligamed MF-2-V and Ligamed MF-2-V-BI samples. MgSt samples are cohesive in nature and poor flowing with Carr's index (> 23) and Hausner ratio (>1.25).

Figure 3.6 shows the Brookfield's powder flow analysis of MgSt samples. It represents the strength developed within the samples when consolidated and the nature of powder flow is described as its flow function (measure of unconfined failure strength versus major principal consolidating stress). Flow index (ff_c) for MgSt samples was calculated by inverse slope of flow function for first two points as shown in Figure 3.6. It can be differentiated into five categories, from non-flowing to free flowing as shown in Figure 3.6. The slope of flow function was calculated from first two points in Figure 3.6 because at unconfined strength of 1kPa, all the MgSt samples started to show easy flowing behaviour. This was due to sliding of the vane lid over outer catch tray due to the lubricant effect of MgSt samples at increased unconfined strength.

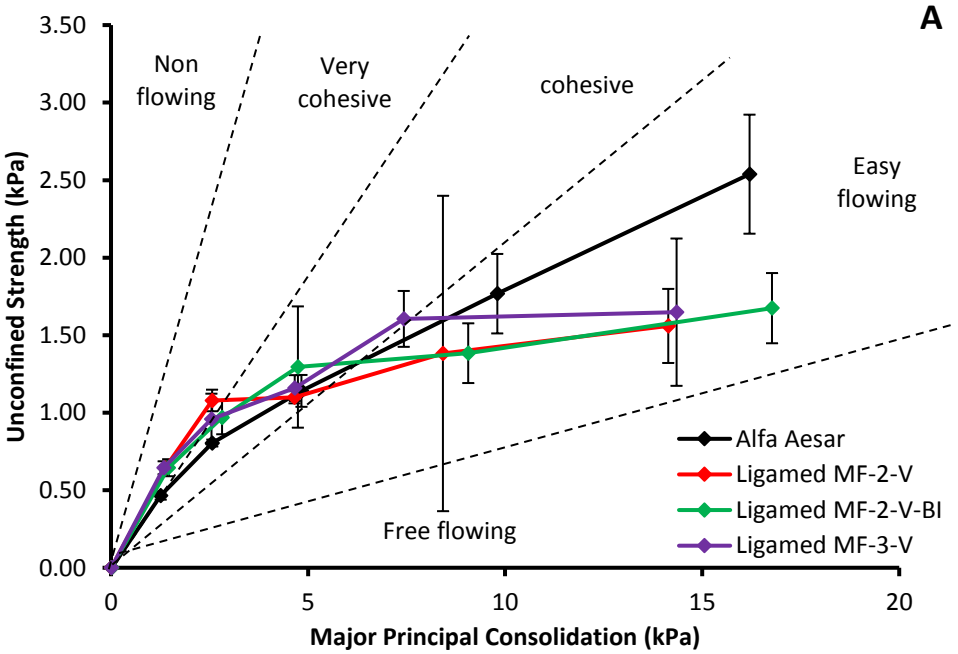


Figure 3.6 Flowability of MgSt samples analysed by Brookfield Powder Flow Tester. Plot shows the unconfined failure strength versus major principal consolidating stress for MgSt samples. Average values shown n=2, y error bars indicate max and min values.

Flow function slope of MgSt samples was observed to be between 0.37 to 0.48 and flow index was between 2.08 to 2.7, indicating the samples are cohesive in nature (Jenike, 1964). Among four samples, Alfa Aesar grade was less cohesive compared to Ligamed samples (Table 3.7)

3.3.3.2 Moisture sorption characteristics of MgSt samples

The dynamic vapour sorption analysis of MgSt samples is showed in Figure 3.7. Moisture uptake and loss capacity of any material depends on its crystalline, amorphous content and specific surface area (Haware et al., 2014). MgSt samples took up water with increase in humidity, from 0% to 90 % at 25^{o}C. The sorption-desorption isotherm of Alfa Aesar showed an open hysteresis loop (Figure 3.7A). A larger amount of water was associated with Alfa Aesar sample during desorption phase relative to the sorption phase. The hysteresis loop might be attributed to the binding and physical fit of water within the disordered and low-density amorphous sites. This kind of behaviour is normally associated with amorphous materials (Haware et al., 2014; Swaminathan and Kildsig, 2001). Ligamed samples showed a more closed hysteresis loop compared to the Alfa Aesar sample (Figure 3.7B-D). The desorption phase of the isotherm is closest to the sorption phase in case of Ligamed MF-3-V sample, which indicates desorption of nearly all of the adsorbed water. Such behaviour is commonly associated with crystalline materials (Haware et al., 2014; Swaminathan and Kildsig, 2001). The order of hysteresis loop with respect to Ligamed samples was Ligamed MF-3-V < Ligamed MF-2-V-BI < Ligamed MF-2-V, indicating MF-3-V was more crystalline compared to other Ligamed samples.

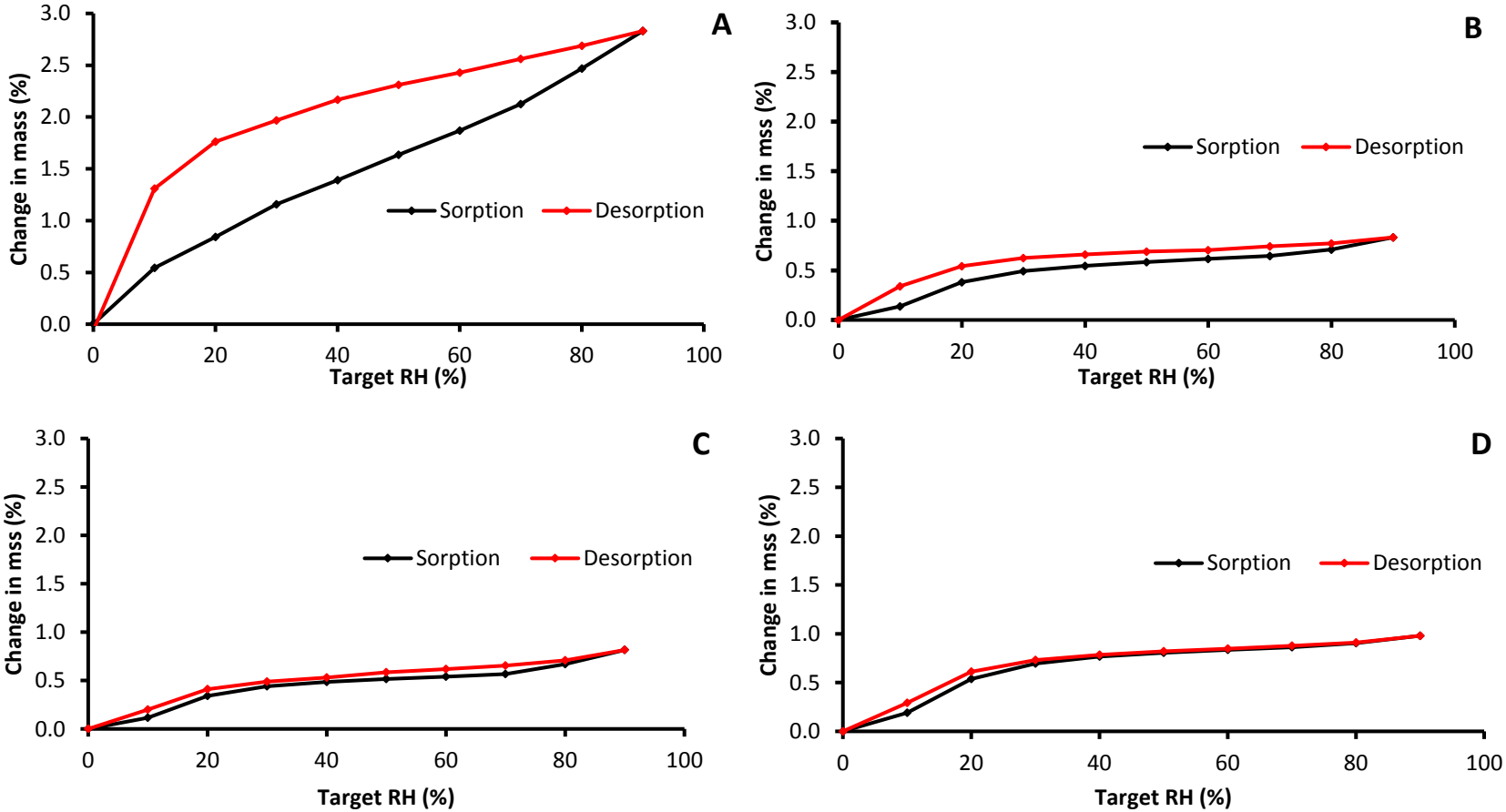


Figure 3.7 Moisture adsorption isotherms of MgSt samples at 25^0C. (A) Alfa Aesar (B) Ligamed MF-2-V (C) Ligamed MF-2-V-BI (D) Ligamed MF-3-V

3.3.4 Impact of MgSt on tablet properties

3.3.4.1 Impact on compression

The effect of selected grades of MgSt samples on tablet properties (tabletability, compactibility and compressibility) was investigated. Figure 3.8 shows the tabletability profile of paracetamol tablets prepared from an unlubricated and lubricated blends each prepared with one of the 4 MgSt samples.

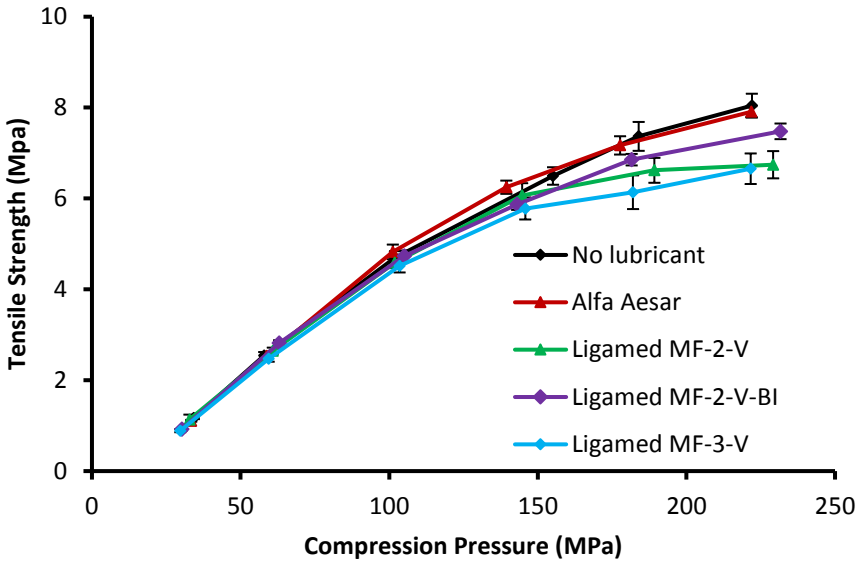


Figure 3.8 Tabletability profiles of paracetamol tablets unlubricated and lubricated, prepared with MgSt samples. Average values shown n=20, y error bars indicates standard deviation.

The effect of MgSt on tabletability of paracetamol tablets was compared over a compression pressure range of 30 – 234 MPa which produced tablets of relative density range 0.55 – 0.95, and with tensile strength range between 0.8 - 8 MPa. Tablet tensile strength increased with increasing compression pressure for all five samples. Unlubricated tablets and tablets produced with MgSt Alfa Aesar grade

showed similar TS at higher compression pressures. Tablets produced from with Ligamed MF-2-V, MF-2-V-BI and MF-3-V showed similar tensile strength up to 150 MPa. However above 150 MPa the tensile strength of compacts was reduced compared to the unlubricated tablets and those produced with the Alfa Aesar sample (Figure 3.8).

Figure 3.9 depicts the compactibility profile, which shows the relationship of tensile strength as a function of the tablet solid fraction. Compactibility profiles show the tablet relative density or solid fraction that would have to be achieved to produce a tablet with a desired tensile strength (Tye et al., 2005).

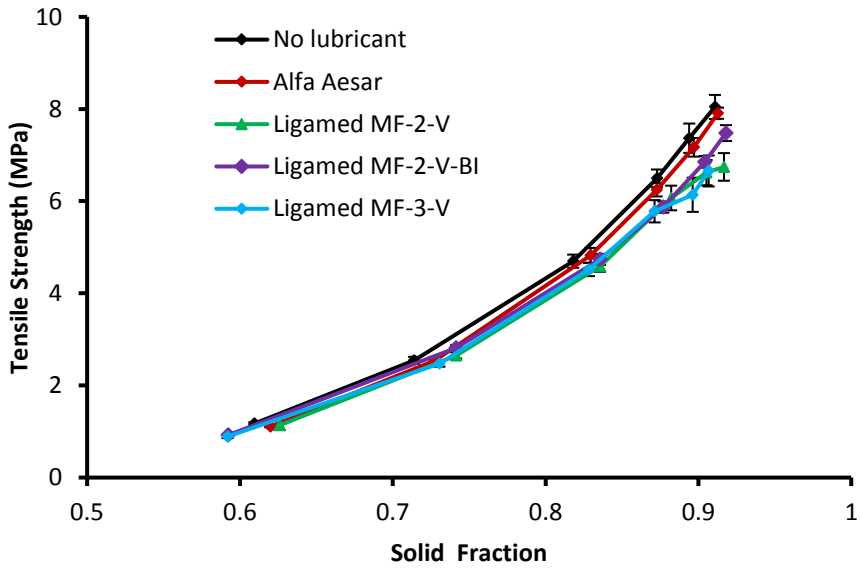


Figure 3.9 Compactibility profiles of paracetamol tablets unlubricated and lubricated, prepared with MgSt samples. Average values shown n=20, y error bars indicates standard deviation.

The tablets compactibility behaviour was consistent with the tabletability profile. Tablets produced with Ligamed MF-2-V, MF-2-V-BI and MF-3-V MgSt samples at

higher solid fractions showed lower compactibility (lower tensile strength). This result shows effect of MgSt supplier variability on compactibility performance.

Figure 3.10 shows the compressibility profile, which assesses the change in volume of powder blend when it is compressed (Joiris et al., 1998; Tye et al., 2005).

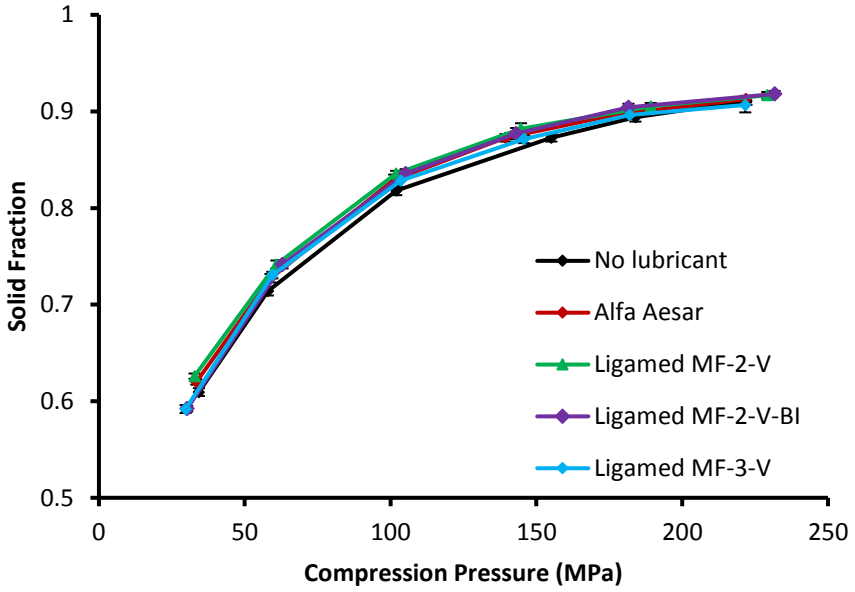


Figure 3.10 Compressibility profiles of paracetamol tablets unlubricated and lubricated, prepared with MgSt samples. Average values shown n=20, y error bars indicates standard deviation.

As the compression pressure was increased, material solid fraction increased for the unlubricated and formulations with different MgSt samples. At a given compression, no differences were noticed in the compressibility profiles of tablets with and without lubricants. Inclusion of different grades of MgSt also did not show any differences in the compressibility of the tablets.

3.3.4.2 Impact on dissolution

Tablets produced at tensile strength of 2 MPa are selected across all batches for dissolution testing. USP specification for paracetamol tablets is not less than 80% of the labelled amount should be released in 30 minutes in 900 mL dissolution media using the paddle apparatus operated at 50 rpm (Stosik et al., 2008). In this study, water was used as dissolution media.

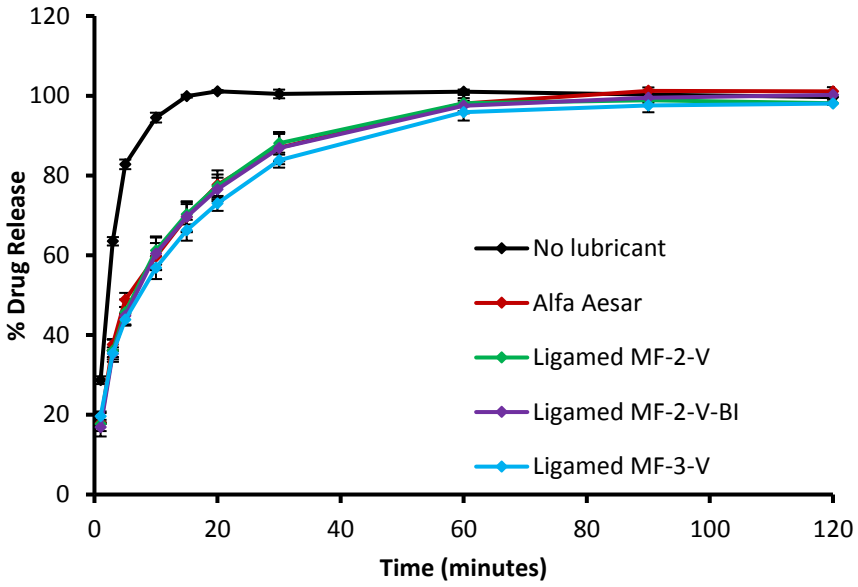


Figure 3.11 Dissolution profiles of paracetamol tablets unlubricated and lubricated, prepared with one of the 4 samples of magnesium stearate, produced at 2 MPa and tested in water at 37^{o}C. Average values shown n=3, y error bars indicates standard deviation.

Figure 3.11 shows *in-vitro* dissolution studies of the unlubricated and lubricated paracetamol tablets. It clearly shows the effect of lubricant in % release of paracetamol over time. Faster release was observed in unlubricated tablets with 100% release within 15 minutes and slower release was seen in lubricated tablets.

Tablets lubricated with all MgSt samples showed similar *in-vitro* drug release profiles (Figure 3.11). However, tablets lubricated with MF3V showed further minor delay in drug release profile compared to tablets with other MgSts. All formulations showed 80% drug release within 30 minutes, which is *in-vitro* standard USP 26 specification (USP 26 – NF21, 2003).

3.4 Discussion

Characterisation of four grades of MgSt showed that they differ in solid state, particulate and bulk properties. Solid state analysis of MgSt samples showed differences in crystallinity and thermal behaviour (Figure 3.1 and Figure 3.2). Ligamed MF-2-V and MF-2-V-BI showed similar thermal behaviour. Thermal analysis of Ligamed MgSt samples showed higher enthalpy of melting compared to Alfa Aesar, which indicates the greater molecular order or higher crystallinity in these samples. All samples showed a moisture loss between 3.30% and 4.26%, which is slightly below the theoretical 1.5 water molecules to per mole of MgSt (4.36%) that Wada and Matsubara determined for different combinations of commercial MgSts (Wada and Matsubara, 1994). DSC thermogram of Ligamed MF-3-V showed the most narrow melting point range suggesting the lowest level of impurities, whereas Alfa Aesar showed broad melting point range indicating the presence of high level of impurities (Wada and Matsubara, 1992). Within supplier variability was evident as the material properties of Ligamed MF-3-V were variable from Ligamed MF-2-V and MF-2-V-BI. Supplier to supplier variability was seen as Alfa Aesar has more amorphous in nature, which is evident from differences in PXRD and thermal analysis properties.

Morphological study of MgSt samples showed that particles of the Alfa Aesar sample appeared to be plate and needle shaped. All the Ligamed samples are also visualised as plate and needle shaped but organised as a deck of cards with micro agglomerates (Figure 3.3). Alfa Aesar showed smallest surface area and MF-3-V showed larger surface area with smaller particle size (Figure 3.4 and Table 3.4).

Ligamed MF-2-V and MF-2V-BI showed similar particulate properties. All samples showed decrease in particle size, with increase in air pressure indicating de-agglomeration and a very low deagglomeration was observed for MF-2-V-BI compared to other samples (Figure 3.5 and Table 3.5).

During sorption and desorption studies Alfa Aesar displayed an open hysteresis loop, which is mainly due to the binding and physical fit of water within the amorphous sites of Alfa Aesar. A study by Swaminathan and Kildsig showed that, this kind of behaviour is mainly associated with materials which have more amorphous content (Swaminathan and Kildsig, 2001). Ligamed samples showed less hysteresis compared to Alfa Aesar. Such behaviour is commonly associated with crystalline materials (Swaminathan and Kildsig, 2001). The order of hysteresis loop with respect to MgSt samples was Ligamed MF-3-V < Ligamed MF-2-V-BI < Ligamed MF-2-V < Alfa Aesar, indicating MF-3-V was more crystalline compared to other samples. Sorption-desorption studies corroborated the PXRD data (Figure 3.1), that indicated Alfa Aesar was more amorphous in nature compared to Ligamed samples.

Flowability analysis including powder flow testing and Carr's Index showed that all samples are very cohesive to cohesive in nature, indicating Ligamed MF-3-V having good flow compared to other samples (Figure 3.6 and Table 3.6). Brookfield's FT4 showed the same result, indicating all samples are cohesive, with the Alfa Aesar possessing the better flow compared to other samples (Figure 3.6 and Table 3.7).

The objective of this chapter was to determine the relevance of this variability on performance within blends. Though similar tabletability and compactibility profiles were seen for unlubricated tablets and tablets with Alfa Aesar (Figure 3.8 and

Figure 3.9), they differed in *in-vitro* drug release, where Alfa Aesar showed delayed drug release (Figure 3.11). At compression pressure above 150 MPa the tensile strength of compacts prepared using Ligamed samples was reduced compared to tablets prepared with Alfa Aesar and the unlubricated tablets (Figure 3.8). Tablets with Ligamed MgSt, showed lower compactibility at higher solid fraction (Figure 3.9). No real differences were observed in compressibility of blends, when different MgSt samples were included (Figure 3.10). Paracetamol tablets with Alfa Aesar, MF-2-V and MF-2-V-BI as lubricants showed similar *in-vitro* drug release profiles (Figure 3.11). Whereas a slight reduction in drug release was observed in tablets with MF3V, which may be due to its higher surface area and smaller particle size provides better lubrication around bulk powder particles (Haware et al., 2014).

3.5 Conclusions

Selected lots of MgSt samples analysed, showed variability in solid state and particulate properties. Unlubricated tablets showed lowest solid fraction and higher compactibility compared to lubricated tablets. At higher compression pressures, tablets with Ligamed samples showed slightly less tabletability and compactibility, compared to tablets with Alfa Aesar. Tablets lubricated with all MgSt samples showed similar in-vitro drug release profiles except for tablets with MF3V.

The next chapter-4 is focused on in investigating the influence of this variability in MgSt properties on continuous feeding performance and significance of continuous feeding on MgSt properties and their effect on tablet quality.

Chapter - 4

The behaviour of magnesium stearate during continuous feeding

4. The behaviour of MgSt during continuous feeding

4.1 Introduction

In chapter – 3, we investigated the differences in MA of four grades of MgSt from two different suppliers. The main emphasis of this chapter - 4 is to study the effect of those different material properties on the continuous feeding performance of the MgSt grades. As mentioned in chapter – 1, there is a growing interest amongst pharmaceutical companies and academic researchers in the area of continuous manufacturing which is evident by the increase in number of publications in this area (Ervasti et al., 2015; Fonteyne et al., 2015; Mascia et al., 2013; Simonaho et al., 2016; Vanarase et al., 2010; Vanarase and Muzzio, 2011). A major advantage of continuous processing it that it allows for reengineering of the process train and the introduction of engineering solutions (Plumb, 2005).

Feeding of excipients and active ingredients into the continuous processing line is the first step in continuous processing. The presence of highly accurate feeding systems and their optimal performance is essential to produce products with target quality properties. Powder feeding into subsequent downstream processes is regarded as one of the critical process parameter in overall continuous manufacturing (Ervasti et al., 2015; Pernenkil and Cooney, 2006). A continuous powder feeder should be able to feed the raw materials at their specific ratios needed continuously and consistently for a specific formulation, and this is a challenging feat for the raw materials which have poor flowability (Engisch and Muzzio, 2014). One such material is MgSt, which is very cohesive in nature.

Though MgSt is used in very small amounts as lubricant in the tablet blends, if the addition of MgSt is not properly monitored it can have negative effects on the tablet quality properties as discussed in chapter 1 and 3. Feeding materials like MgSt continuously and consistently into downstream processing is challenging as it tends to coat metal tooling and to be shear sensitive (Engisch and Muzzio, 2014). Engisch and Muzzio investigated the feeding behaviour of MgSt in K-Tron KT20 and K-Tron MT12 loss in weight feeders. In this study they used CCS and FCS, which are self-cleaning screws, with five different screen combinations to study the feeding behaviour of MgSt. This study showed that the K-Tron MT12 with FCS-no screen combination performed better and a comparative long term feeding performance between two feeders showed that the K-Tron MT12 performed better compared to the K-Tron KT20 feeder (Engisch and Muzzio, 2014).

4.2 Aim and objectives

The main aim of this chapter is to understand the continuous feeding process of MgSt.

The main objectives of the chapter are:

- To investigate the effect of physical attributes variability of four different MgSt samples on its continuous feeding performance.
- To investigate the effect of continuous feeding on the particulate properties of MgSt samples
- To determine if physical changes induced in MgSt due to continuous feeding effects the final tablet quality (compaction and dissolution behaviour).

4.3 Results

4.3.1 K-Tron MT12 set-up optimisation using Alfa Aesar

The initial feeding trial with the Alfa Aesar sample was conducted to determine the optimal feeding parameters and to identify any issues regarding feeding that could be rectified prior to testing and comparing the four MgSt samples. Self-cleaning concave screws were selected over auger screws for this feeder optimisation based on recommendations from the study conducted by Engisch and Muzzio, 2014. Experimental conditions examined for feeder optimisation are shown in Table 4.1.

Table 4.1 Feeding configurations investigated for Alfa Aesar feeder set-up optimisation study and associated feeding performance expressed at feeding rate % RSD

Run	Screw type	Screen	Feed factor (kg/hr)	Target feed rate set Point (kg/hr)	Average Feed Rate (kg/hr)	Feed Rate % RSD
1	CCS	No Screen	1.90	0.15	0.15	5.72
2	CCS	No Screen	1.90	0.25	0.25	3.55
3	CCS	CSqS	1.89	0.15	0.15	5.07
4	CCS	CSqS	1.89	0.25	0.25	3.75
5	CCS	FSqS	1.95	0.15	0.15	4.95
6	CCS	FSqS	1.95	0.25	0.25	3.10
7	FCS	No Screen	1.64	0.15	0.15	11.37
8	FCS	No Screen	1.64	0.25	0.25	4.83
9	FCS	CSqS	1.12	0.15	0.15	19.87
10	FCS	CSqS	1.12	0.25	0.25	13.57
11	FCS	FSqS	1.55	0.15	0.15	8.96
12	FCS	FSqS	1.55	0.25	0.25	9.10

As expected due to its cohesive nature, Alfa Aesar proved to be a difficult material to feed within the continuous feeder. There was a build-up of material on hopper walls in non-agitated zones and on the screws selected (Figure 4.1). It formed clumps within the pockets of screws. It fell off in lumps even with and without the use of discharge screens (Figure 4.2). A larger amount of MgSt adhered to the outlet of the feeder, when no screen was used (Figure 4.2A). To surpass the effect of the electrostatics, feeder was instrumented with earthing, which did not reduce the effect of the MgSt adhering at the feeder outlet.

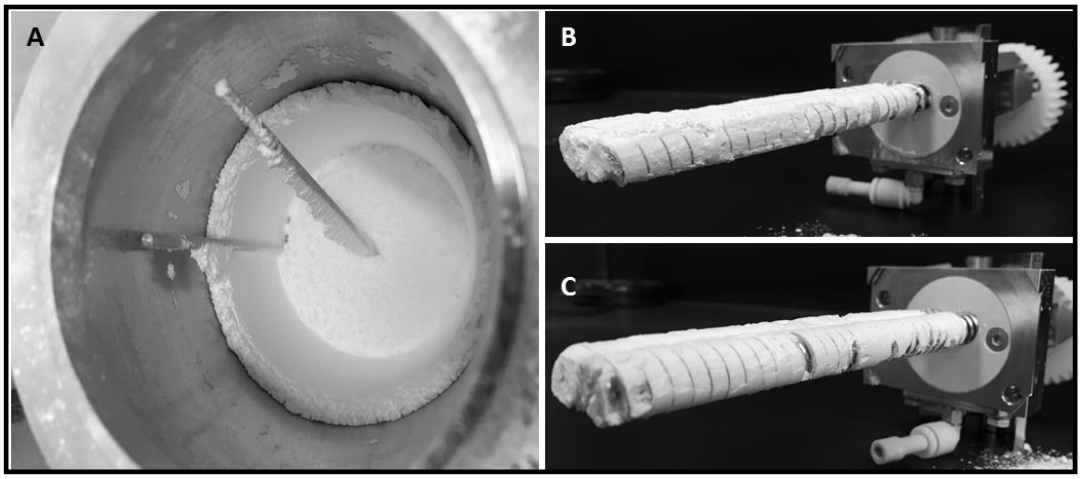


Figure 4.1 Pictures showing (A) build-up of material on hopper walls in non-agitated zones, (B) coating of MgSt on coarse concave screw and (C) coating of MgSt on fine concave screws, during continuous feeding.

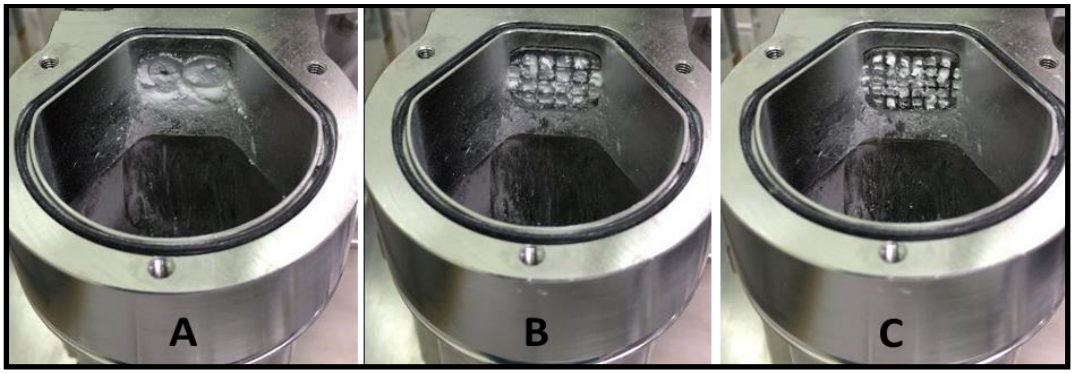


Figure 4.2 Pictures of MgSt build up near discharge outlet (A) no screen, (B) CCS (C) FSqS

The feed rate data generated from the K-Sampler software for different time intervals (1 second, 5 seconds, 10 seconds, 15 seconds, 30 seconds and 60 seconds) over a period of 30 minutes was recorded for all the runs examined as per Table 4.1. To understand the influence of sampling interval and impact of averaging on RSD, one specific run 5 is chosen from Table 4.1. Feed data of the MgSt Alfa Aesar from K-Tron MT12 with CCS and FSqS is shown in Figure 4.3. The moving averages of feed rate were plotted for 1 second interval of data collection, it showed large sinusoidal oscillations with higher standard deviation (Figure 4.3A and C). When the sampling interval is increased the sinusoidal oscillations of the feed rate around the target feed rate set point (0.15 kg/hr) and the RSD is decreased (Figure 4.3A - C).

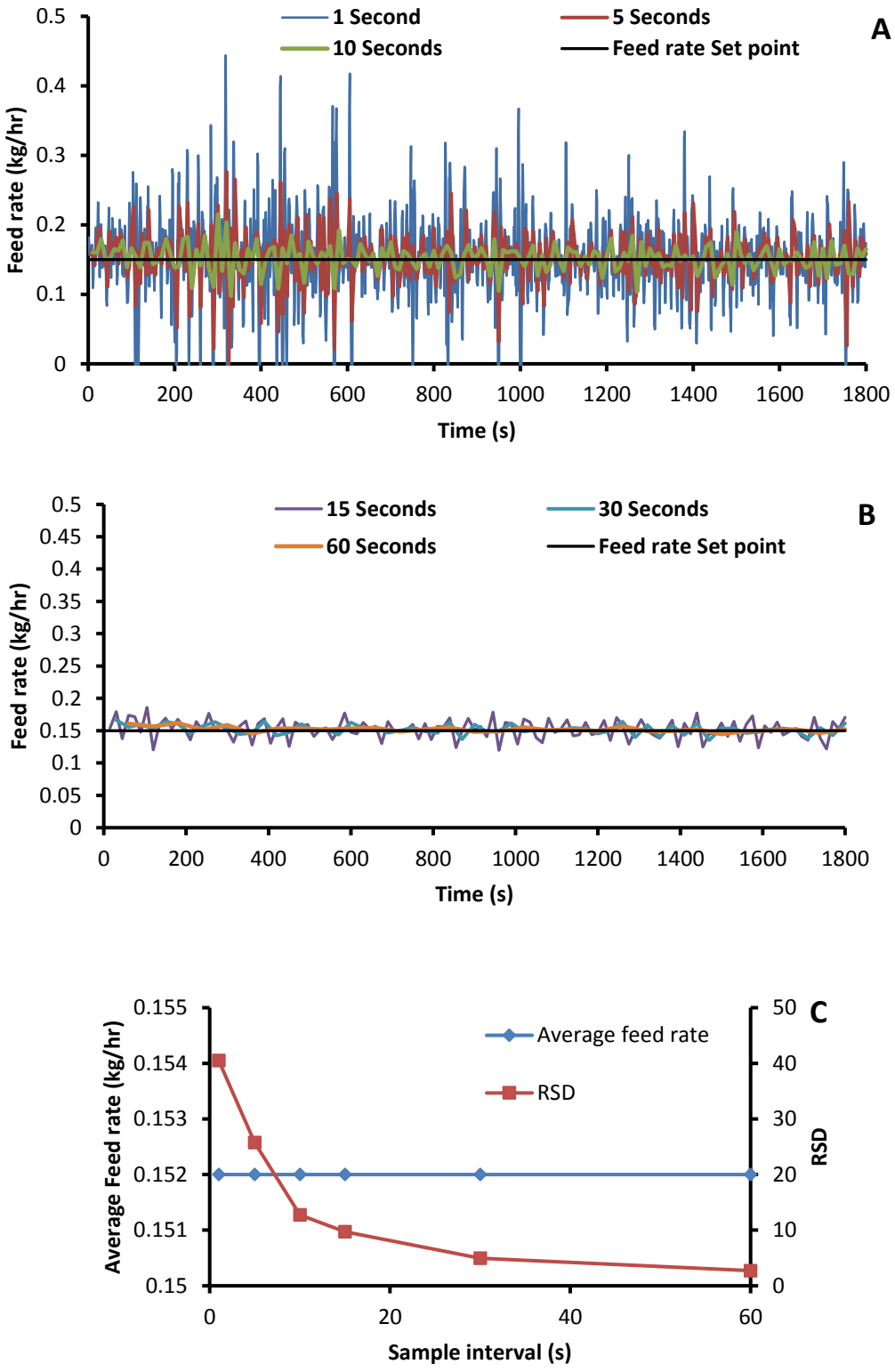


Figure 4.3 Feed rate data as function of time during feeding of Alfa Aesar fed from MT12 with CCS and FSqS displayed (A and B) using different moving averages. (C) The effect of sampling interval on RSD.

For this optimisation study the RSD of feed weight recorded for 30 seconds sample intervals was chosen and compared across different feeder settings. Figure 4.4 shows the feeding performance data of MgSt Alfa Aesar for three different screen conditions: no screen, CSqS and FSqS at two different feed rate set points.

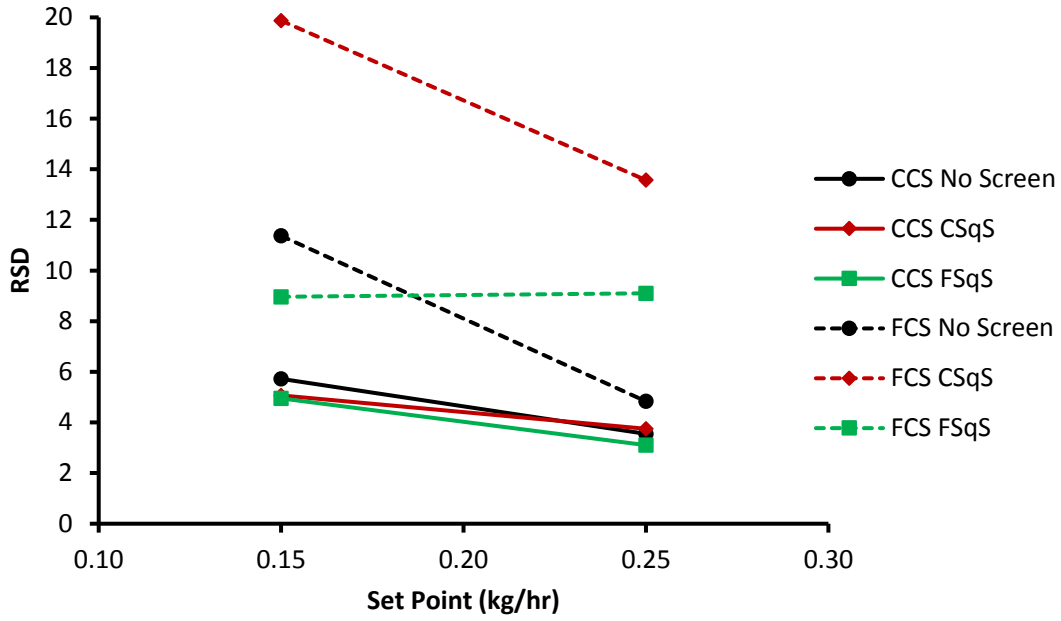


Figure 4.4 Feeding performance of Alfa Aesar (% RSD) with CCS and FCS with three different screen combinations: no screen, CSqS and FSqS at two different feed rate set points

Greater variation in RSD was seen when FCS were used compared to CCS, with different screen conditions (Figure 4.4). This may be due to the pocket sizes of the screws used; CCS have larger pockets, resulting in formation of heavier lumps of MgSt which are less prone to electrostatic effect at the feeder outlet, as previously reported by Engisch and Muzzio for feeding trials of silicon dioxide (Engisch and Muzzio, 2014). In contrast, FCS have smaller pockets resulting in smaller clumps of MgSt, which are more prone to electrostatic effects at the feeder outlet. The higher feeder set point of 0.25 kg/hr resulted in a lower RSD than lower set point of 0.15

kg/hr. This may be due to a lower residence time of powder within the flights of the screws and reduced clumping. Coarse concave screw at all screen configurations gave the lowest RSD for the all trials of Alfa Aesar. The screen configuration had less of an effect on feed rate RSD. A CCS with a FSqS configuration was chosen to compare the feeding behaviour of the other sample of MgSt.

4.3.2 Comparison of feeding behaviour of MgSt samples

Compared to Alfa Aesar, MgSt Ligamed samples were marginally more cohesive and therefore difficult powders to feed through KTRON MT12, due to formation of electrostatics and tool coating. Material build-up was evident in the hopper during the feeding procedure creating stagnant zones despite the presence of an agitator in the hopper. CCS with FSqS was chosen and two different feed rate set points of 0.15 kg/hr and 0.25 kg/hr were studied. The FF is the gravimetric speed equivalent for 100% screw speed with a specific screw and screen setting. FF was recorded for all the MgSt samples, before carrying out the feeding at above mentioned set points. The bulk density of MgSt samples determined the initial feed factor achieved. For example MF-3-V had the lowest bulk density of 0.14 g/cm^3 and lowest feed factor. Alfa Aesar had the highest bulk density and showed highest FF (Figure 4.5).

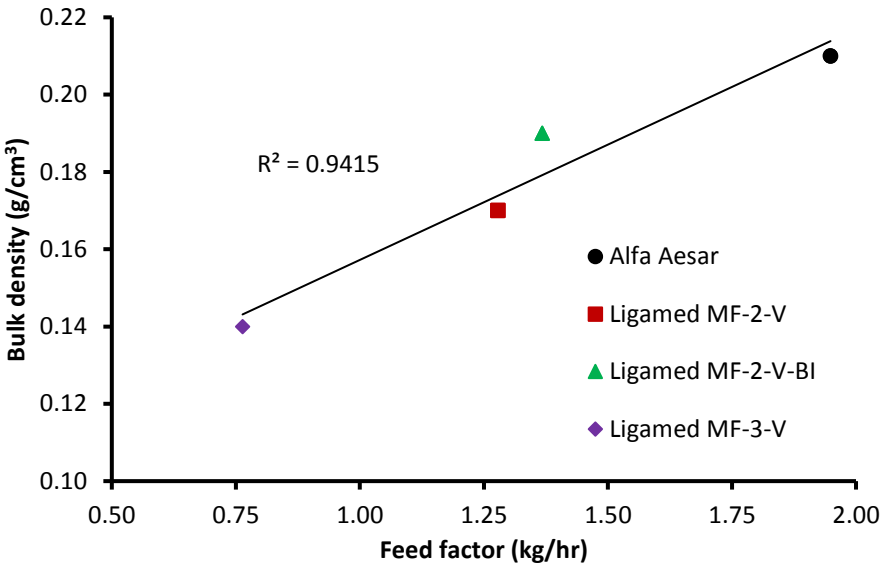


Figure 4.5 Effect of MgSt bulk density on samples feed factor

Comparisons of feeding performance (% RSD) demonstrated that the variability of MgSt feeding was clearly influenced by feed rate set point. Greater variability was observed between samples when fed at lower feed rate of 0.15 kg/hr compared to the variability of samples fed at 0.25 kg/hr as shown in Figure 4.6.

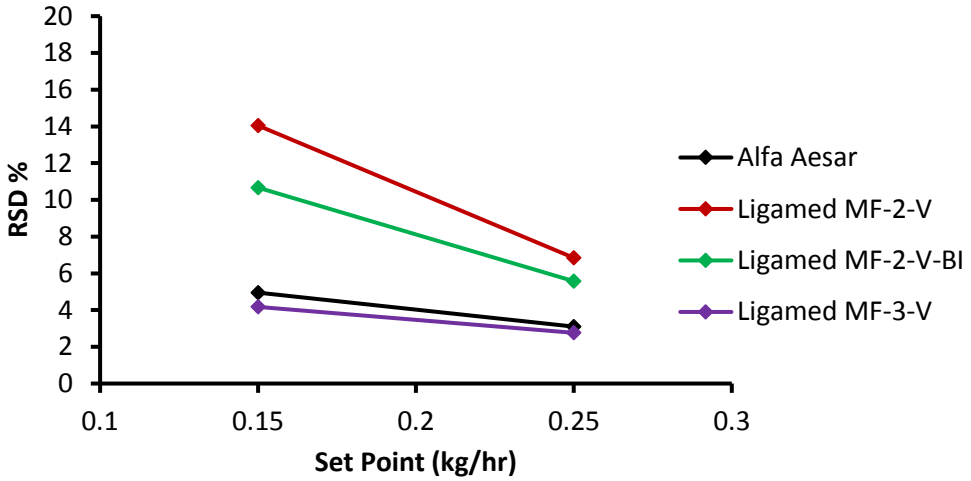


Figure 4.6 Feeding behaviour of four different grades of MgSt using CCS with FSqS at two feed rates. RSD is shown as function of feed rate for K-Tron MT12 feeder.

RSD for all samples decreased with increase in feed rate. Alfa Aesar and Ligamed MF-3-V which had the lowest and highest surface area and flow function parameters showed the lowest RSD when fed at two different feed rates. However, Ligamed MF-2-V and Ligamed MF-2-V –BI which showed similar characteristics as discussed in chapter-3, showed a greater RSD at two different feed rates (Figure 4.6). With all the processing variables kept constant, the differences between the feeding performances clearly corresponds to characteristics of the fed MgSt sample.

4.3.3 Effect of feeding on MgSt particulate properties

4.3.3.1 Effect of Feeding on Particle size distribution

As shown in chapter-3, four different grades of MgSt used in this study existed in agglomerated states. PSD of unfed and post fed (0.15 kg/hr and 0.25 kg/hr) MgSt samples determined using dry powder laser diffraction at 1.5 bar dispersive pressure is shown in Figure 4.7. To understand the effect of feeding on PSD of samples, the percentage reduction of particle size was calculated and discussed here, for samples fed at both feed rates. The statistical analysis for each sample at different feed rates, is shown in supplementary information.

Table 4.2 shows the percentage reduction in particle size for MgSt samples, fed at both feed rates. Focussing on D10, at both feed rates, Ligamed MF-3-V is least effected by feeding with no significant reduction in D10. A higher reduction of 5.54% in D10 was observed for Ligamed MF-2-V when fed at 0.15 kg/hr and at 0.25 kg/hr. Alfa Aesar showed reduction in D10 by 3.27%. At both feed rates D50 of Alfa Aesar was greatly affected, which showed approximately 6% reduction. D50 of

Ligamed MF-2-V-BI and Ligamed MF-3-V were least affected when fed at 0.15 kg/hr and 0.25 kg/hr sample respectively. D90 of Alfa Aesar and Ligamed MF-2-V samples was highly affected by feeding and showed approximately 11% reduction when fed at 0.15 kg/hr and approximately 10% reduction when fed at 0.25 kg/hr. Very less affect was seen in D90 of Ligamed MF-3-V, when fed at 0.15 kg/hr and Ligamed MF-2-V-BI when fed at 0.25 kg/hr. All samples showed greater percentage reduction in particle size, when fed at lower feed rate of 0.15 kg/hr.

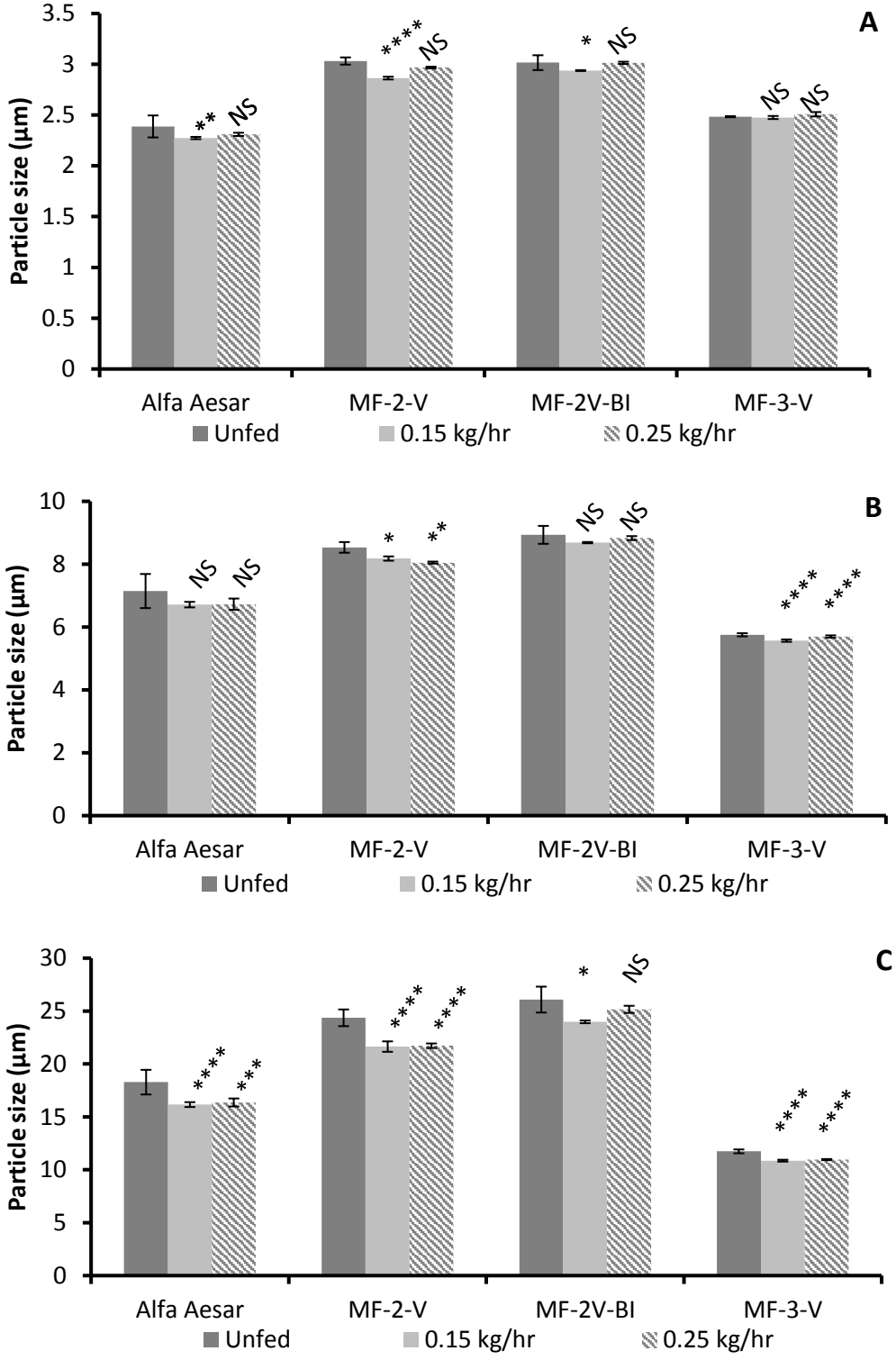


Figure 4.7 Effect of continuous feeding on particle size analysed by laser diffraction at 1.5 bar air pressure for four grades of MgSt. (A) D10, (B) D50 and (C) D90. Average values shown, n=5. ± indicates standard deviation.

Where, * represents P≤0.05, ** represents P≤0.01, *** represents P≤0.001 and **** represents P≤0.0001.

Table 4.2 Particle size and percentage reduction in particle size (relative to unfed material) due to feeding of MgSt samples at two feed rates. Average values shown n=5. ± indicates standard deviation. NA indicates not applicable and NC indicates no change.

Particle size	Feed rate (kg/hr)	Alfa Aesar		Ligamed MF-2-V		Ligamed MF-2-V-BI		Ligamed MF-3-V	
		Particle size (µm)	% reduction	Particle size (µm)	% reduction	Particle size (µm)	% reduction	Particle size (µm)	% reduction
D10	Unfed	2.388±0.10	NA	3.032±0.03	NA	3.016±0.07	NA	2.484±0.00	NA
	0.15	2.274±0.01	4.77	2.864±0.01	5.54	2.938±0.00	2.59	2.476±0.01	0.32
	0.25	2.310±0.01	3.27	2.968±0.00	2.11	3.014±0.01	0.07	2.508±0.02	NC
D50	Unfed	7.146±0.54	NA	8.534±0.17	NA	8.934±0.28	NA	5.754±0.05	NA
	0.15	6.714±0.08	6.05	8.18±0.06	4.15	8.686±0.02	2.78	5.568±0.03	3.23
	0.25	6.728±0.17	5.85	80.50±0.03	6.56	8.830±0.06	1.16	5.698±0.03	0.97
D90	Unfed	18.28±1.16	NA	24.36±0.78	NA	26.08±1.22	NA	11.74±0.18	NA
	0.15	16.16±0.23	11.60	21.64±0.49	11.17	23.98±0.13	8.05	10.86±0.08	7.50
	0.25	16.36±0.37	10.50	21.72±0.21	10.84	25.16±0.33	3.53	10.96±0.05	6.64

Effect of feed rate on sample de-agglomeration

Prior to feeding, four grades of MgSt showed significant reduction in particle size as the titration pressure increased indicating de-agglomeration, as discussed in chapter-3. In this chapter the effect of feeding was also studied on the ease of de-agglomeration of MgSt samples fed at both feed rates, by performing air pressure titration (1.5 bar, 2 bar and 3 bar) using a dry powder laser diffraction method. As discussed earlier, the decrease in the particle size is given by percentage reduction. Figure 4.8 shows the effect of feeding on particle size. The statistical analysis of particle size data and the percentage reduction in particle size due to feeding is shown in supplementary information. It was anticipated that the higher the % reduction in particle size, the greater the de-agglomeration of samples, the higher the presence of agglomerates within the samples.

The particle size (D10, D50 and D90) of Ligamed MF-2-V showed greater % reduction as the titration pressure increased indicating presence of more agglomerates, compared to other three samples when fed at 0.15 kg/hr (Table 4.3). D10 and D50 of Ligamed MF-3-V and D50 & D90 of Alfa Aesar showed less % reduction in particle size indicating presence of less agglomerates. Table 4.4 shows the % reduction for samples fed at 0.25 kg/hr. The least % reduction in particle size (D10, D50 and D90) for Alfa Aesar sample was observed as the titration pressure increased indicating less agglomerates. However greater % reduction was observed in D10, D50 and D90 as titration pressure increased for Ligamed MF-2-V and MF-2-V-BI samples, indicating presence of agglomerates.

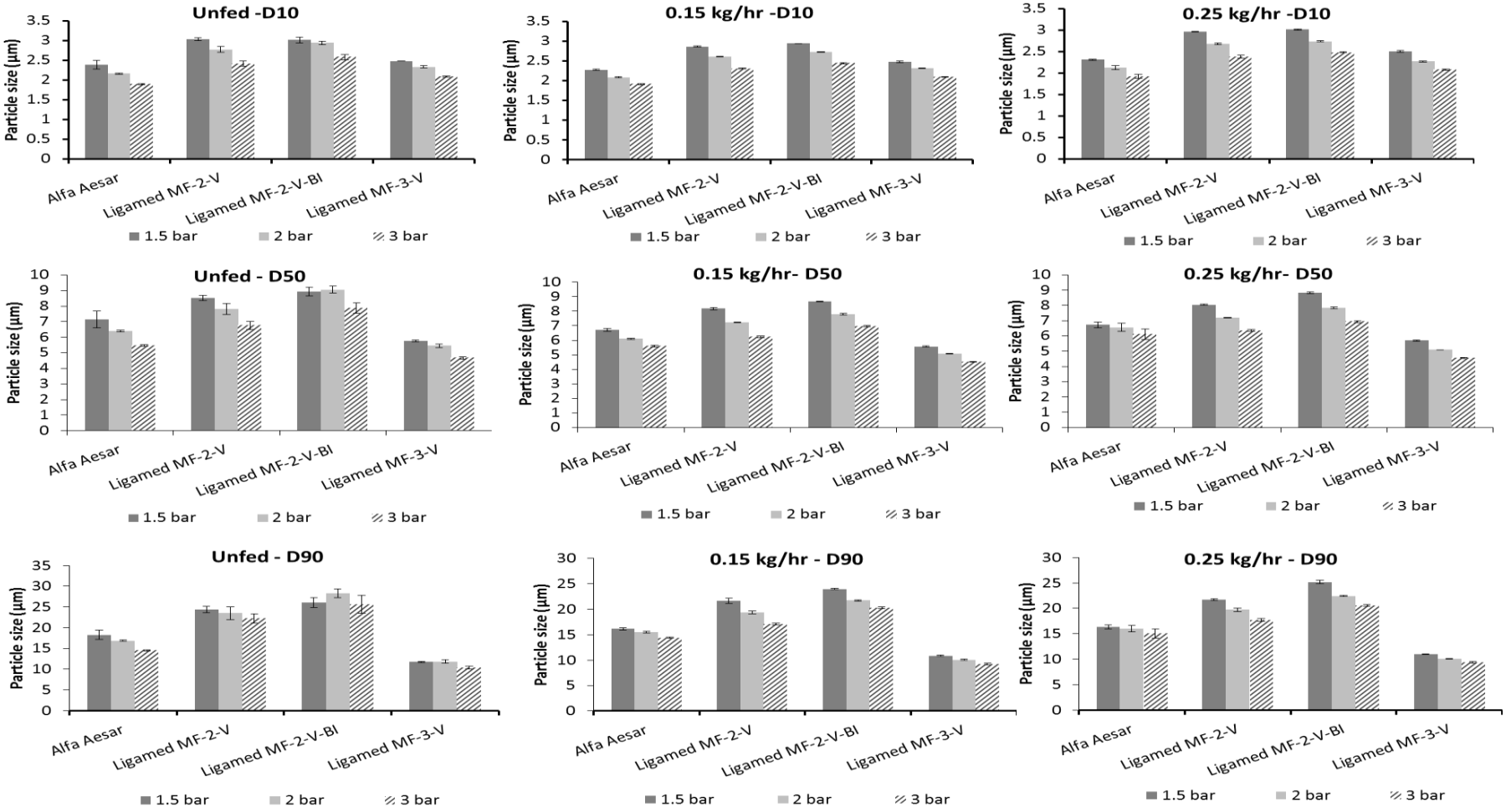


Figure 4.8 Particle size pressure titration analysis of four grades of MgSt unfed and fed at different feed rates. Average values, n=5. ± shows standard deviation

Table 4.3 Particle size and percentage reduction in particle size (relative to material analysed at titration pressures of 1.5 bar) for MgSt samples fed at 0.15 kg/hr analysed at titration pressures of 1.5 bar, 2 bar and 3 bar. Average values shown n=5. ± indicates standard deviation. NA indicates not applicable.

Particle size	Feed rate (kg/hr)	Air Pressure (Bar)	Alfa Aesar		Ligamed MF-2-V		Ligamed MF-2-V-BI		Ligamed MF-3-V	
			Particle size (µm)	% reduction	Particle size (µm)	% reduction	Particle size (µm)	% reduction	Particle size (µm)	% reduction
D10	0.15	1.5	2.27±0.01	NA	2.86±0.01	NA	2.93±0.00	NA	2.47±0.01	NA
		2	2.08±0.00	8.27	2.60±0.00	9.15	2.72±0.00	7.22	2.31±0.01	6.62
		3	1.91±0.01	16.01	2.30±0.01	19.55	2.44±0.01	16.95	2.09±0.01	15.43
D50	0.15	1.5	6.71±0.08	NA	8.18±0.06	NA	8.68±0.02	NA	5.56±0.03	NA
		2	6.10±0.05	9.09	7.24±0.03	11.49	7.78±0.06	10.41	5.08±0.01	8.62
		3	5.60±0.06	16.59	6.24±0.05	23.72	6.98± 0.03	19.62	4.51±0.02	18.93
D90	0.15	1.5	16.16±0.23	NA	21.64±0.49	NA	23.98±0.13	NA	10.86±0.08	NA
		2	15.52±0.16	3.96	19.38±0.24	10.44	21.72±0.14	9.42	10.06±0.13	7.37
		3	14.38±0.13	11.01	17.12±0.17	20.89	20.28±0.16	15.43	9.23±0.16	14.99

Table 4.4 Particle size and percentage reduction in particle size (relative to material analysed at titration pressures of 1.5 bar) for MgSt samples fed at 0.25 kg/hr analysed at titration pressures of 1.5 bar, 2 bar and 3 bar. Average values shown, n=5. ± indicates standard deviation. NA indicates not applicable.

Particle size	Feed rate (kg/hr)	Air Pressure (Bar)	Alfa Aesar		Ligamed MF-2-V		Ligamed MF-2-V-BI		Ligamed MF-3-V	
			Particle size (µm)	% reduction	Particle size (µm)	% reduction	Particle size (µm)	% reduction	Particle size (µm)	% reduction
D10	0.25	1.5	2.31±0.01	NA	2.96±0.00	NA	3.01±0.01	NA	2.50±0.02	NA
		2	2.12±2.12	7.97	2.67±0.021	9.77	2.74±0.01	9.09	2.27±0.01	9.41
		3	1.92±1.92	16.88	2.38±0.03	19.74	2.47±0.01	17.78	2.07±0.01	17.15
D50	0.25	1.5	6.72±0.17	NA	8.05±0.03	NA	8.83±0.06	NA	5.69±0.03	NA
		2	6.57±0.25	2.35	7.19±0.03	10.63	7.85±0.04	11.08	5.09±0.01	10.64
		3	6.10±0.33	9.30	6.35±0.05	21.09	6.94±0.05	21.38	4.56±0.03	19.90
D90	0.25	1.5	16.36±0.37	NA	21.72±0.21	NA	25.16±0.33	NA	10.96±0.05	NA
		2	15.98±0.64	9.12	19.74±0.32	9.12	22.44±0.15	10.81	10.08±0.08	8.03
		3	15.04±0.92	18.51	17.70±0.25	18.51	20.56±0.15	18.28	9.39±0.15	14.32

4.3.3.2 Effect of feed rate on sample surface area

An increase in surface area was expected as a function of increase in feed rate, due to the shearing action of concave screws on the materials. However, no significant differences were noticed within the surface area of samples when fed at different feed rates (Table 4.5). Differences were not observed in the DSC and TGA thermograms of unfed and fed samples of all four grades of MgSt samples (Supplementary information, Figure S1 – S2).

Table 4.5 Impact of feed rate on surface area of MgSt samples. Average values shown, n=3. ± standard deviation.

Specific surface area (m^2/g)			
Sample No.	**Unfed**	**Feed rate 0.15 kg/hr**	**Feed rate 0.25 kg/hr**
Alfa Aesar	03.08 ± 0.09	3.23±0.13	3.15±0.00
Ligamed MF-2-V	10.59 ± 0.12	10.75±0.34	10.71±0.43
Ligamed MF-2-V-BI	10.14 ± 0.14	10.24±0.77	9.77±0.32
Ligamed MF-3-V	15.49 ± 0.12	17.05±0.59	17.07±1.58

4.3.4 Effect of fed MgSt on tablet properties

4.3.4.1 Effect on compression

The tablets formulated using fed MgSt samples as lubricants were compared to tablets prepared with unfed lubricants, to see the effect of feeding on MgSt performance in tabletability, compressibility and compactibility. Tabletability profiles of paracetamol formulations with no lubricant (MgSt), unfed and fed MgSt samples, shown in Figure 4.9.

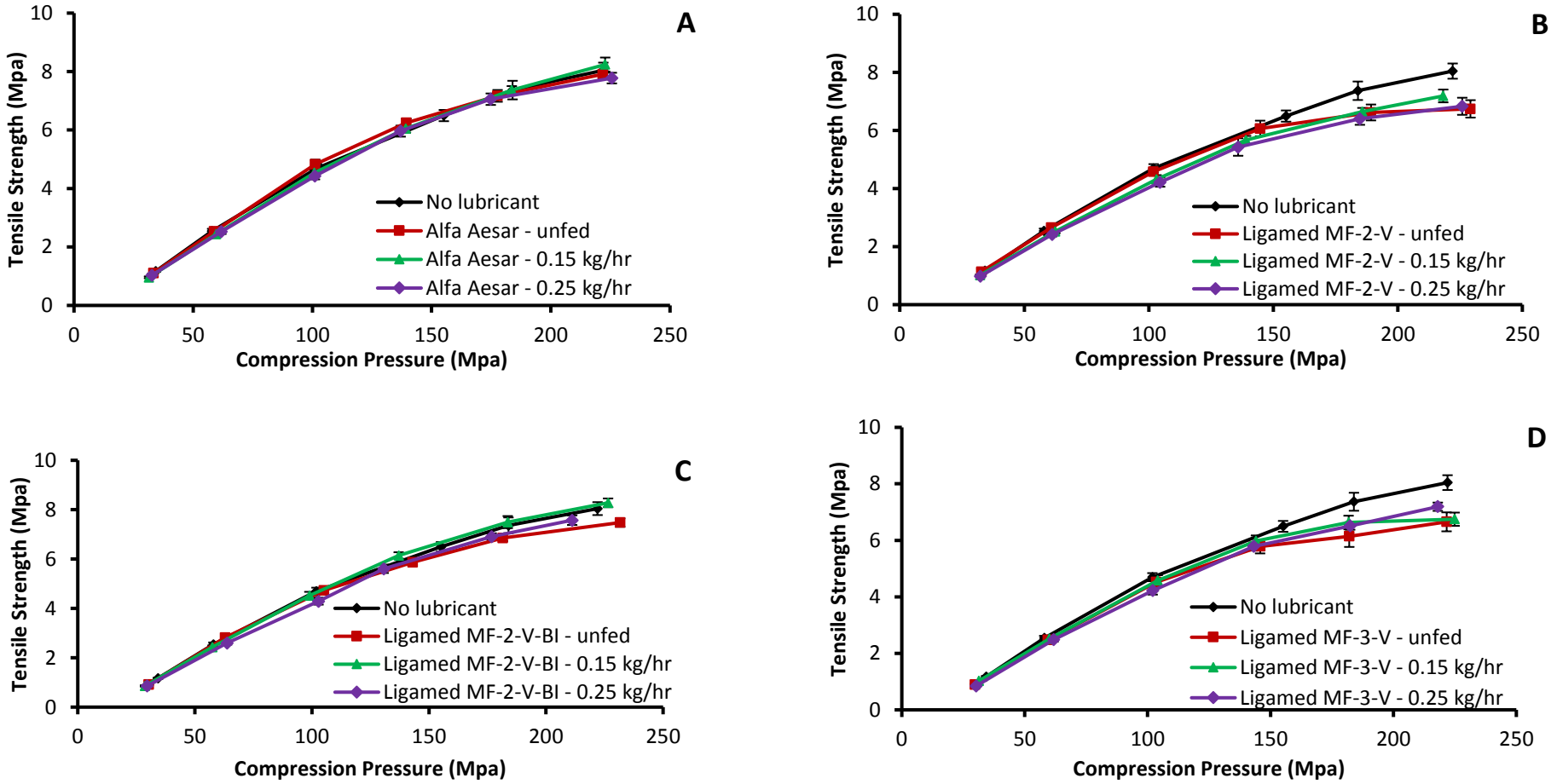


Figure 4.9 Tabletability profiles of tablets with four grades of MgSt (A) Alfa Aesar (B) Ligamed MF-2-V (C) Ligamed MF-2-V-BI and (D) Ligamed MF-3-V. Average values shown n = 20, y error bars indicate standard deviation.

All formulations showed increase in tensile strength as the compression pressure increased up to 150 MPa. Reduction in tablet tensile strength was expected due to inclusion of a lubricant, but for the formulations with fed the MgSt grade of Alfa Aesar no difference was observed compared to the unfed batch (Figure 4.9A). Ligamed MF-2-V-BI sample showed a very minor increase in tensile strength at the highest compression forces when fed lubricants were included, compared to the tablets containing unfed Ligamed MF-2-V-BI (Figure 4.9C). As discussed in previous chapter-3, tablets with Ligamed MF-2-V and Ligamed MF-3-V showed a slight reduction in tablet tensile strength at higher compression forces compared to the formulation without lubricant, as shown in Figure 4.9B and D. No further effect on tensile strength was observed when fed samples were included in tablets.

Figure 4.10 shows the compactibility profiles of tablets with different grades of unfed and fed MgSt. Compactibility depicts the tensile strength of the tablets as a function of solid fraction. As previously shown in chapter 3, tablets with no lubricant and unfed lubricant (Alfa Aesar) behaved similarly at a given solid fraction. Inclusion of Alfa Aesar fed at both feed rates yielded weaker compacts for solid fractions, between 0.65 to 0.85 (Figure 4.10A). For blends with Ligamed samples fed at both feed rates it was difficult to clearly identify differences in behaviour between fed and unfed samples (Figure 4.10B, C and D).

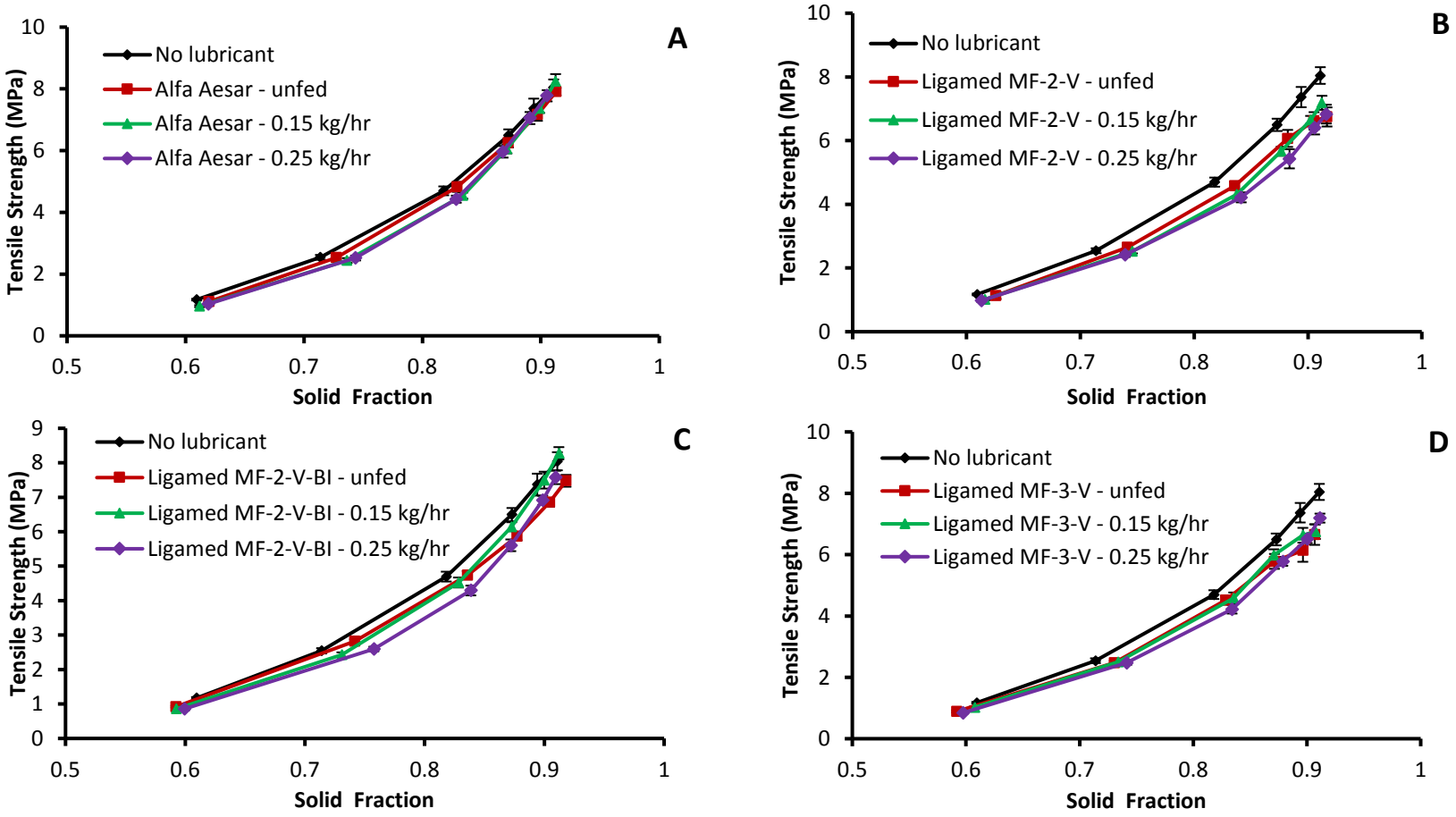


Figure 4.10 Compactibility profiles of tablets with four grades of MgSt (A) Alfa Aesar (B) Ligamed MF-2-V (C) Ligamed MF-2-V-BI and (D) Ligamed MF-3-V. Average values shown n = 20, y error bars indicate standard deviation.

Figure 4.11 shows the compressibility profile, which assesses the change in volume of powder blend when it is compressed. Compressibility describes the change in porosity or relative density or solid fraction of a powder blend changes under pressure. If a tablet has a higher relative density or solid fraction, it results in larger areas of interparticulate bonding thus stronger compacts are formed.

As the compression pressure is increased, material solid fraction is increased. Tablets compacted with fed lubricants from four grades at two feed rates showed similar effect same as that of tablets with unfed lubricants. At a given compression pressure between 50 MPa and 175 MPa, tablets without lubricant yielded the lowest solid fraction compared to lubricated tablets for the four grades of MgSt (Figure 4.11) and tablets with fed lubricants showed similar solid fraction.

4.3.4.2 Effect of feeding on tablet dissolution

Figure 4.12 shows the dissolution profiles of paracetamol tablets formulated with no MgSt, unfed and fed MgSt of four different grades. Dissolution experiments clearly showed the delayed release of API after inclusion of lubricant. To discriminate the effect of feeding on lubrication performance, the dissolution profiles were compared using one way ANOVA followed by Tukey posthoc multiple comparison test was performed as showed in Table 4.6.

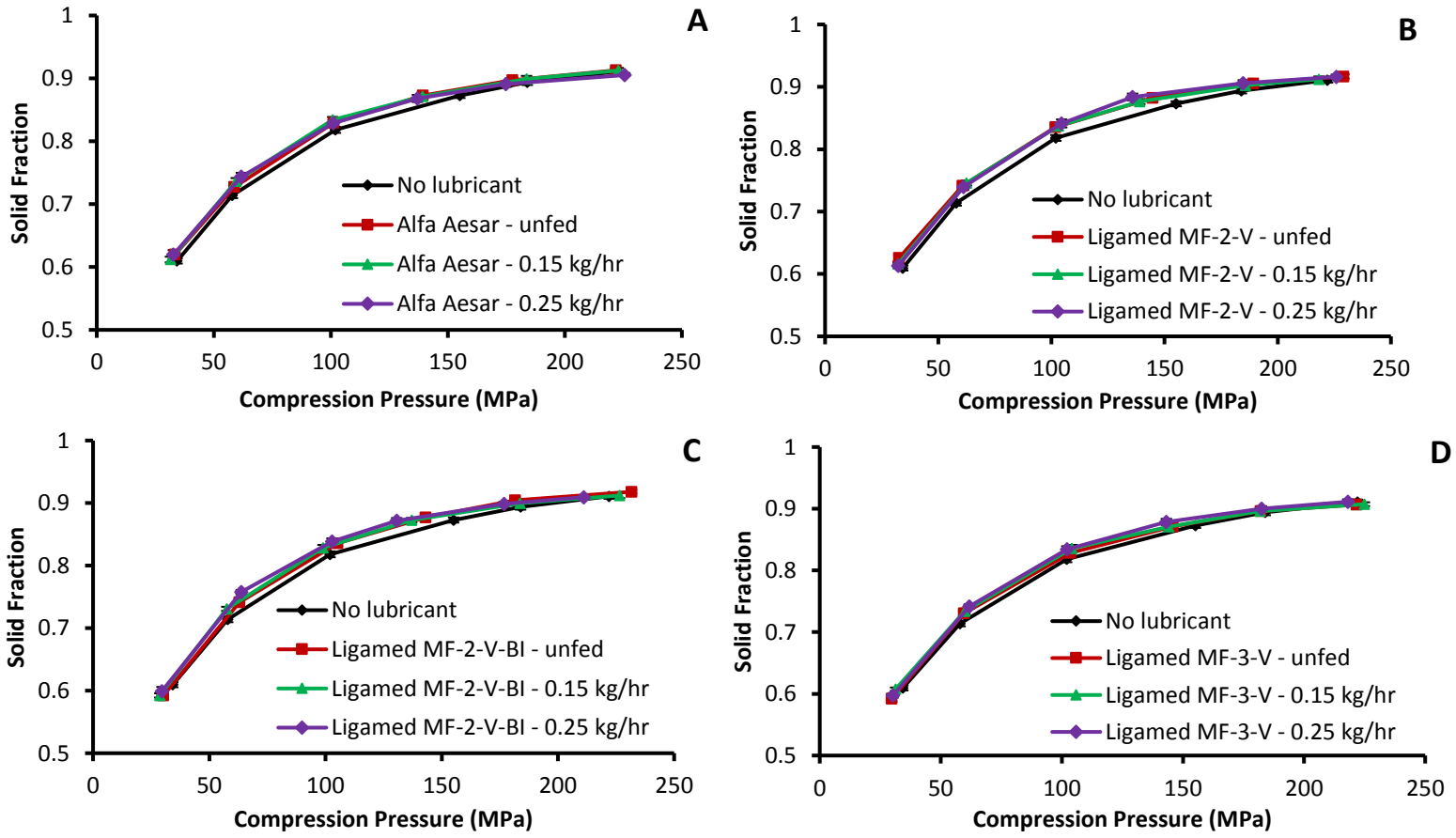


Figure 4.11 Compressibility profiles of tablets with four grades of magnesium stearate (A) Alfa Aesar (B) Ligamed MF-2-V (C) Ligamed MF-2-V-BI and (D) Ligamed MF-3-V. Average values shown n = 20, y error bars indicate standard deviation.

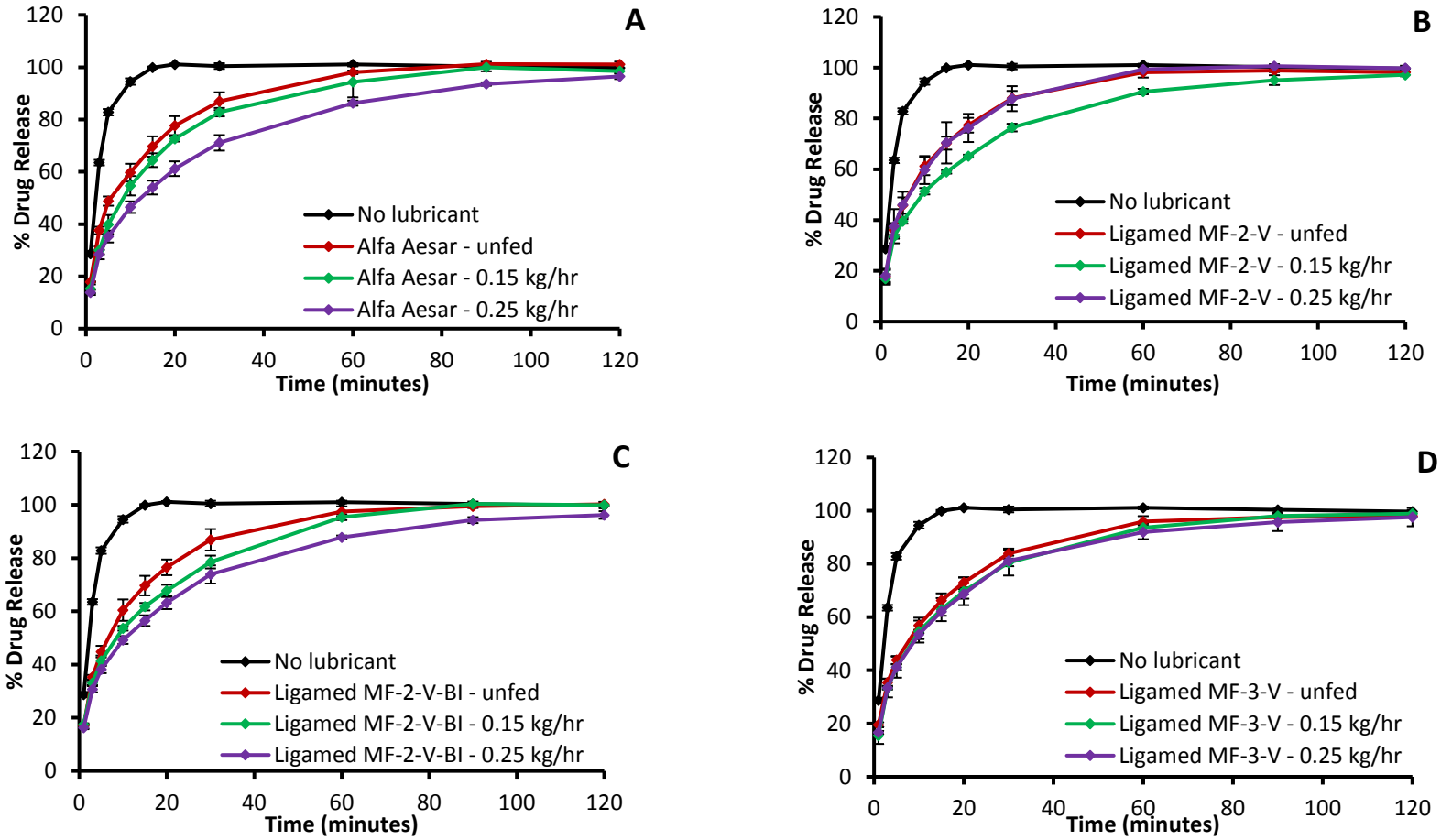


Figure 4.12 Effect of fed MgSt samples on dissolution profiles of Paracetamol tablets produced at 2 MPa and tested in water at 37°C. (A) Alfa Aesar (B) Ligamed MF-2-V (C) Ligamed MF-2-V-BI and (D) Ligamed MF-3-V. Average values shown n = 3, y error bars indicate standard

Table 4.6 Tukey's multiple comparison tests for dissolution profiles of paracetamol tablets prepared with different MgSt samples

Not compared

Sample	Feed rate (kg/hr)	0.15	0.25
		Alfa Aesar	
Alfa Aesar	Unfed	*	***
	0.15		***
Ligamed MF-2-V		Ligamed MF-2-V	
	Unfed	***	NS
	0.15		***
Ligamed MF-2-V-BI		Ligamed MF-2-V-BI	
	Unfed	*	***
	0.15		**
Ligamed MF-3-V		Ligamed MF-3-V	
	Unfed	***	***
	0.15		NS

Where, * represents p≤0.05, ** represents p≤0.01, *** represents p≤0.001 and **** represents p≤0.0001.

Percentage drug release was significantly reduced, when unfed and fed MgSt grades of Alfa Aesar and Ligamed MF-2-V-BI were used as lubricants in tablet formulations. This significant reduction was higher when the formulations are prepared with lubricant samples fed at higher feed rate 0.25 kg/hr (Figure 4.12A and C). No differences in dissolution profiles were observed between formulations with Ligamed MF-2-V unfed and fed at 0.25 kg/hr, whereas formulation containing 0.15 kg/hr fed Ligamed MF-2-V showed significant reduction in drug release (Figure 4.12B). Formulations with Ligamed MF-3-V as lubricant showed a significant reduction in drug release when fed samples were used. However, this difference was not further observed, when samples fed at different feed rates were incorporated in the blends (Figure 4.12D).

4.4 Discussion

The initial study with Alfa Aesar demonstrated the variability of feeding due to processing variables related to the feeder configuration. The feeding set up was optimised using CCS and FCS with different screen settings, showed the impact that these processing variables have an impact on the feed rate % RSD (Figure 4.4). CCS showed lower RSD compared to FCS; this was possibly due to the CCS possessing the wider pockets facilitating the mass flow of MgSt due to its cohesiveness. The impact of feed rate was also seen with, a higher feed rate resulting in lower RSD due to lower residence time of MgSt within screws (Engisch and Muzzio, 2014).

Four different grades of MgSt chosen for this study were different in bulk density, surface area, particle size, flow properties, crystallinity and thermal properties as discussed in chapter-3. Comparing across all four grades, the variability of the materials on feeding performance was quite evident. Bulk density of the materials was shown to be directly related to the feed factor achieved for each grade of MgSt (Figure 4.5). All MgSt samples showed higher feed rate variability at a lower feed rate of 0.15 kg/hr, this effect was more pronounced in Ligamed MF-2-V and Ligamed MF-3-V. Though Ligamed MF-2-V and Ligamed MF-2-V-BI have similar properties they differed in feeding performance (Figure 4.6).

Among the 4 grades of MgSt, particle size of Ligamed MF-2-V was most affected by feeding and Ligamed MF-2-V-BI was least effected by feeding, though they have similar properties. No real differences were seen in tabletability of formulations with fed and unfed lubricants. Differences were only seen at higher compression pressures for Ligamed MF-2-V and Ligamed MF-3-V (Figure 4.9). Inclusion of fed

lubricants (all four grades) in formulations showed reduced compactibility between 50 and 175 MPa of compression pressure compared to formulations with unfed lubricants (Figure 4.10). Inclusion of fed lubricants did not show any effect on the compressibility of the formulations (Figure 4.11).

As discussed in earlier chapter-3, presence of lubricants showed significant decrease in drug release. In this chapter, the effect of fed lubricants on drug release was studied and a significant decrease in the percentage drug release was observed by inclusion of fed lubricants in formulations (Figure 4.12). Inclusion of fed lubricants of Alfa Aesar and Ligamed MF-2-V-BI showed significant reduction in drug release, but it was difficult to attribute this effect as a result of reduction in particle size due to feeding. With respect to D50 of the samples measured at 1.5 bar pressure, feeding at two different feed rates did not show any significant effect on the particle size reduction (Figure 4.7). Lubricant samples (Alfa Aesar and Ligamed MF-2-V-BI) that showed reduction in drug release, did show a significant reduction in particle size reduction, when the feed rate was increased, however reduction was much greater for Alfa Aesar compacted to Ligamed MF-2-V-BI.

Greater decrease in the particle size was observed when Ligamed MF-2-V was fed at 0.15 kg/hr and inclusion of this sample in tablets showed delayed drug release compared to the tablets with unfed and 0.25 kg/hr fed Ligamed MF-2-V lubricant (Figure 4.12B). Significant reductions were seen in the D50 and D90 of Ligamed MF-3-V due to feeding and no significant change between different feed rates, with no effect on D10 (Figure 4.7). Tablets prepared with fed Ligamed MF-3-V showed significant decrease in percentage drug release compared to tablets with unfed MF-

3-V as lubricant (Figure 4.12D and Table 4.6). A study by Kato et al. showed that tablet quality properties become more affected by the effects of over blending, if the D50 of the MgSt is 10µm or less, particularly 5µm or less (Kato et al., 2005). In this chapter, all the samples studied had an initial D50 in the range of 5.75 – 8.93 µm when measured at standard titration pressure of 1.5 bar and for all samples majority of particles were above 5 µm. Therefore it was difficult to attribute the slight reduction in dissolution of the tablets with fed lubricants observed to any decrease in particle size of the samples determined. For these formulations with paracetamol as API, the reduction in the dissolution was minimal and would not have any further impact in the efficacy of the paracetamol *in-vivo.*

4.5 Conclusions

The four grades of MgSt investigated showed differing solid state properties and their physical attributes were shown to impact on gravimetric powder feeding behaviour. For the experimental set-up in this study the sample bulk density determined the FF achieved. Feed variability was influenced by the feed rate set point. Greater variability was observed between samples at the lower feeding rate. Ligamed MF-2-V was most effected by feeding and Ligamed MF-2-V-BI was least effected by feeding. Alfa Aesar, Ligamed MF-2-V and Ligamed MF-2-V-BI, when fed at different feed rates, affected the drug release. Fed samples of MF-3-V did not show any effect on tablet dissolution. The results of this chapter were limited to four different grades of MgSt, which clearly demonstrate the requirement to fully understand the properties of lubricants used and how they impact the pharmaceutical continuous processing.

The objective of the next chapter-5 was to understand the continuous feeding behaviour of tablet blends through K-Tron MT12 feeder and applicability of BARDS, to study the wettability of lubricated blends following continuous feeding.

Chapter 5

Broadband Acoustic Resonance Dissolution Spectroscopy (BARDS) Analysis of Lubricated Blends

(*Results from this chapter were published in Peddapatla et al., 2018.*)

Peddapatla, R.V.G., Ahmed, M.R., Blackshields, C.A., Sousa-Gallagher, M.J., McSweeney, S., Kruse, J., Crean, A.M., Fitzpatrick, D., (2018). Broadband Acoustic Resonance Dissolution Spectroscopy (BARDS): A Novel Approach to Investigate the Wettability of Pharmaceutical Powder Blends. Mol. Pharm. 15, 31–39. https://doi.org/10.1021/acs.molpharmaceut.7b00658

5. BARDS Analysis of Lubricated Blends

5.1 Introduction

In chapter - 4, the continuous feeding behaviour of four grades of MgSt and effect of fed MgSt samples on tablet properties was studied. In this chapter, applicability of BARDS, to detect differences in the distribution of powder lubricant within pharmaceutical powder blends following continuous feeding of blends is investigated.

BARDS works on the principle of frequency change of acoustic resonances that are mechanically provoked in a solvent using a stirrer bar when a solute is added (Fitzpatrick et al., 2012a). The acoustic resonances correlate with the compressibility of the solvent system with or without solute. When a powder is introduced into a solvent it introduces gas (air) into the solvent, which changes the compressibility of the solvent. As the powder is wetted or dissolved, the associated gas is eliminated and solvent compressibility returns to a steady state. The acoustic resonance generated depends on different physical and chemical parameters of the powder that is added into the solvent. BARDS monitors the acoustic profile of solvent as a powder disperses and dissolves. It correlates the acoustic profile of the solvent to changes in the compressibility of the solvent as a result of powder dispersion and dissolution within the solvent (Fitzpatrick et al., 2012a, 2012b).

BARDS Spectrometer consists of a dissolution vessel equipped with a magnetic stirrer and a micro-phone set above the dissolution vessel, which receives and records the responses from the vessel. There is access at the front of the dissolution vessel and a tripper motor with a weighing boat on it to introduce the sample into

the dissolution medium. The glass tumbler containing 25 mL of deionised water is placed on the stirrer plate. The stirrer motor underneath is positioned so as to allow the magnetic stirrer bar to gently tap the inner glass wall, which will act as the source of broadband acoustic excitation. This will induce various acoustic resonances in the glass, liquid and the air column above the liquid. The audio is sampled at a rate of 44.1 kHz. The resonances of the liquid vessel are recorded in a frequency band of 0-20 kHz. A frequency time course is generated as shown in Figure 5.1.

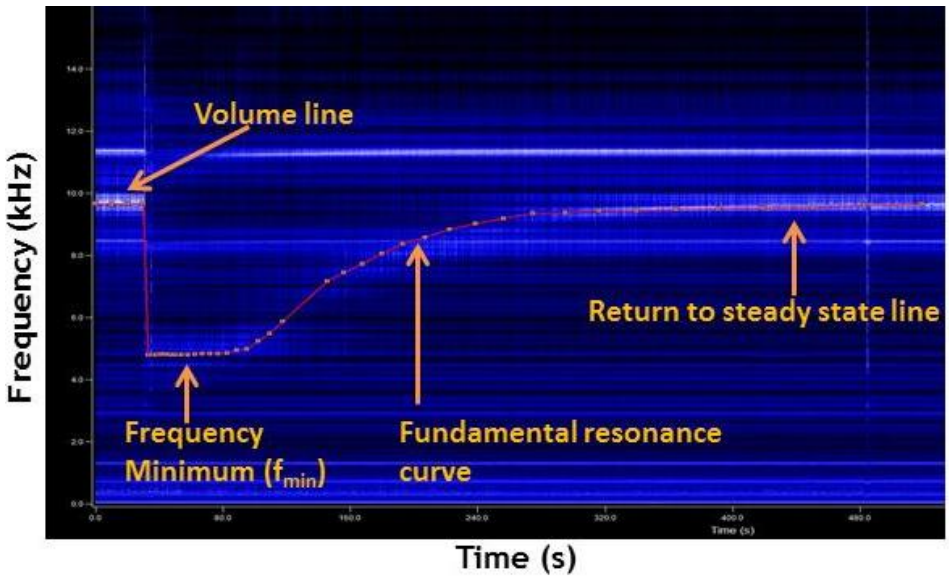


Figure 5.1 Representative BARDS raw spectrum of 250 mg MCC in 25 mL water

Acoustic spectra are characterized by specific nomenclature. The first 30 seconds of the spectrum corresponds to steady state resonances of vessel 10 kHz as shown as volume line in Figure 5.1. When the sample is tipped into the solvent at the 30 second time point, a decrease of resonance frequencies due to a change in the velocity of sound is observed. This resonance line is called the fundamental curve

(Fitzpatrick et al., 2012a). The time taken to reach the frequency minimum (f_{min}) is designated as Δt. The time for which the response maintains f_{min} is known as the lag phase. The approximate time taken for the fundamental curve to progress from f_{min} to steady state is designated as ΔT. In this study all the time points shown are specific to each phase of the acoustic response. Lag phase and ΔT were used to identify the degree of wetting of the individual powders and blends (Evans-Hurson et al., 2016; Fitzpatrick et al., 2014; Vos et al., 2016)

Fitzpatrick et al. successfully demonstrated the differences between various chemical compounds and commercially available pharmaceutical powder blend products using BARDS (Fitzpatrick et al., 2013, 2012b). Another study by Fitzpatrick et al. showed that the BARDS was able to discriminate the distinctive acoustic signature profiles of the enteric coated core spheres of varying size distributions as they dissolve in acoustic media (Fitzpatrick et al., 2014). A study by Evans Hurson et al. showed that the dissolution rate of enteric coated drug spheres depended on the pH of the BARDS dissolution media (Evans-Hurson et al., 2016). A recent study by Vos *et al.* showed the potential of BARDS to detect the transfer of water into milk protein concentrate (MPC) powder particles with different rehydration characteristics (Vos et al., 2016). The work presented in this chapter focuses on demonstrating the ability of BARDS to detect the degree of lubrication within tablet blends. The distribution of a hydrophobic lubricant, such as MgSt, in tablet blends is a critical formulation factor due to its capability to alter the wetting behaviour of MCC and API within the blend and hence drug dissolution.

5.2 Aim and objectives

The main aim of this study was to demonstrate the ability of BARDS to detect differences in lubricant distribution in powder blends. The blends compared using the BARDS technique were of equivalent composition but prepared under a range of processing conditions.

Main objectives of this chapter are:

- To analyse the functionality of BARDS technique to detect the wetting behaviour of MCC, MgSt (Alfa Aesar grade) and a model API (metoclopramide hydrochloride) as single components.
- To determine the ability of BARDS to differentiate between unlubricated and lubricated blends containing MCC, MgSt (Alfa Aesar grade) and a model API (metoclopramide hydrochloride).
- To determine the ability of BARDS to detect differences in the distribution of MgSt within blends generated using K-Tron MT12 LIW feeder.
- To compare the ability of BARDS to detect differences in the blends wetting behaviour of blends with more widely reported wetting measurement techniques such as contact angle and wetting time.

5.3 Results

5.3.1 Preliminary BARDS studies – proof of concept

The BARDS acoustic spectra of the individual blend components, 25 mg of metoclopramide 225 mg of MCC, and 250 mg of a metoclopramide HCl/MCC blend are shown in Figure 5.2. Table 5.1 details the lag times and steady state time points for the individual components and blends. All samples were added to 25 mL water following the period (30 s) of steady state resonance. The acoustic response generated for MgSt upon addition to water was a straight line without any frequency decrease (acoustic spectra shown in supplementary information, Figure – S3). The MgSt sample did not disperse in water due to its hydrophobic nature. Hence no air was introduced into the water and no change in resonance frequency was observed. There was a slight frequency decrease of 0.3 kHz for metoclopramide HCl samples and gradual return to steady state after approx. 50 s as shown in Figure 5.2. The acoustic profile after addition of metoclopramide was a V-shaped response to f_{min}, which is a good indication of trapped and adhered gases that are introduced into the solvent with a fast gas release. The frequency change was sustained only for a short period of approx. 15 s due to the high solubility and rapid dissolution of metoclopramide hydrochloride in water.

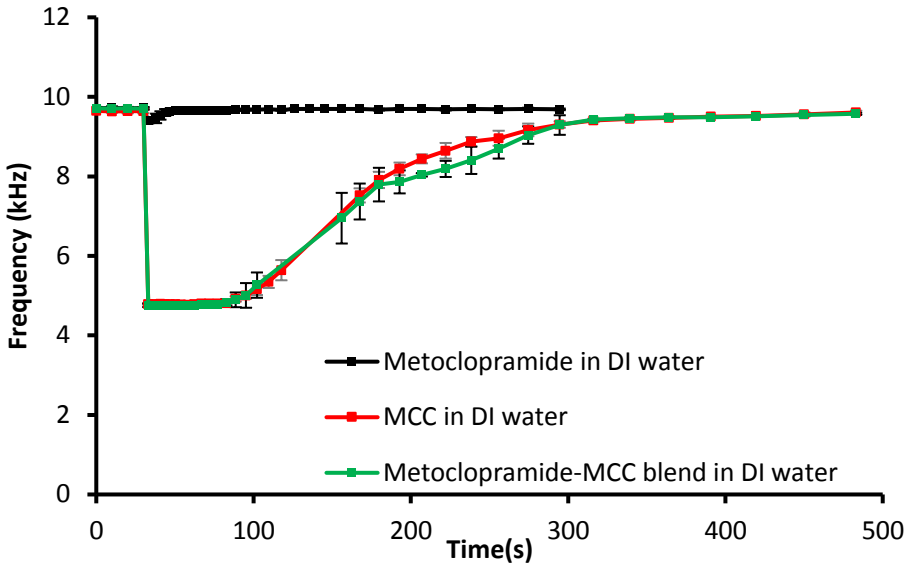


Figure 5.2 BARDS acoustic response of Metoclopramide (25mg), MCC (225 mg) and blend of metoclopramide (10% w/w) and MCC (90% w/w) (250 mg) in 25 mL deionised water (DI). Average values shown, n =3, y error bars indicate standard deviation

In contrast, the frequency of MCC and metoclopramide/MCC blend was decreased to approx. 5 kHz and sustained a lag time up to approx. 80 s after sample addition was observed. Both the spectra gradually returned to steady state (ΔT) at approx. 310 s (Table 5.1), with a slight deflection of acoustic response for metoclopramide/MCC blend in the range of 190 – 270 s (Figure 5.2). The U-shaped acoustic response of the MCC and metoclopramide/MCC blend indicates the gas oversaturation in the solvent (Fitzpatrick et al., 2012a). The greater frequency decrease observed for MCC, compared to metoclopramide, relates to the larger sample weight and hence the volume of entrained gas introduced. MCC does not dissolve in water but hydrates in water resulting in the prolonged lag time.

Figure 5.3 shows the BARDS profiles of metoclopramide/MCC lubricated and unlubricated blends after varied degrees of manual rotation. The blend frequency decreases to a f_{min} of approx. 5 kHz for all blends. The frequency is sustained at f_{min} for approx. 120 s and 145 s for the lubricated blends prepared at 5 rotations and 100 rotations respectively, which is designated as lag phase (start of f_{min} to finish of f_{min}). This differentiates the effect of lubricant presence and blending time on the lag time. In contrast the unlubricated blend lag phase was sustained for approx. 80 s. Similarly the time taken to return to steady state resonance (ΔT) was approx. 600 s for the lubricated blend rotated 5 times and approx. 800 s for 100 times rotated blend Figure 5.3 and Table 5.1. The notable shift in the lag times and the time taken to return to steady state was attributed to the increased coating of metoclopramide and MCC with hydrophobic MgSt which delayed the wetting of the blend and hence displacement of gas from powder to water phase.

This phenomenon of powder lubricants retarding the wetting and dissolution of blend components is a commonly observed effect of MgSt when over blended (Duong et al., 2017; Gupta et al., 2009a; Rao et al., 2005). The end of lag time signifies the starting point of wetting of blends, which is similar to the results obtained by Hurson *et al.,* on enteric coated drug spheres (Evans-Hurson et al., 2016). Lag time can be potentially used to indicate the coating thickness or the degree of lubrication of the blends by hydrophobic MgSt and the start of return to steady state frequency can be related to the wetting of blend and outgassing of the oversaturated gases. The results of this preliminary proof of concept study demonstrated the potential of BARDS to detect differences in the wetting of blends due to the presence of MgSt and the degree of blending of MgSt.

Table 5.1 BARDS profile lag times and time to return to steady state for metoclopramide, MCC, blend of metoclopramide – MCC, and blend of metoclopramide-MCC-MgSt prepared by manual rotation.

Components	Approx. Lag time (s)	Approx. Time to return to steady state (s)
Metoclopramide	Not observed	50
MCC	80	310
Metoclopramide/MCC (5 rotations)	80	310
Metoclopramide/MCC/MgSt (5 rotations)	120	600
Metoclopramide/MCC/MgSt (100 rotations)	145	800

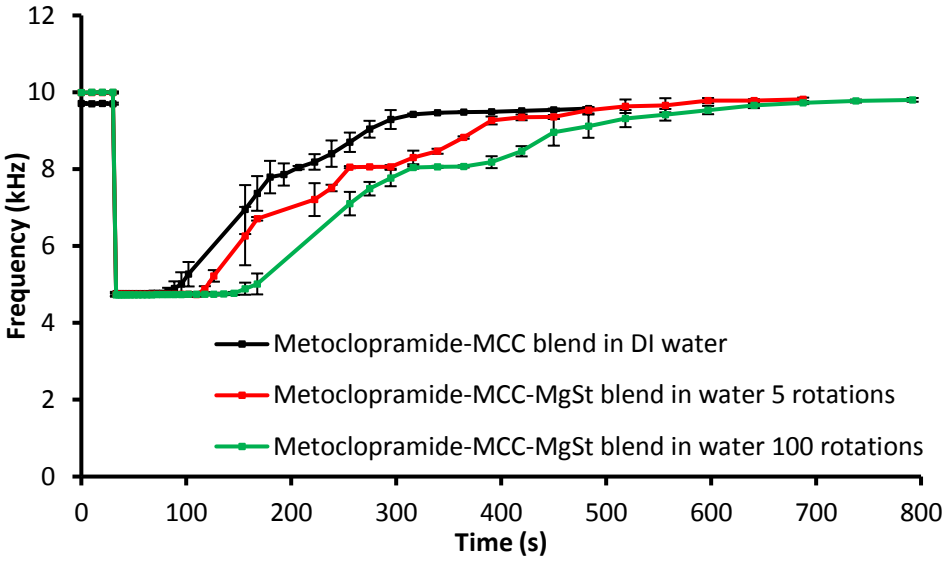


Figure 5.3 BARDS acoustic response for blends manually blended in 25 mL deionised water. Metoclopramide 10% w/w and MCC 90% w/w (250mg) after 5 rotations, metoclopramide 10% w/w, MCC 89.5% w/w and 0.5% w/w MgSt (250mg) after 5 rotations and after 100 rotations. Average values shown, n =3, y error bars indicate standard deviation.

5.3.2 Comparison of unlubricated and lubricated formulations by BARDS

Following on from the preliminary proof of concept study, the ability of BARDS to detect differences in the wetting behavior of lubricated and unlubricated blends prepared using a lab scale double cone blender and subsequently fed at different feed rates through a LIW screw feeder (K-Tron MT12) was assessed.

5.3.2.1 BARDS analysis of blends prior to feeding

Figure 5.4 shows the BARDS profiles of unlubricated and lubricated formulations, prior to feeding collected from blender immediately after blending, from six different locations. Following addition of the sample to water there was a decrease to a plateau frequency of approx. 5 kHz after 30 s. Unlubricated blend (API/MCC) showed a lag time of approx. 80s and lubricated blend (API/MCC/MgSt) showed a lag time of approx. 100 s. The lag phase indicates that the rate of gas evolution in the water phase is equal to the rate of gas loss from the water phase. The disappearance of gas from the solvent after f_{min} proceeded more slowly for lubricated blend, which resulted in notable extension in time of approx. 640 s for acoustic resonance to return to steady state, whereas for unlubricated blend it was found to be approx. 450 s. The differences between acoustic responses between the two blend formulations as shown in Figure 5.3 and Figure 5.4, is mainly due to the volume of gas introduced into the solvent after blend sample addition, the amount of gas generated, the rate of gas released from the blend and the rate of gas eliminated from the solvent during the wetting of unlubricated and lubricated formulations. All these parameters were examined in depth by determining the changes in gas volumes using equation 6.

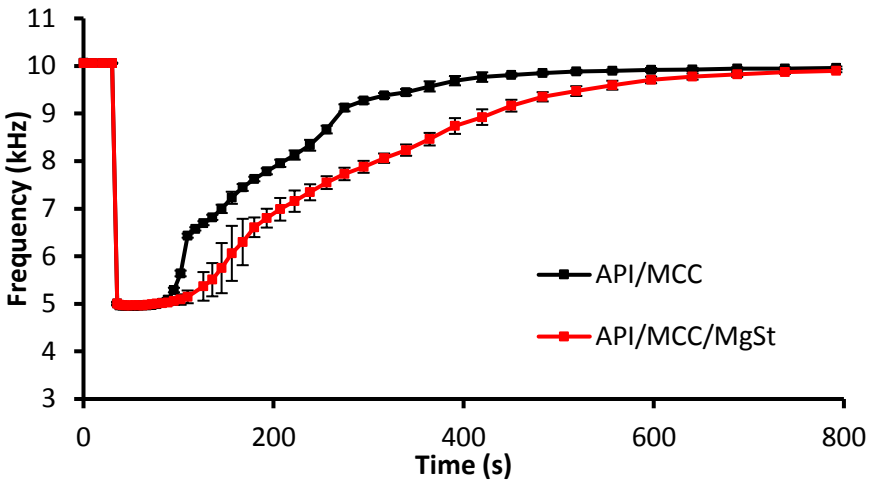


Figure 5.4 BARDS acoustic response for blends prepared using lab scale blender in 25 mL deionised water. Unlubricated blend (metoclopramide 10% w/w and MCC 90% w/w) (250mg) and lubricated blend (metoclopramide 10% w/w, MCC 89.5% w/w and 0.5% w/w MgSt) (250mg). Samples analysed were collected from 6 different locations in the blender and analysed in duplicate. Average values shown, n =12, y error bars indicate standard deviation.

Equation 6 was applied to BARDS frequency data to analyze the fractional gas volume (fa) occupied by compressible gas following the introduction of powder samples and during the wetting of the formulations. Both formulations quickly immersed when added into the water and reached a constant gas volume which lasted for a lag phase of approx. 45 s and 65 s for unlubricated and lubricated formulations respectively, Figure 5.5A. The curves represent an evolution and gas release from the water surface. No difference in the gas evolution following the addition of sample into the water was noted between the formulations. However, the release of gas from the water following sample addition was extended in the lubricated blend data.

Figure 5.5A is plotted in a logarithmic scale as shown in Figure 5.5B. The gas or air elimination rate constant (k) for the compressible gas in solution was assumed to be a first order process and was determined from the descending slope of the log plots shown in Figure 5.5B

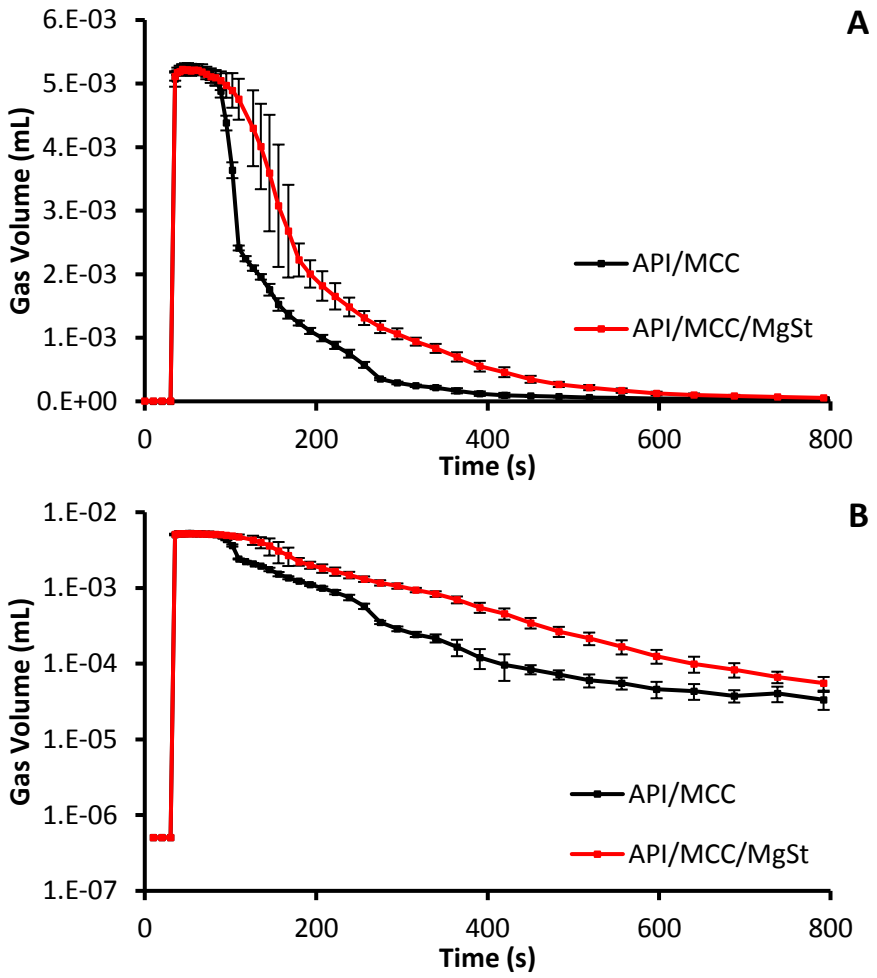


Figure 5.5 Gas volume plots for blends prepared using lab scale blender in 25 mL deionised water. (A) Plot of calculated gas volume versus time and (B) Plot of log of calculated gas volume versus time for unlubricated (API/MCC) and lubricated blends (API/MCC/MgSt). Samples analysed were collected from 6 different locations in the blender and analysed in duplicate. Average values shown, n =12, y error bars indicate standard deviation.

Table 5.2 shows the gas elimination rate constants (*k)* and the time range for which this constant is calculated. The gas elimination rate constants calculated for all samples of unlubricated blend were consistent ($k \approx 1 \times 10^{-5}$ s^{-1}), whereas the presence of MgSt in lubricated formulation resulted in a reduction in gas elimination constant ($k \approx 7 – 8 \times 10^{-6}$ s^{-1}), and greater variability between samples.

This result is generally in agreement with the previous study on milk protein powder concentrates (Vos et al., 2016). The slow gas generation of lubricated blends strongly inhibits hydration of the powder. In order to validate this hypothesis, these blends were fed through K-Tron MT12 loss in weight feeder, to obtain blends of varying degrees of lubrication to determine the influence of increased distribution of MgSt in blends on the BARDS acoustic response. These blends were also analysed for tabletability, wetting time and contact angle measurements which are more recognized methods to determine degree of lubrication on blend hydration (Pabari and Ramtoola, 2012; Rajpurohit et al., 2011).

Table 5.2 Calculated gas volume elimination rate constant (*k*) and time ranges used for the calculation of the rate constant for samples of unlubricated and lubricated blend formulations. Samples were taken from various locations in the lab scale blender.

Blend Location	**Unlubricated blend**		**Lubricated blend**	
	Time range (s)	***k* (s^{-1})**	**Time range (s)**	***k* (s^{-1})**
Top – 1	95-390	1.E-05	109-556	8.E-06
Top – 2	95-390	1.E-05	167-556	7.E-06
Top – 3	95-390	1.E-05	109-556	8.E-06
Bottom – 1	95-390	1.E-05	109-556	8.E-06
Bottom – 2	95-390	1.E-05	156-556	7.E-06
Bottom – 3	95-390	1.E-05	126-556	8.E-06

5.3.2.2 Feeding of blends through K-Tron MT12 feeder

Unlubricated and lubricated blends were each fed through a K-TRON MT-12 twin screw micro-feeder to achieve different levels of MgSt distribution within blends in a controlled manner. The feeder set up used in this study comprised of a FCS and FSqS, with the objective of minimizing MgSt build-up on screws, feeding rate of blends and promote over-lubrication of blends. The FF is the theoretical 100% feed rate that can be achieved with a given set of tooling and material and was determined through equipment calibration. The FF determined for both blends was 1.11 kg/hr for unlubricated blend and 2.41 kg/hr for lubricated blend. The feed rate set points were set for 20% (0.2238 kg/hr), 50% (0.5594 kg/hr) and 90% (1.006kg/hr) of the feed factor for the unlubricated blend. The same feed rates were used for lubricated blend for direct comparison. Figure 5.6 shows image of

two blends at three different feed rates. Figure 5.6A shows feeding behaviour of unlubricated blend and lubricated blend through FCS. It was visually evident that some of the powder adhered to the feeder outlet while feeding lubricated blend, this is may be due to the electrostatic properties of MgSt. Figure 5.6B shows the post feeding assessment of screws, in which unlubricated blend is adhered within screws and no such behaviour is noticed with lubricated blend.

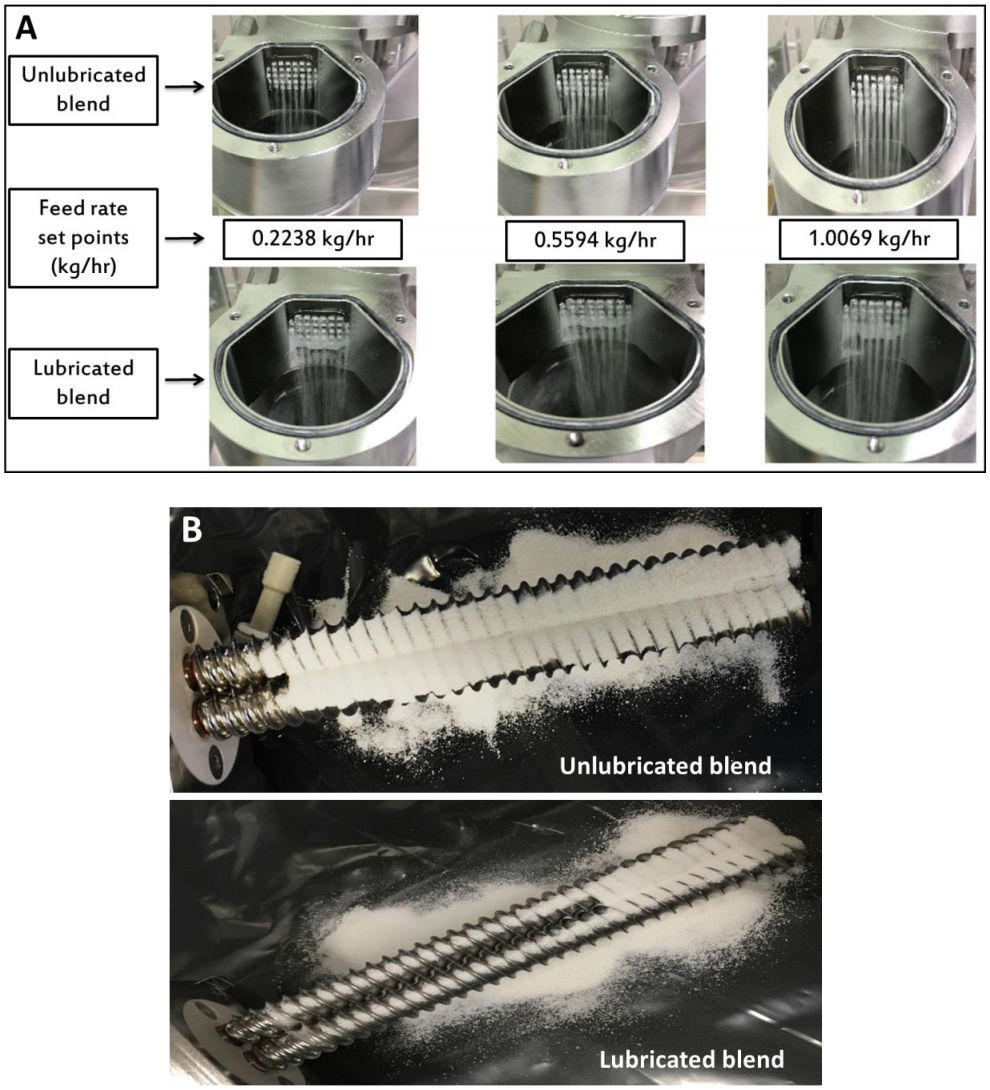


Figure 5.6 Feeding of unlubricated and lubricated blend (A) Image of blends during feeding at three different feed rates and (B) Post feeding assessment of screws.

Figure 5.7 shows the performance data of K-TRON MT12 feeder for unlubricated and lubricated blends. As the feed rate increased, the feeder performance (% RSD weight) decreased for both blends. The lubricated blend demonstrated lower %RSD compared to unlubricated blend at three feed rates. For both blend formulations, lowest feed rate of 0.2238 kg/hr showed highest %RSD. Drive command (%) of the feeder is the value that indicates how much of the controller output is used or required to deliver indicated actual mass flow value (feed rate set point). Drive command during feeding of unlubricated blend at three different feed rates was found to be approx. 20, 50 and 90%. The drive command halved (10%, 25% and 45%) during the feeding of lubricated blend. This may be due to the effect of lubricant on screws. The ability of MgSt to reduce the shear stress in contact with metal objects was observed in the Brookfield flow results of chapter 3. These blends fed through the feeder are further compacted into tablets and tabletability was analysed to see the effect of lubricant in these blends on tablets due to feeding.

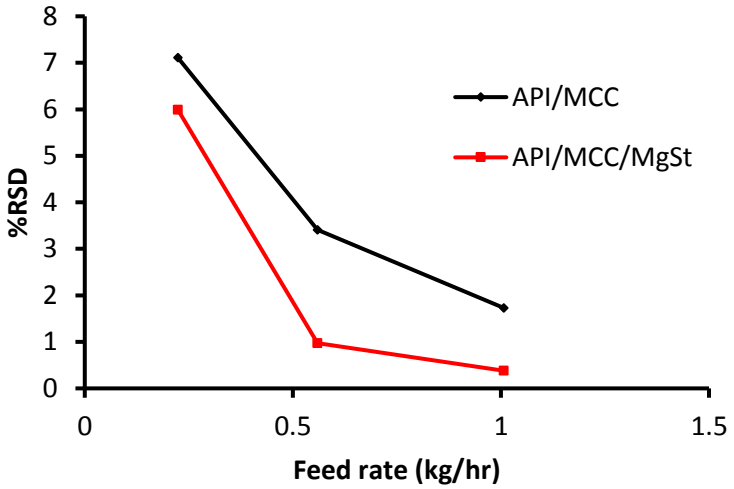


Figure 5.7 Feeding performance of unlubricated blend (API/MCC) and lubricated blends (API/MCC/MgSt) at different feed rates through K-Tron MT12 feeder.

5.3.2.3 Tabletability of blends fed through K-Tron MT12 feeder

Tabletability profiles of unlubricated and lubricated blends fed through MT-12 feeder are shown in Figure 5.8. Tabletability is represented by a plot of tensile strength versus compaction pressure. As the compression pressure increased tablet tensile strength increased. The unlubricated blend fed at three different feed rates did not show any significant effect on tabletability. However, lubricated blend was more affected by feeding. As the feed rate was increased, the tabletability decreased resulting in a reduction in tablet hardness (Figure 5.8). This data demonstrates that the feeding affected the distribution of MgSt in the lubricated blend which resulted in a lower tensile strength of the tablets from this blend as the feed rate increased. This behaviour indicates overlubrication.

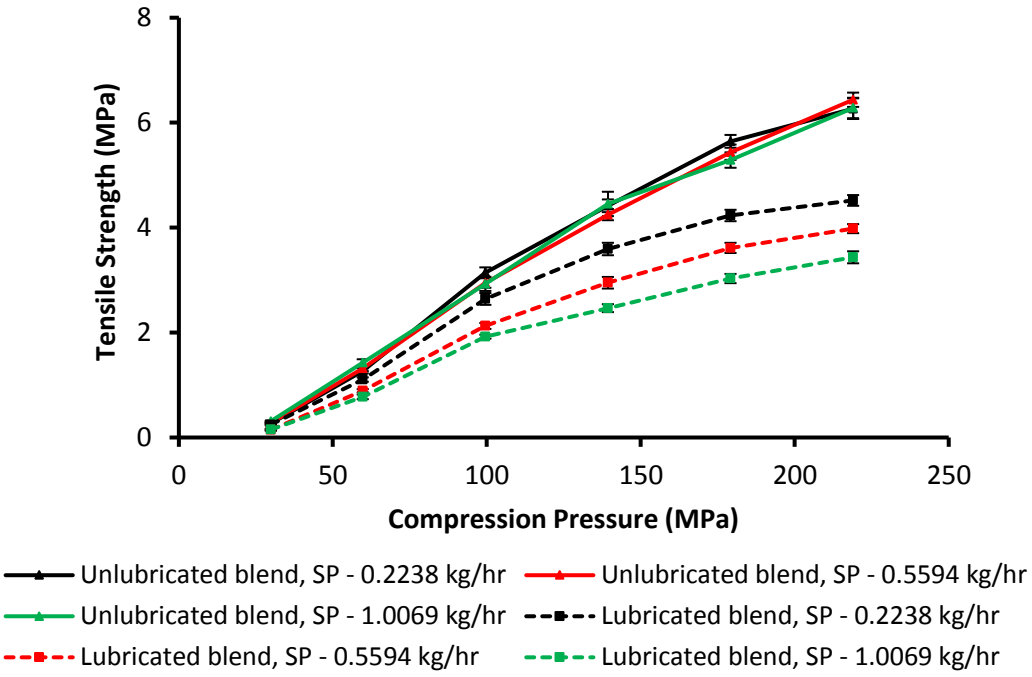


Figure 5.8 Tabletability profiles of unlubricated and lubricated blend fed at different feed rates and compacted at a range of compression pressures. Average values shown, n=20 at each compression pressure, y error bars indicate standard deviation. (Feed rate SP = Set point).

5.3.2.4 BARDS analysis of blends following to feeding

The overlubrication of the lubricated blends was confirmed by analysing the tabletability of the fed blends (Figure 5.8). The subsequent objective was to demonstrate differences in the wetting behaviour of lubricated blends with equivalent lubricant composition but different degrees of lubricant distribution obtained using a feeding system. The hypothesis of this chapter was that the BARDS technique could detect differences in blend wetting behaviour related to the degree of lubrication.

The unlubricated blend was unaffected by feed rate when analysed by BARDS as shown in Figure 5.9A. The lag phase lasted for approx. 90 s and the acoustic response reached steady state after approx. 420s as shown in Figure 5.9A. In contrast, lubricated blend formulation showed a slight extension in the lag phase as the feed rate increased and all the lubricated blends returned to steady state after approx. 790 s. as shown in Figure 5.9B. The extension in lag phase was attributed to increased coating of the MCC and drug particles with MgSt due to increased feeding rate and hence prolonged wetting as discussed previously.

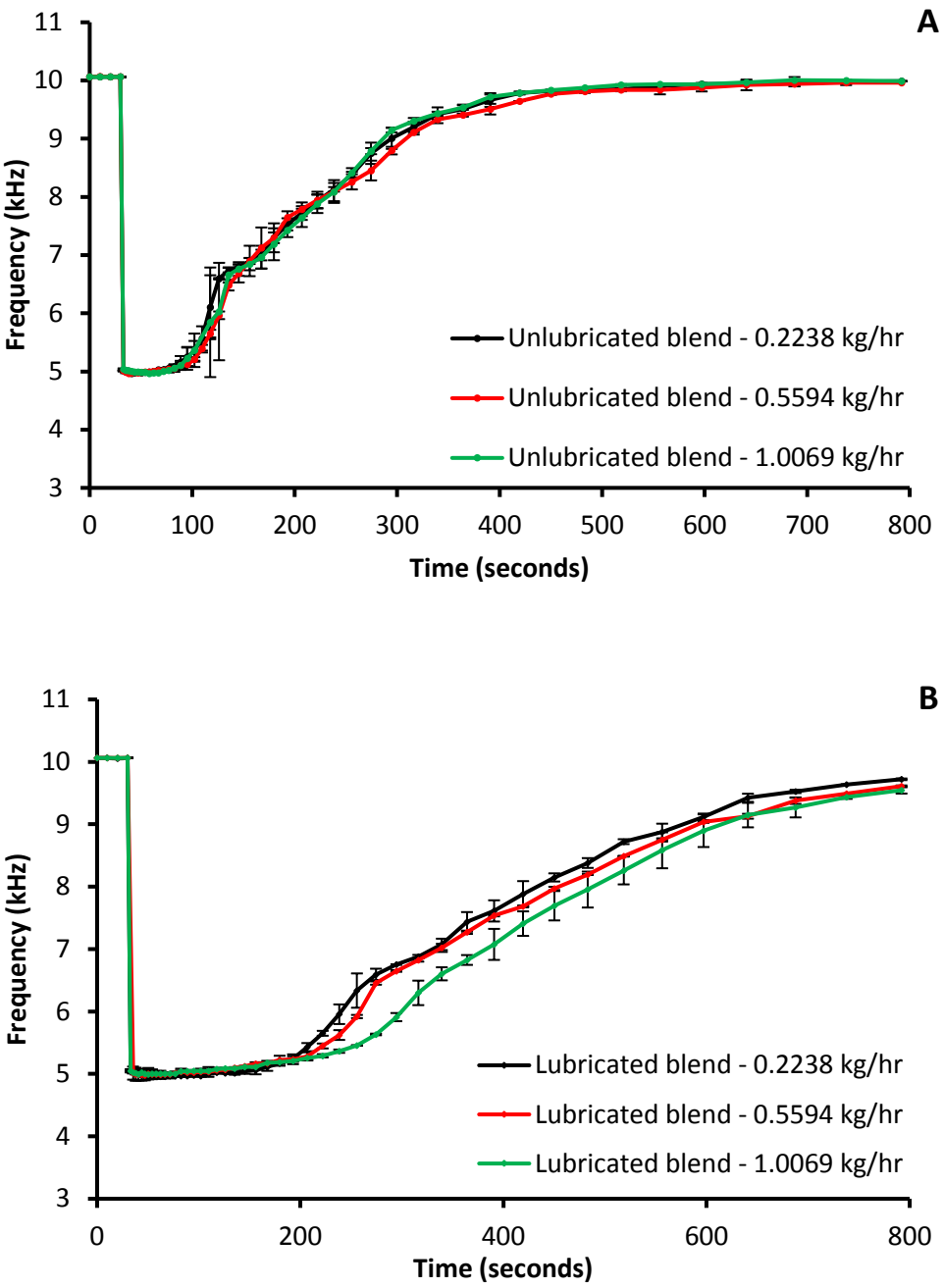


Figure 5.9 BARDS acoustic response for blend samples in 25 mL deionised water. Blends were prepared using lab scale blender and fed at different rates through a screw feeder. (A) Unlubricated blend and (B) Lubricated blend. Average values shown, n =2, y error bars indicate max and min values.

The unlubricated blend when fed at different feed rates, showed constant gas volumes over the time period of approx. 60s, with a relatively rapid gas elimination rate constant thereafter ($k \approx 1.17 - 1.21 \times 10^{-5}\ s^{-1}$), Figure 5.10A and Table 5.3. Lubricated blends show an increase in gas volume during the gas elimination stage with increase in formulation feed rate, Figure 5.10C. Slower gas elimination rate constants were observed for the lubricated blend ($k \approx 5.99 - 6.74 \times 10^{-6}\ s^{-1}$), Table 5.3.

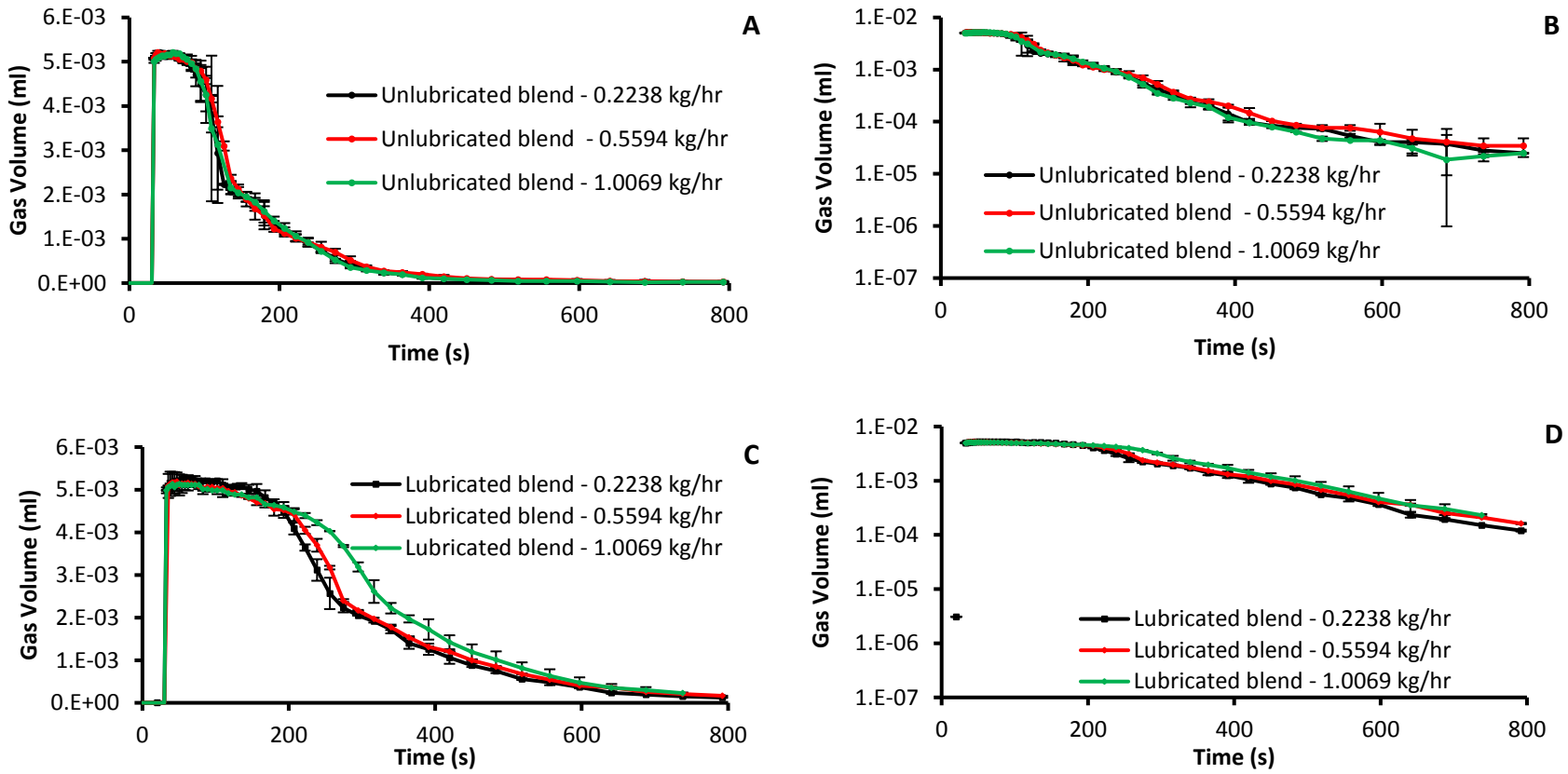


Figure 5.10 Gas volume plots for blends in 25 mL deionised water. Blends were prepared using lab scale blender- and fed at three different rates through a screw feeder. (A) Unlubricated blend plot of calculated gas volume versus time, (B) Unlubricated blend plot of log of calculated gas volume versus time, (C) Lubricated blend plot of calculated gas volume versus time, and (D) Unlubricated blend plot of log of calculated gas volume versus time. Average values shown, n =2, y error bars indicate max and min values.

Table 5.3 Lag time, time to return to steady state, calculated gas volume elimination rate constant (k) and time ranges used for calculation of the constant for samples of unlubricated and lubricated blends.

Feed rate (kg/hr)	Unlubricated blend				Lubricated blend			
	Approx. Lag time (s)	Time to return to steady state (s)	*k* (s^{-1})	Time range (s)	Approx. Lag time (s)	Time to return to steady state (s)	*k* (s^{-1})	Time range (s)
0.2238	90	420	1.17E-05	95-419	210	790	5.99E-06	207-792
0.5594	90	420	1.19E-05	95-419	220	790	6.02E-06	222-792
1.0069	90	420	1.21E-05	95-419	240	790	6.74E-06	255-792

5.3.2.5 Contact angle and wetting time of formulations before and after feeding

Contact angle is a commonly employed technique used to investigate the wetting of powders. When the surface of compacted powder is exposed to a liquid drop, the rate of change of the contact angle is monitored and recorded until the it reaches equilibrium (Ji et al., 2016). In this study, the major diluent used in preparing blends was MCC, which swells upon contact with water (Hattori and Otsuka, 2014). The contact angle reported is the initial angle of contact between compacted powder and water droplet, after the droplet is stabilized. Compacts with similar porosity were prepared for contact angle measurements. Contact angle results are shown in Figure 5.11. It was anticipated that presence of lubricant and degree of distribution of MgSt within tablet blend would delay the wetting of compacts. The compact from unlubricated blend showed a contact angle of approx. 10^0, and the compact from lubricated blend showed a 4 fold increase in the contact angle, which was attributed to the presence of MgSt. The feed rate did not show any effect on the contact angle measurements for compacts of the unlubricated blend as anticipated. However, for compacts of lubricated blend as the feed rate increased the average

contact angle increased but it was not statistically significant, possibly due to variability in measurements. The contact angle method detected differences in wetting behaviour between lubricated and unlubricated blends, however due to inherent test variability the technique was unable to detect differences between lubricated blends fed at different feed rates.

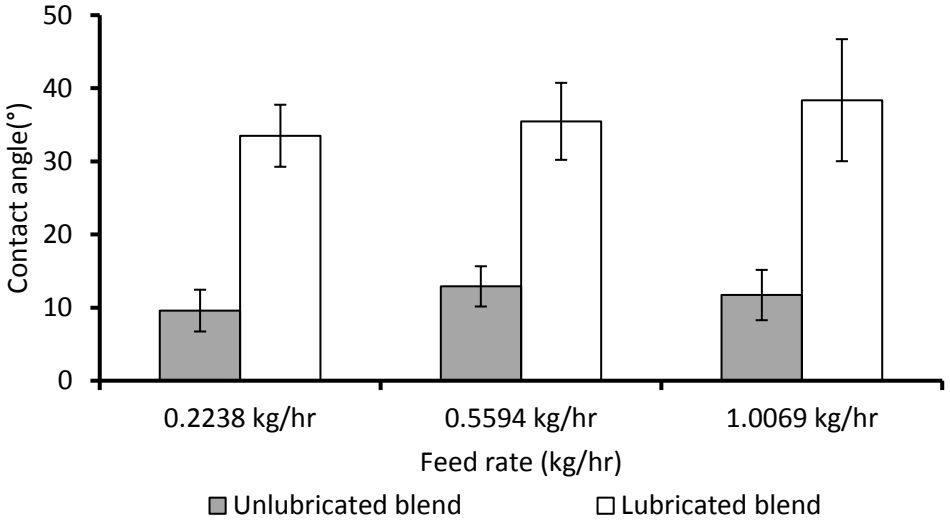


Figure 5.11 Contact angle (^{0}) of deionized water on unlubricated and lubricated blend compacts with similar porosity. Average values shown, n =3, y error bars indicate standard deviation.

The wetting time method is an alternative method that can used to determine the wetting behaviour of powders. Figure 5.12 shows the differences in the wetting time for the unlubricated and lubricated blend compacts of equivalent porosities. An increase in the feed rate was expected to result in an increased degree of lubrication for lubricated blend compacts. However increased feed rate did not show significant differences in wetting times (54.6s ± 0.5 and 52s ± 2.6) between the blends fed at 0.2238 kg/hr and 0.5594 kg/hr respectively. However, lubricated

blend formulation fed at 1.0069 kg/hr, showed an increased wetting time of 74.3 s ± 10.96 s. These results support the attribution of differences in BARDS profiles to differences in blend wetting behavior.

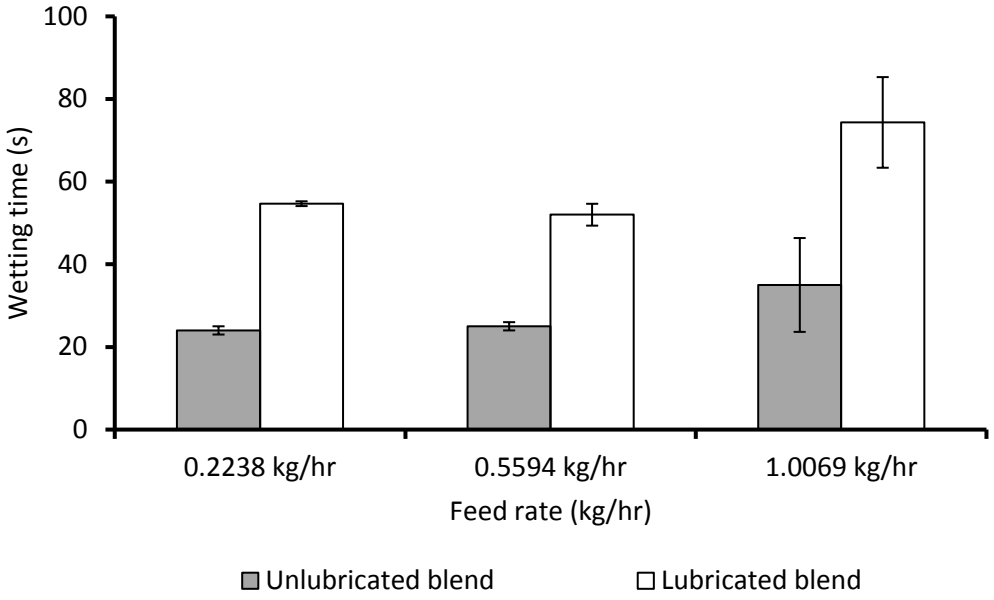


Figure 5.12 Wetting time of blend compacts with aqueous amaranth solution of unlubricated and lubricated blend compacts with similar porosity. Average values shown, n =3, y error bars indicate standard deviation.

Compared to both techniques assessed, the BARDS method was easier to perform and analysed the blends in their powdered form without the need for compaction prior to analysis.

5.4 Discussion

MgSt is one of the most commonly used lubricants in tablet manufacturing and due to its hydrophobic nature, if not properly monitored during blending has the potential to overcoat powders in the blend thereby compromising the tablet quality (Moreton, 2006; Pernenkil and Cooney, 2006). This chapter demonstrated the capability of BARDS to identify differences in wetting behaviour of blends due to different degrees of MgSt distribution, at a fixed MgSt concentration (Figure 5.4). BARDS analysis generated reproducible, qualitative data that could be related to powder wetting in a timeframe suitable for its use as an at-line process analytical technology (PAT) tool. Other PAT tools like near infrared and Raman spectroscopy, have been successfully used to measure the MgSt homogeneity within blends (Lakio et al., 2013), in-line and at-line (Liew et al., 2010; Nakagawa et al., 2013), with the objective of identifying differences in subsequent blend behaviour including hydration. Compared to these techniques, the BARDS method proposed studies blend wetting behaviour by immersion of powder in the liquid system of interest. Previous BARDS hydration studies focused mainly on single component milk protein powders (Vos et al., 2016) here we demonstrated the applicability of BARDS in multi-component pharmaceutical powder blends for the first time and specifically to the study of blend lubrication.

Individual components and blends yield significantly different acoustic profiles specific to the amount of sample and composition of blend as shown in Figure 5.2 and Figure 5.3. Compound solubility has an effect on the acoustic response (Fitzpatrick et al., 2012a). The results demonstrated that a soluble API

(metoclopramide hydrochloride) sustained a short V- shaped frequency change for only very short duration compared to insoluble MCC, which wets but does not dissolve in water. Preliminary testing of blends prepared manually showed notable shift in the acoustic response for blends rotated 100 times compared to blends prepared with 5 rotations. This was further demonstrated by preparing lab scale blends in a controlled manner.

Blends were prepared using V-cone blender, with and without MgSt. Lubricated blends showed extended acoustic response compared to unlubricated blends as shown in Figure 5.4. Equation 6 was used to convert this BARDS frequency data, to generate fractional gas volume (f_a) occupied by the compressible gas during wetting or dissolution of the powders. From this the log plots of gas volume were plotted to calculate the gas elimination rate constants to allow the quantitative comparison of the wetting behavior of powders, which signifies the degree of lubrication caused by MgSt. Unlubricated blend showed faster gas elimination rate constant compared to lubricated blend Table 5.2. These blends were fed through K-Tron MT-12 feeder to get varied distribution of MgSt within lubricated blend. Lubricated blend showed less %RSD compared to unlubricated blend. It was established that the blends were over lubricated as there was a decrease in tensile strength in tablets compacted from lubricated blend, as they were fed at higher feed rates (Figure 5.8). As expected no change in acoustic response was seen for unlubricated blends as the feed rate increased. However in lubricated blends extended acoustic response was seen as the feed rate increased (Figure 5.9).

Results generated in this chapter by BARDS were also compared to more standard wetting techniques of contact angle and wetting time. However, there are some limitations to these techniques. For both methods the powder was compacted prior to analysis in order to achieve reproducible results. The nature of this formulation, in particular the hydrophilic and swelling behavior of MCC, undermines the reproducibility and accuracy of the contact angle technique. However despite these limitations, the contact angle results demonstrated a significant change in the measurements between lubricated and unlubricated formulations. BARDS offers some key advantages compared to traditional techniques; powder can be directly analysed without packing or compacting and the acoustic profile is generated by dispersion of the blend in water, akin to disintegration and dissolution experiments. BARDS experiments require only 25 mL of solvent with 10-300 mg of sample, which greatly minimizes the quantities of powder required in comparison to comparable wetting tests (Alghunaim et al., 2016).

The results from this chapter highlights the ability of BARDS as a novel technique to identify over or under lubricated blends and could potentially assist in predicting dissolution behavior of specific batches. BARDS can also be used to identify batch to batch variability (Fitzpatrick et al., 2012b). BARDS can also be used to rapidly monitor the degree of lubrication and wetting behavior of pharmaceutical blends demonstrating its potential as an at-line PAT screening tool during development and routine pharmaceutical production for enhanced quality control and finished product quality.

5.5 Conclusions

Results from this chapter demonstrate the ability of the BARDS to detect differences in the wetting behavior of commonly used tablet excipients MCC, MgSt and a model API (metoclopramide hydrochloride) as single component and multi-component powder blends. BARDS was capable of detecting the differences in the wetting behaviour of lubricated and unlubricated blends and was compared with the wetting measurement techniques of contact angle and wetting time. The BARDS technique was also shown to be capable of detecting differences in the wetting behavior of lubricated blends, of equivalent composition, following different blending processes and feeding rates. The results of this study highlight the ability of the BARDS technique as a relatively rapid, at-line technique for in-process analysis of pharmaceutical blend lubrication and potentially the wetting behaviour of pharmaceutical powders and blends.

The next chapter focuses in demonstrating behaviour of tablets in BARDS media, formulated at range of compression forces.

Chapter 6

Broadband Acoustic Resonance Dissolution Spectroscopy (BARDS) analysis of Lubricated Tablets

6. BARDS analysis of Lubricated Tablets

6.1 Introduction

In chapter 5, the BARDS technique was successfully used to study the wetting behaviour of pharmaceutical powders as single and multiple components, with and without varied degrees of lubricant distribution. This chapter is focused on using BARDS to study lubricated tablet behaviour in an aqueous medium. BARDS is a novel technique that has been applied to study the *in-vitro* behaviour of pharmaceutical dosage forms. To date there has been limited publications on the application of BARDS to study pharmaceutical compounds and dosage forms. (Evans-Hurson et al., 2016; Fitzpatrick et al., 2014, 2012b; Howick et al., 2018; Peddapatla et al., 2018). A study by Evans Hurson et al. showed that BARDS could determine the dissolution rate of enteric coated drug loaded spheres dissolution media at difference pH values (Evans-Hurson et al., 2016). Peddapatla et al., showed the applicability of BARDS to study the wettability of pharmaceutical powder blends with different degrees of lubrication (Peddapatla et al., 2018). Howick et al., recently used BARDS, as a complementary technique to confirm the results seen in USP dissolution studies of a novel ghrelin receptor agonist, FHI-2571 (Howick et al., 2018). A study by Alfarsi et al. showed BARDS as a rapid test to determine the enteric coating thickness and integrity of controlled release formulations (Alfarsi et al., 2018). In this chapter BARDS technique was used to explore the behaviour of lubricated and unlubricated pharmaceutical tablets with a range of physical properties (porosity and tensile strength) in aqueous media.

As discussed earlier, BARDS works on the principle of frequency change of acoustic resonances (mechanically provoked in a liquid using a stirrer bar) when a material is added to a liquid (Fitzpatrick et al., 2012a). The frequency of acoustic resonances correlates with the compressibility of the liquid system. The addition of gas to the liquid system alters the compressibility of the liquid system and causes a reduction in the acoustic frequency. Studies to date have shown how the addition of a powder sample to a liquid medium reduces the acoustic frequency recorded by the BARDS instrument, and as the material wets or dissolves the acoustic frequency returns to the initial steady state frequency (Fitzpatrick et al., 2012a; Peddapatla et al., 2018; Vos et al., 2016). The reduction in frequency has been attributed to the introduction of air associated with the powder into the liquid upon adding the powder sample. The return to a steady state frequency has been related to the elimination of the air introduced from the system. In this study we were interested to determine what information could be gained by studying tablets using the BARDS technique.

In its simplest form, a pharmaceutical tablet can be described as a mixture of a compacted solid material and gas. The gas is the air contained in the pores of the tablet. When pharmaceutical tablets are introduced into an aqueous system, the air entrapped within the tablet's surface pores is displaced into the liquid as the compact is wetted. As the tablet proceeds to disintegrate and dissolve gas entrained within the tablet is released into the aqueous system. Therefore, the process of air introduction from the tablet into the liquid media would result in a change into the compressibility of the liquid and hence the frequency spectrum

recorded by the BARDS instrument. It was our hypothesis that the BARDS spectra for each tablet would provide information related to the behaviour of the tablets in the liquid media and this behaviour could in turn be related to the physical properties of the tablets

In aqueous medium wicking, water imbibition or penetration into the pores of tablets occurs (Markl and Zeitler, 2017; Nogami et al., 1967). Liquid penetration into the tablet compact initiates a range of mechanisms such as swelling (particles enlarge omni-directionally), strain recovery (particles enlarge uni-directionally) and dissolution (particles dissolve from the pore walls) (Markl and Zeitler, 2017). These mechanisms can rupture the particle-particle bonds in the tablet and result in tablet disintegration. Wicking and tablet disintegration can result in further release of gas into the liquid media. Tablet disintegration behaviour depends on the nature of bonds formed between the particles of the tablet blend during compression. The nature of the bonds formed between tablets is dependent on their porosity, tensile strength and the compactibility and ratio of blend components (Luangtana-Anan and Fell, 1990).

The tablet formulations selected for this study are composed of the blends which were previously studied in chapter 5. They consist of a model drug metoclopramide HCl 10% w/w, with or without MgSt 0.5% w/w and MCC. In this study tablets prepared from blends compressed at different compression forces are investigated. At increased compression forces, the volume and amount of gas entrapped within the powder bed is initially reduced (Tye et al., 2005). Earlier studies have indicated that tablet quality is sensitive to MgSt which can lead to problems such as reduced

tablet tensile strength, chipping, lamination and a change in the drug product release profile (Abe and Otsuka, 2012; Gupta et al., 2009a; Iranloye and Parrott, 1978; Roberts et al., 2004; Uzunović and Vranić, 2007). In this chapter, the effect of the presence of MgSt on tablet behaviour in an aqueous media was also investigated using the BARDS technique.

6.2 Aim and objectives

The aim of this chapter was to demonstrate the capability of BARDS to study differences in tablet behaviour in an aqueous medium.

The main objectives of the chapter are:

- To determine the effect of tablet tensile strength and porosity on the BARDS acoustic profiles of tablets
- To determine the differences between BARDS acoustic profiles of unlubricated and lubricated tablets

6.3 Results

6.3.1 Tablet characterisation

Prior to BARDS analysis of tablets, tablets were characterised in terms of tensile strength and porosity. Data related to tablet properties are shown in Table 6.1. For both the lubricated and unlubricated blends, tablets were produced at a range of compression pressures. As anticipated, an increase in compression pressure showed an increase in the tablet tensile strength and decrease in the tablet porosity as shown in Figure 6.1.

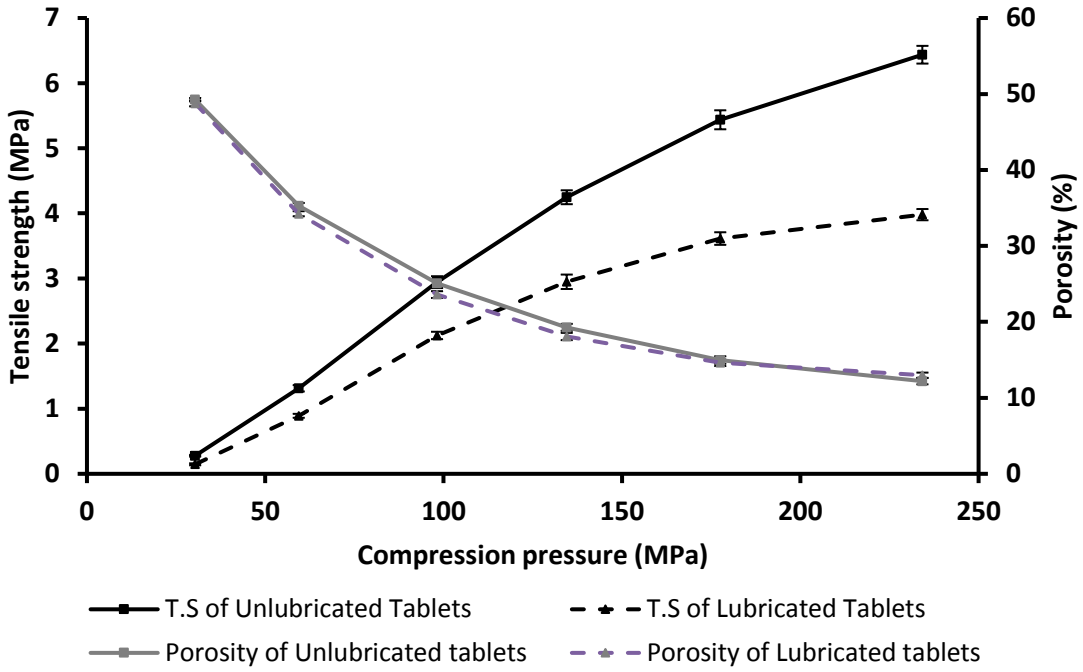


Figure 6.1 Tensile strength (T.S.) and porosity of unlubricated and lubricated blends compressed at different compression forces. Average values shown n=20, y-error bars indicate standard deviation.

Table 6.1 Properties of tablets compressed from unlubricated and lubricated blends at a range of compression pressures. Average values shown, ± indicate standard deviation.

Compression Pressure (MPa)	Weight (mg) (n=20)		Thickness (mm) (n=20)		Tensile Strength (MPa) (n=20)		Porosity (%) (n=20)		Disintegration time (minutes) (n=3)	
	Unlubricated Tablets	Lubricated Tablets	Unlubricated Tablets	Lubricated Tablets	Unlubricated Tablets	Lubricated Tablets	Unlubricated Tablets	Lubricated Tablets	Unlubricated Tablets	Lubricated Tablets
30	256.5±0.9	258.3±1.2	6.26±0.02	6.29±0.00	0.27±0.01	0.15±0.02	49.24±0.22	48.76±0.39	1	1
59	257.8±0.8	260.7±0.8	4.96±0.02	4.97±0.01	1.31±0.04	0.89±0.03	35.27±0.37	34.23±0.33	1	1
98	258.0±0.9	259.7±0.9	4.31±0.01	4.29±0.01	2.94±0.09	2.12±0.06	25.06±0.44	23.59±0.44	1	1
135	256.6±0.6	261.3±1.2	3.99±0.01	4.03±0.01	4.24±0.10	2.95±0.11	19.28±0.45	18.08±0.47	1	1
178	257.2±0.6	261.1±0.9	3.80±0.02	3.88±0.01	5.43±0.14	3.61±0.10	14.97±0.49	14.61±0.42	3	3
234	257.7±1.1	260.0±1.1	3.69±0.01	3.79±0.01	6.43±0.13	3.98±0.09	12.19±0.41	12.98±0.34	5	3

The presence of lubricant did not show any significant effect on tablet porosity. However, a decrease in the tablet tensile strength for lubricated blend, relative to the unlubricated blend, was observed. The relationship between tablet relative density and applied pressure for both blends was determined using the Heckel equation (Heckel, 1961; Ilkka and Paronen, 1993). Heckel plots for the unlubricated and lubricated tablets are shown in Figure 6.2. The yield pressures for plastic deformation for unlubricated and lubricated blends were found to be, 98 and 102 MPa respectively. Above the yield pressure particles undergo densification and form stronger inter-particulate bonds, which can affect tablet disintegration behaviour (Markl and Zeitler, 2017). In this study we were interested to investigate differences in the behaviour of tablets prepared above and below the yield pressure in an aqueous media.

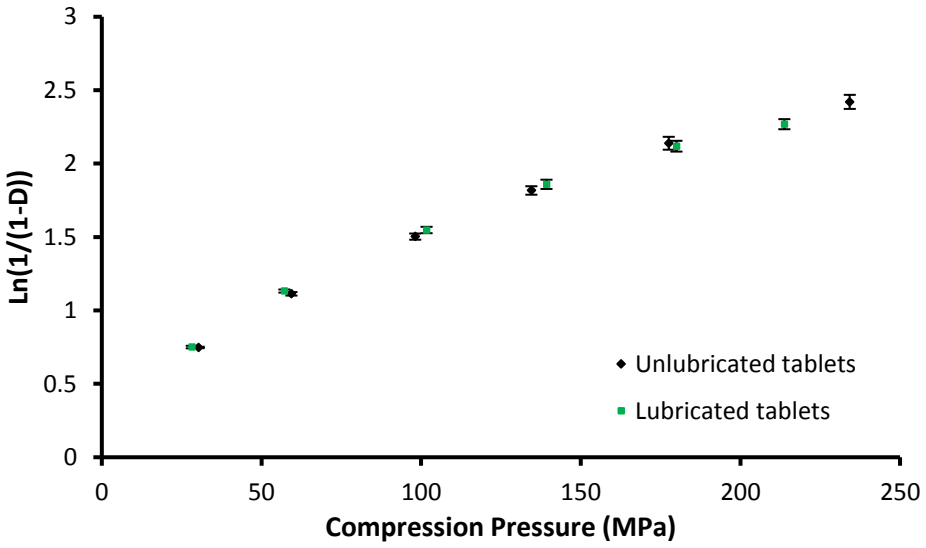


Figure 6.2 Heckel plots derived from relative density and compression forces for unlubricated tablets and lubricated tablets. The points between 25 MPa and 150 MPa were used to calculate the yield pressure with R^2 of 0.99 for both unlubricated and lubricated tablets. Average values shown n=20, y-error bars indicate standard deviation.

The disintegration times for all tablet samples are listed in Table 6.1. All tablets compacted from both formulations, had disintegration times of less than 15 min when tested under USP 30 conditions which agrees with the standard disintegration test specifications for uncoated tablets (Hirschfelder, 1930). Unlubricated and lubricated blends compressed at lower compression pressures <135 MPa disintegrated in less than one minute. Whereas unlubricated and lubricated tablets compacted at 178 MPa and lubricated tablets compaction at 234 MPa disintegrated within 3 minutes. Unlubricated tablets compacted at 234 MPa disintegrated in approx. 5 minutes. Slow disintegration of unlubricated tablet compressed at 234 MPa was attributed to its high tensile strength compared to lubricated tablet compacted at the equivalent compression force (Table 6.1).

6.3.2 Interpretation of BARDS results

During BARDS analysis it was observed that all tablets disintegrated in aqueous media to which they were added. When a tablet is introduced into aqueous media, the gas adhered to the tablet surface is instantly liberated into the solution resulting in an increase in gas volume in the medium. Secondly, the gas that is entrapped between the particles within a tablet is introduced to the media during tablet disintegration. Finally additional gas is introduced as agglomerates disintegrate to primary particles and individual particles are wetted or dissolve. As gas is introduced into the media for the tablet, the volume of gas exceeds steady state and gas is liberated from the solution until the volume of gas returns to steady state. These changes in gas volume in the solvent, alter the solvent's compressibility

and hence the acoustic frequency spectrum as shown for a representative tablet, Figure 6.3.

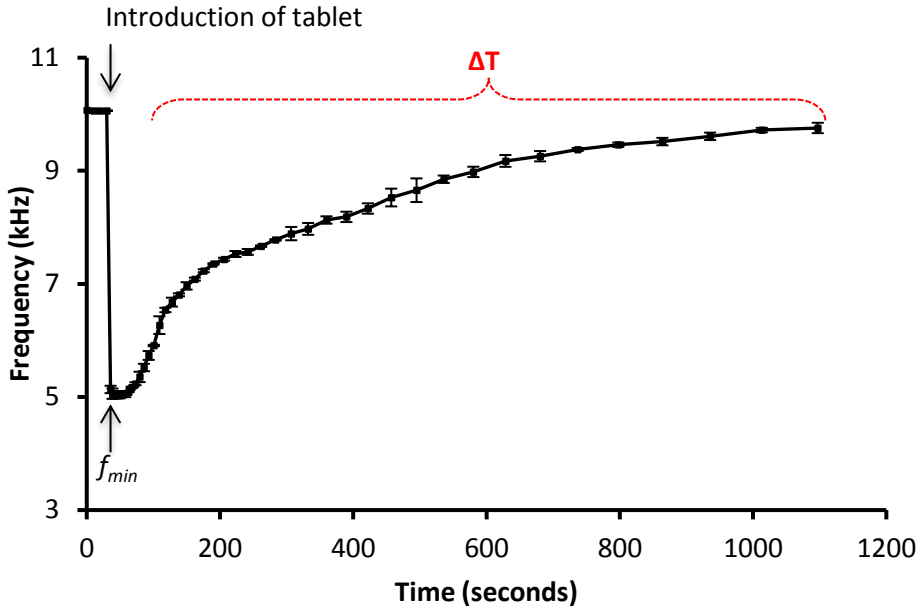


Figure 6.3 BARDS raw spectrum of lubricated tablet compressed at 135 MPa in 25 mL of water at room temperature. Average values shown n=2, y-error bars indicate max and min values.

The f_{min} and time to reach steady state ΔT were determined for each tablet sample from the frequency-time profiles as shown in Figure 6.3. The f_{min} was considered to be related to the initial volume of gas released from the tablet introduced. ΔT is indicative of the combined time for the tablet to disintegrate and all gas introduced with the tablet to be released into the aqueous media and eliminated.

To track the gas volume changes following the introduction of the tablet to the aqueous media, the BARDS frequency-time profiles were transformed to gas volume-time profiles using the equation 6. A representative BARDS Gas volume-time profile is shown in (Figure 6.4).

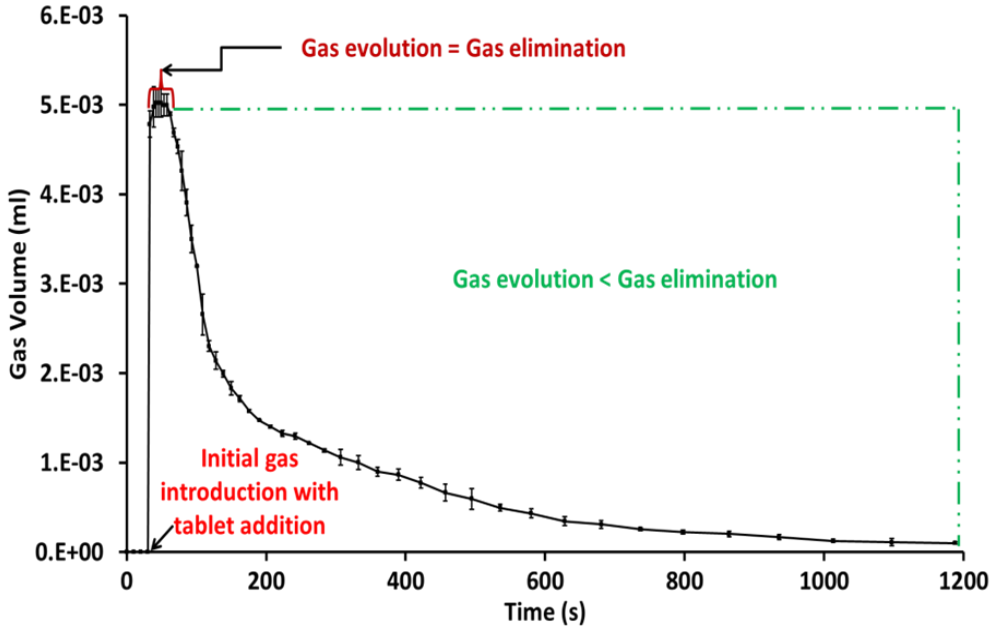


Figure 6.4 Gas-volume plot showing different phases of gas introduction and elimination following addition of a tablet to aqueous media. Tablet compressed from lubricated blend at 135MPa. Average values shown n=2, y-error bars indicate max and min values.

As shown for in Figure 6.4 when a tablet is added into the aqueous media there is a rapid increase in gas volume in the medium, followed by a period when the rate of gas evolution into solution from the tablet and the rate of gas elimination at the surface of the liquid are equal (gas evolution = gas elimination), finally gas evolution from the tablet is decreased relative to gas elimination. The analysis of changes in the compressible gas volume during the elimination stage is given by the descending slope of gas-volume. A gas elimination rate was calculated from the gas-volume profiles assuming it as a first order process (Fitzpatrick et al., 2012a). To determine the gas elimination rate constant (*k*) for aqueous media the gas volume

data shown in Figure 6.4 was plotted using a logarithmic scale as shown in Figure 6.5

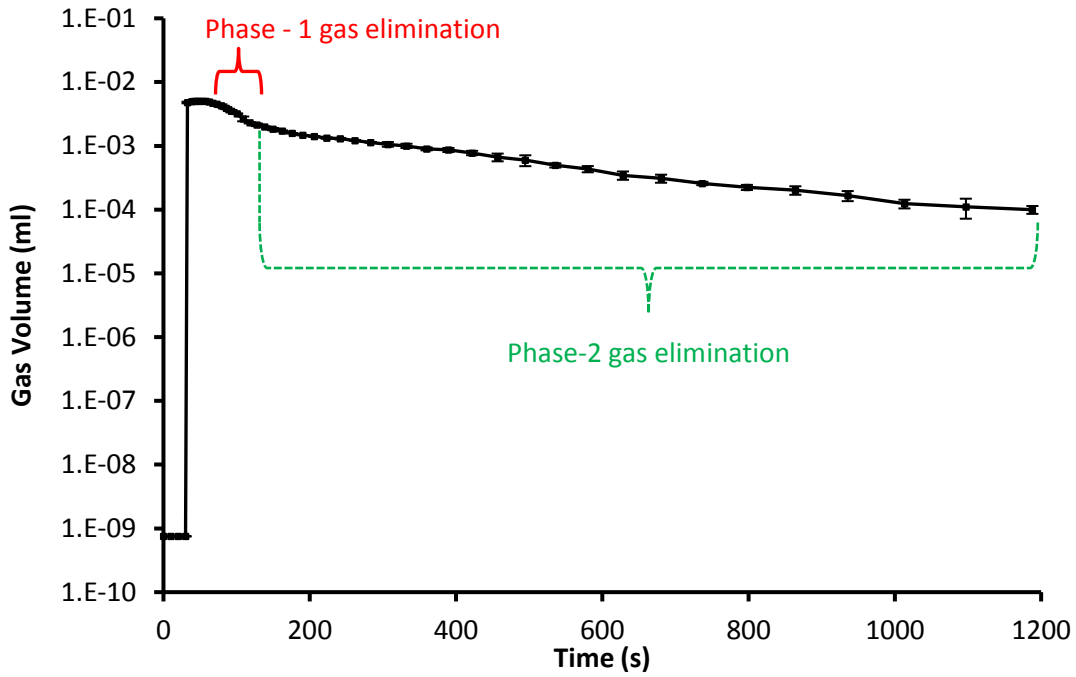


Figure 6.5 A log gas-volume showing time range for different phases of gas elimination. Tablet compressed from lubricated blend at 135MPa. Average values shown n=2, y-error bars indicate max and min values.

6.3.3 Frequency-time profiles of tablets

The BARDS frequency-time profiles for unlubricated and lubricated tablets compressed at increasing compression pressures are shown in Figure 6.6. To aid understanding of the effect of compression at low compression pressures, the frequency-time profile for powder blends prior to compaction were also included in this figure.

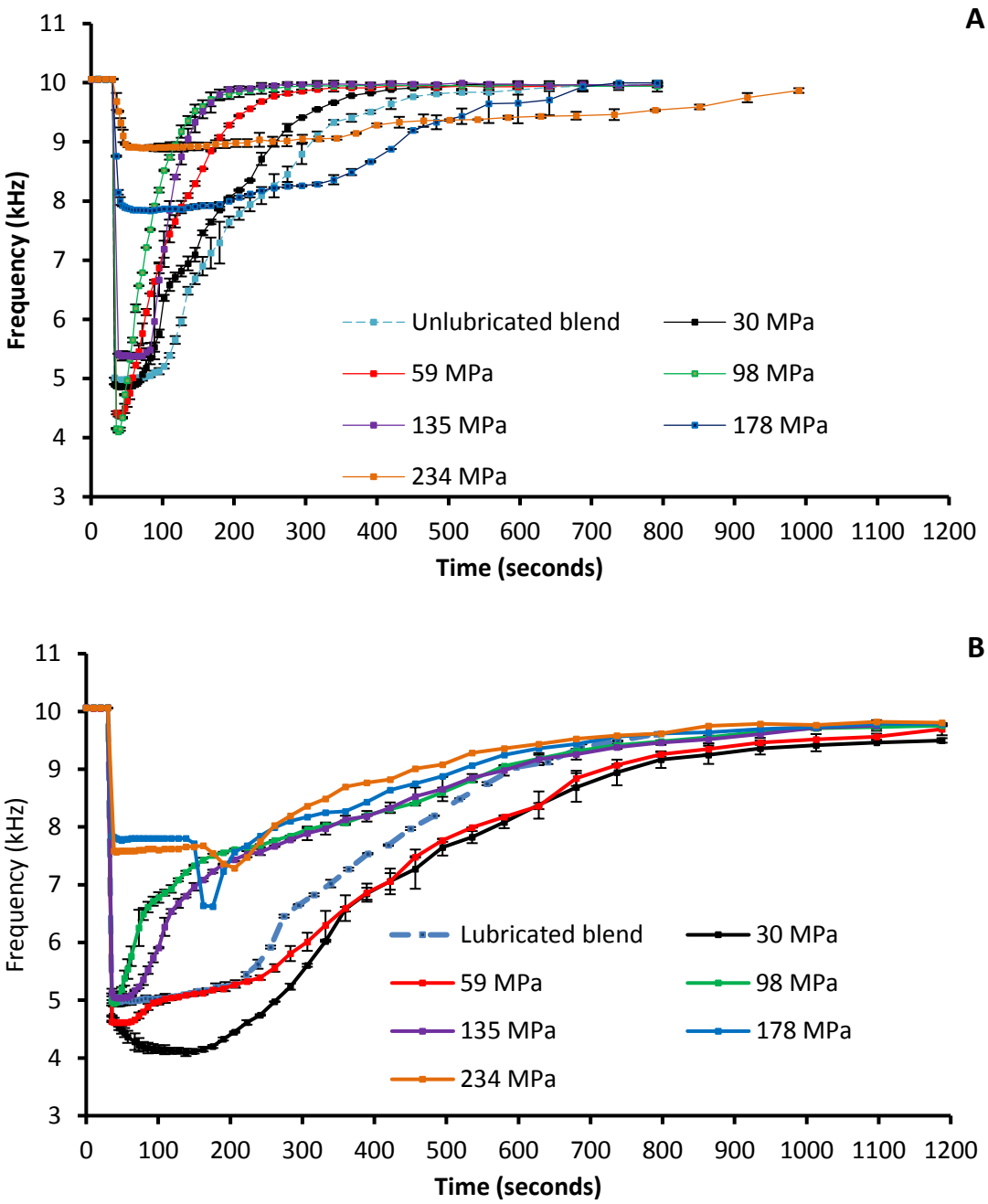


Figure 6.6 Frequency-time profiles of tablets compressed at different compression forces analysed by BARDS in 25 mL of water at room temperature. (A) Unlubricated tablets, (B) Lubricated tablets. Average values shown n=2, y-error bars indicate max and min values. For lubricated tablets, at higher compression pressures of 178 MPa and 234 MPa, n=1

Clear differences in the profiles can be observed with respect to tablet compression force and the presence or absence of MgSt. Compared to unlubricated tablets, lubricated tablets compressed at similar compression pressures showed differences in time (Δt) to reach the frequency minimum (f_{min}), a longer time to return to reach steady state (ΔT) frequency and showed a prolonged acoustic response at f_{min} (Table 6.2).

The frequency-time profile for unlubricated blend prior to compaction and unlubricated tablets prepared at the lowest compression pressures were similar (Figure 6.6A). However differences were observed between lubricated tablets produced at 30 MPa and corresponding blends (Figure 6.6B). Compared to unlubricated and lubricated tablets at lower compression forces, tablets compressed at higher compression forces, showed a smaller decrease in frequency upon introduction of the tablet to the media, and a shallower with more prolonged frequency-time profile (Figure 6.6).

Table 6.2 Time periods associated with time taken to reach frequency minima (f_{min}) Δt, the gas equilibrium phase at f_{min} and time taken to reach steady state (ΔT) for unlubricated and lubricated tablets compressed at different compression forces. Values are calculated from the BARDS frequency-time profiles. (n=2). * indicates gas equilibrium phase time range before tablet lamination in BARDS medium

	Unlubricated tablets			Lubricated tablets		
Compression Pressure (MPa)	**Time taken to reach f_{min} (Δt) s**	**Gas equilibrium phase (s)**	**Steady state return (ΔT)**	**Time taken to reach f_{min} (Δt)**	**Gas equilibrium phase (s)**	**Steady state return (ΔT)**
Blend	3	70	350	5	186	570
30	3	38	320	6	155	545
59	5	11	230	6	50	710
98	5	8	135	6	13	815
135	8	50	90	6	51	850
178	15	157	450	6	114*	695
234	22	335	550	9	123*	715

Both unlubricated and lubricated tablets compressed at 30 and 59 MPa gave rise to U shaped acoustic response at the f_{min}. The U shaped response was more pronounced for the lubricated tablets compared to unlubricated tablets. In contrast tablets compressed at intermediate pressure gave rise to a V shape acoustic response. V-shape acoustic response is an indication of a reproducible number of bubble growth centres in the acoustic suspension (Fitzpatrick et al., 2012a). Tablets compressed at higher compression forces showed a significant increase in f_{min} with increase in compression force and show a sustained U shaped acoustic response. Interestingly, lubricated tablets compacted at higher compression pressures, showed a second f_{min} (Figure 6.6B).

6.3.4 Gas volume - time profile

The gas volume plots for unlubricated and lubricated tablets are presented in Figure 6.7. Clear differences were observed between the gas-volume profiles for unlubricated and lubricated tablets produced at range of compression pressures. The gas volume-time profiles for unlubricated blends and unlubricated tablet prepared at the lowest compression pressures were similar (Figure 6.7A). However, differences were observed between lubricated tablets produced at 30 MPa and lubricated blend (Figure 6.7B). Compared to unlubricated and lubricated tablets at lower compression forces a more prolonged gas volume-time profile was observed for tablets produced at higher compression forces (Figure 6.7).

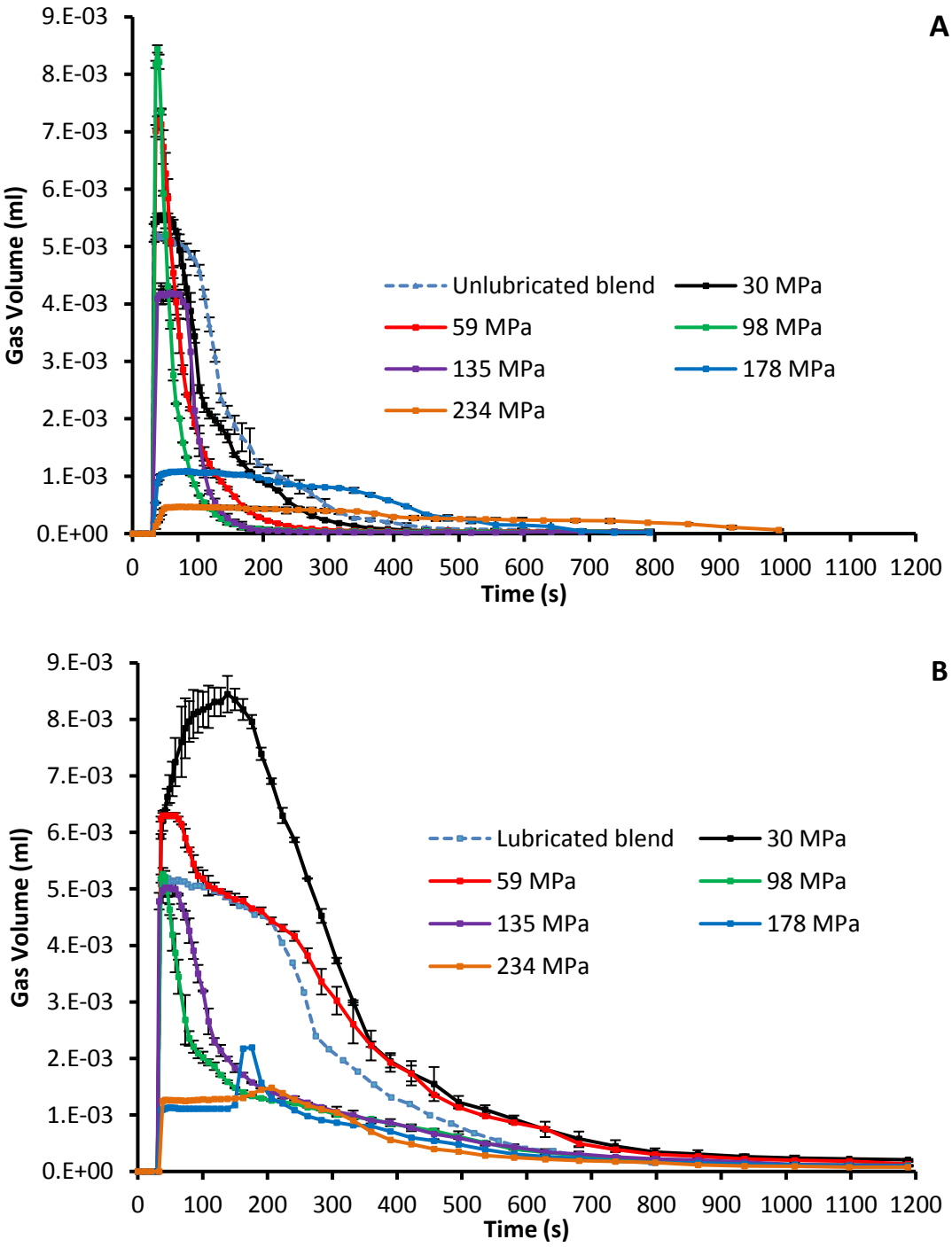


Figure 6.7 Gas volume-time plots derived from BARDS frequency data: (A) Unlubricated tablets (B) Lubricated tablets. Average values shown n=2, y-error bars indicate max and min values. For lubricated tablets, at higher compression pressures of 178 MPa and 234 MPa, n=1

Lubricated tablets produced at 178 MPa and 234 MPa, showed a delayed gas volume introduction, with a second step of gas volume introduction which can be attributed to the due to tablet delamination (Figure 6.8).

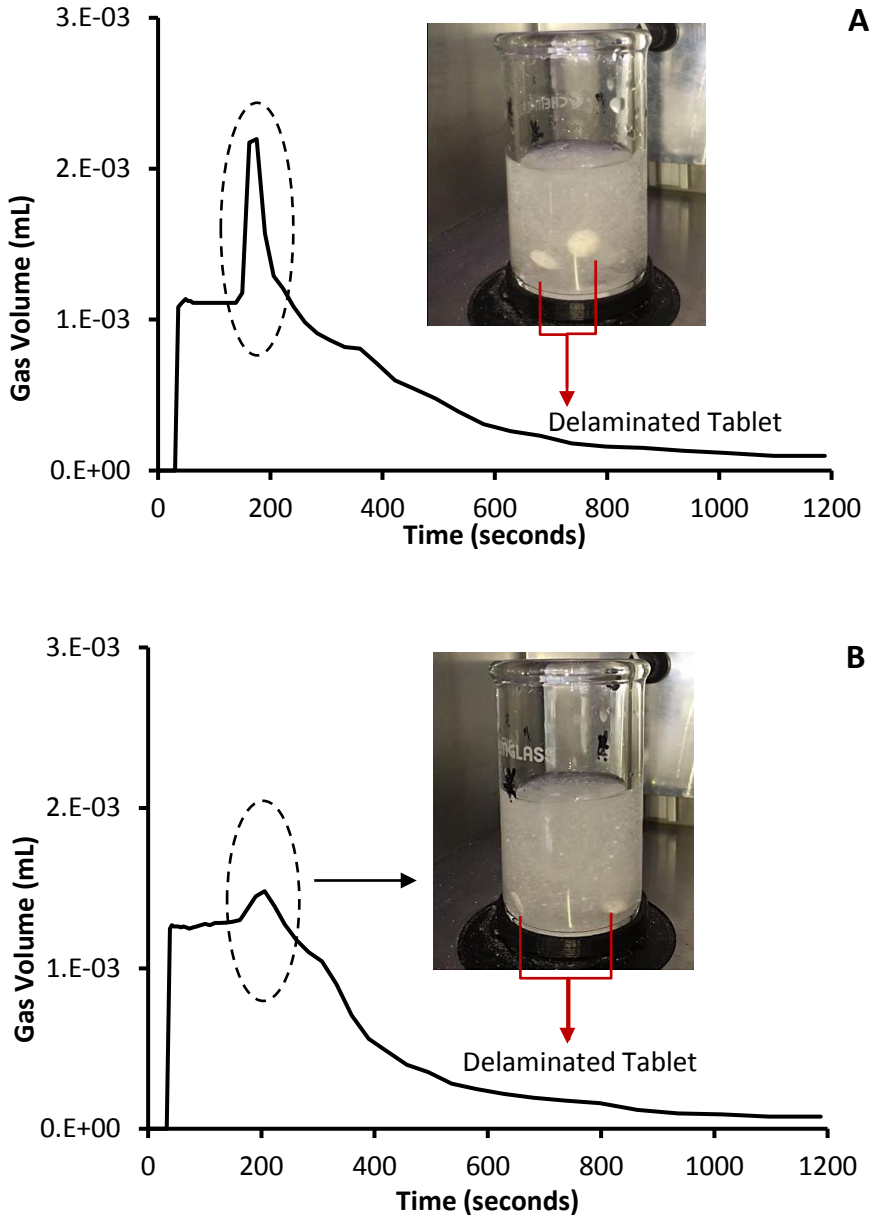


Figure 6.8 Gas volume time plots for tablets showing a second gas release due to tablet delamination in lubricated tablets. (A) 178 MPa and (B) 234 MPa. Photographs in insert show delamination behaviour captured by video recording during disintegration process.

Figure 6.9 shows the area under the gas volume profile (AUVC) for unlubricated and lubricated tablets. Clear differences can be seen in AUVC between unlubricated and lubricated tablets. Unlubricated tablets showed smaller AUVC compared to lubricated tablets at similar compression force (Figure 6.9). For both formulations, as the compression force increased, AUVC decreased up to yield pressure, and above yield pressure, AUVC did not show any specific trend.

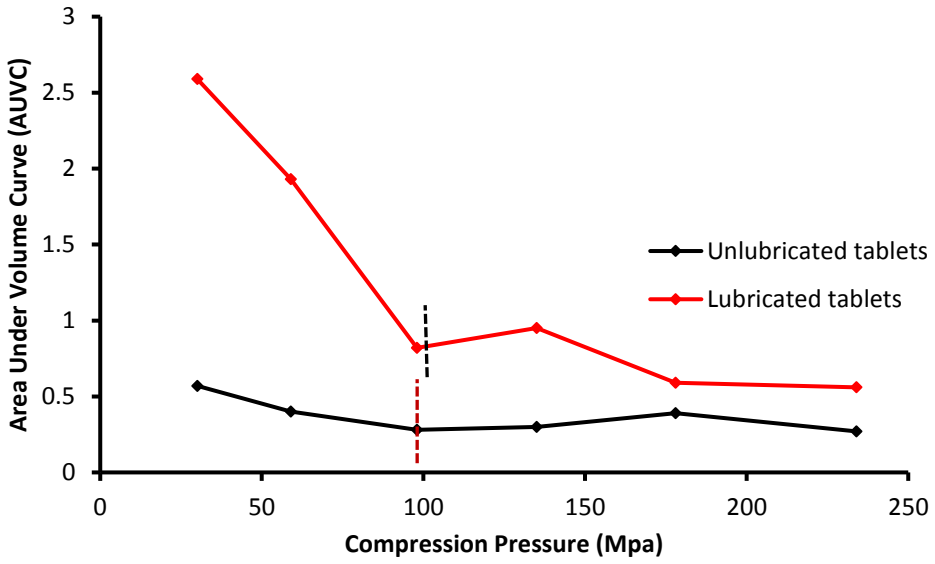


Figure 6.9 Area under volume curve for unlubricated and lubricated tablets, compressed at different compression pressures. Dotted lines on graph indicate the respective yield pressures of unlubricated and lubricated blends.

Gas elimination rate for the tablets was calculated for tablets from the descending slopes of log plots of gas volume plots shown in Figure 6.7. BARDS profiles for both unlubricated and lubricated prepared ≥178 MPa did not fit the first order gas elimination process and therefore gas elimination rate constants are not reported. Unlubricated tablets showed single gas elimination phase, whereas in lubricated tablets showed a change in gas elimination behaviour changed with time and was

modelled considering two gas elimination phases; an initial short faster phase followed by a terminal longer slower phase. The gas elimination rate constant for tablets and associated time ranges are shown in Table 6.3.

A low gas elimination rate constant was observed for unlubricated blend (k ≈1.04 ×10^{-2} s^{-1}) and as the compression pressure is increased up to 135 MPa, the gas elimination rate constant increased moderately from k ≈1.28×10^{-2} s^{-1} to 3.89×10^{-2} s^{-1} for unlubricated tablets (Table 6.3). The lubricated blend showed a slower gas elimination rate constant of k ≈5.56×10^{-3} s^{-1} and this was increased upon applying compression pressure. Lubricated tablets showed two phase gas elimination, an initial phase and terminal phase. The initial phase showed a faster gas elimination rate compared to terminal phase. No specific trend was observed in the elimination rate constants for the initial phase for lubricated tablets in relation to compression pressures. The elimination rate constant was similar for the 2^{nd} elimination phase for lubricated tablets with respect to compression pressure. Unlubricated tablets showed faster gas elimination compared to lubricated tablets at similar compression pressures (Table 6.3).

Table 6.3 Gas elimination rate constant (k(s^{-1})) for unlubricated and lubricated tablets compressed at different compression forces. Values are calculated from the BARDS log gas volume-time profiles and the time ranges used for the calculation are also shown. R- Squared indicates the linear fit for the selected time ranges for the gas elimination rate constants. (n=2)

Tablets	Parameter		Blends			30 MPa			59 MPa			98 MPa			135 MPa		
			Range (s)	*Const.*	R^2	Range (s)	*Const.*	R^2	Range (s)	*Const.*	R^2	Range (s)	*Const.*	R^2	Range (s)	*Const.*	R^2
Unlubricated Tablets	**Gas elimination rate constant - k_{el}(s^{-1})**		102-450	1.04E-02	0.99	72-391	1.28E-02	0.99	47-275	1.96E-02	0.99	44-180	3.22E-02	0.98	89-180	3.89E-02	0.99
Lubricated Tablets	**Gas elimination rate constant – k_e(s^{-1})$_I$**	**Phase I**	222-792	5.56E-03	0.99	190-360	6.85E-03	0.97	68-93	6.29E-03	0.99	49.-79	2.26E-02	0.99	86-118	1.66E-02	0.99
		Phase II				390-1188	3.08E-03	0.94	99-1188	3.82E-03	0.98	85-1188	2.91E-03	0.98	128-1188	3.01E-03	0.99

6.4 Discussion

The results of this study show that BARDS analysis successfully discriminated the behaviour of tablets compressed at different compression forces and tablets with and without MgSt. Though unlubricated and lubricated tablets showed similar porosity, they showed different acoustic behaviour in BARDS. The time taken to reach f_{min} is approx. 3 s in unlubricated blends and tablets produced at 30 MPa. As the compression pressure increased tensile strength is increased and porosity of the tablets is decreased (Figure 6.1). For unlubricated tablets as the porosity decreased, the time taken to f_{min} increased (Table 6.2). However, for lubricated blend and tablets with different porosities, showed similar f_{min} except for tablet produced at 234 MPa (Table 6.2).

The yield pressures for unlubricated and lubricated blends were found to be 98 and 102 MPa respectively. Above the yield pressure particles undergo densification and form stronger inter-particulate bonds, which can affect tablet disintegration behaviour (Markl and Zeitler, 2017). In this study, BARDS discriminated the tablets that were produced below and above yield pressures. There was a significant change in the frequency decrease and gas volume introduction after tablet addition to BARDS media for both unlubricated and lubricated tablets produced above yield pressure (Figure 6.6 and Figure 6.7). Below yield pressure, as the compression pressure increased from 30 MPa to 98 MPa, the acoustic response of unlubricated and lubricated tablets changed from prolonged U shape to V shape. This prolonged U shape response at lower compression pressures, may be due to the lower swelling force generated at lower compression pressures due to high void spaces

which increased the time to break up the inter-particular bonds (Lowenthal, 1972; Markl and Zeitler, 2017).

Similarly the gas equilibrium phase or lag phase is decreased for unlubricated and lubricated tablets compressed at 30 MPa, compared to that of respective blends (Table 6.2). For tablets of both blends produced at increasing compression pressures, the lag time decreased (U shape to V shape) up to their respective yield pressures. However, above yield pressures, the lag time for the tablets started to increase. Unlubricated tablets showed a shorter gas equilibrium phase, compared to lubricated tablets, at respective compression pressures (Table 6.2, Figure 6.6 and Figure 6.7). Initially it may appear that this may be attributed in part to the presence of hydrophobic MgSt, which delayed the disintegration of tablet within BARDS media. However, disintegration results show similar disintegration times for lubricated and unlubricated tablets which would suggest this behaviour may be due to prolonged wetting of disintegrated particles from tablets.

The return to steady state (ΔT), for unlubricated tablets decreased from 320 s to 90 s, as the compression pressure increased up to 135 MPa. However BARDS spectra for tablets produced at higher compression pressure of 178 MPa and 234 MPa took 450 s and 550 s return to steady state. This may be due to the formation of stronger bonds resulting in higher tensile strength and densification above the yield pressure (Figure 6.2). Disintegration data and video imaging of the tablet during BARDS analysis did show complete tablet disintegration at a time point prior to return to steady state frequency such would suggest that these longer time periods are also related to disintegration of tablet fragments to primary particles. An increase in the

ΔT values for lubricated tablets was observed from 545 s to 850 s, as the compression pressure increased up to 135 MPa. Interestingly the lubricated tablets produced at 178 and 234 MPa, showed shallow response and lower ΔT values indicating speedy return to steady state. This can be attributed to the delamination effect of lubricated tablets at higher compression forces due to decrease in tensile strength, which showed second f_{min} resulting in rapid disintegration of the tablets, but slower wetting compared to unlubricated tablets produced at similar compression pressures. The return to steady state is more rapid in unlubricated tablets compared to lubricated tablets at similar compression pressures (Table 6.2).

Lubricated tablets showed extended frequency time profile and gas volume time profiles compared to unlubricated tablets (Figure 6.6 and Figure 6.7). Lubricated tablets showed higher area under volume curve compared to unlubricated tablets (Figure 6.9). This may be due to an increase in outgassing time due to gas oversaturation or slow generation of gas bubbles in the solution (Fitzpatrick et al., 2013), due to the presence of hydrophobic MgSt delaying in wetting of lubricated tablets.

Previous studies on BARDS showed the importance of gas elimination rate constant in understanding the wetting of materials. A study by Vos et al., and Peddapatla et al., showed that a lower gas elimination rate constant corresponds to slower wetting and higher gas elimination constant corresponds to faster wetting of milk protein powders and pharmaceutical powder blends (Peddapatla et al., 2018; Vos et al., 2016). A lower gas elimination rate constant was observed for the unlubricated blend compared to unlubricated tablet compressed at 30 MPa. The

gas elimination rate constant increased as the compression pressure increased up to 135 MPa for unlubricated tablets (Table 6.3). The lubricated blend showed a gas elimination rate constant which increased upon applying compression pressure of 30 MPa. Gas elimination rate constant did not follow any specific tendency for lubricated tablets as the compression pressure increased. Conversely, the initial phase gas elimination is faster compared to terminal phase elimination, for tablets at different compression pressures. However, unlubricated tablets showed faster gas elimination compared to lubricated tablets at similar compression pressures (Table 6.3). Tablets produced at higher compression pressures of 178 MPa and 234 MPa did not fit first order rate elimination kinetics, therefore elimination rate constant for these tablets was not determined. Though the lubricated tablets showed slower gas elimination rate constants across different compression pressures, standard dissolution test performed on these formulations did not show any change in the percentage drug release (Supplementary information, Figure – S4), this is mainly due to the delamination effect of the tablets and the drug used in this study is metoclopramide HCl is a salt of weak base with a pKa of 9.2 which was highly water soluble.

6.5 Conclusions

BARDS was capable of detecting differences in wetting behaviour of the tablets studied. The gas volume plots generated from the BARDS analyses provided new understandings into the tablet wetting mechanism for lubricated and unlubricated tablets produced at a range of compression forces. BARDS analysis parameters such as Δt, ΔT and gas elimination rate constants were identified as useful parameters to quantify differences in tablet wetting in BARDS media.

Chapter 7

General Discussion

7. General Discussion

The problems associated with MgSt in pharmaceutical products are not new, and well-studied since first reported (Iranloye and Parrott, 1978). Previous studies have indicated that tablet quality is sensitive to MgSt, and the product quality may be compromised if it does not perform as expected, leading to processing problems, like poor tablet hardness, chipping, lamination, etc. or change in the drug product release profile (Abe and Otsuka, 2012; Gupta et al., 2009b; Roberts et al., 2004; Uzunović and Vranić, 2007). To date a huge amount of studies have been undertaken regarding the performance of MgSt performance during batch processing. There has been growing interest in continuous manufacturing for oral solid dosage forms, as it provides a suitable platform to apply suitable monitoring and control design, to improve the product quality and minimise product rejection and operating expenses. Moving towards continuous process raises new challenges, when handling hydrophobic, cohesive materials such as MgSt.

The main aims of this thesis were to investigate the role of MgSt supplier variability during continuous feeding through a LIW feeder and to investigate the capability of BARDS to discriminate between blends and tablets with variable MgSt distribution.

7.1 Magnesium stearate variability and continuous feeding

As mentioned in chapter – 1, during the continuous manufacturing of oral solid dosage forms it is critical to maintain a consistent, accurate and reliable feed stream of the raw materials resulting in the initial feeding stage being important to the entire manufacturing process. Although used in small quantities in tablet manufacture, MgSt is an excipient that plays a critical role in pharmaceutical

tableting process. Very little was published on the feeding behaviour of MgSt. Engisch and Muzzio, showed the feeding performance of MgSt in K-Tron MT12 and K-Tron KT20 (Engisch and Muzzio, 2014). This study showed, that the long term performance of MT12 was better compared to KT20 in feeding MgSt. Whereas this thesis was focused not only on the feeding performance, but also looked at the material characteristics and variability (chapter-3) that affect the feeding performance across four different grades of MgSt (chapter-4). Post feeding characterisation of MgSt samples was also performed, to study the effect of feeding on MgSt samples. Continuous fed MgSt samples were also included in tablet blends to study their effect on tablet quality (chapter-4).

The results presented in chapter 3, showed large variability in the solid state, particulate and bulk properties between the lots of MgSt selected for this study (Figure 3.1 – Figure 3.7) which was in agreement with previous study by Gupta et al., and Rao et al. (Gupta et al., 2009a; Rao et al., 2005). This variability did not show any effect in the tabletability and compactibility of paracetamol tablets up to compaction pressures 150 MPa. However, tablets with Ligamed MgSt samples produced tablets with slightly less tabletability and compactibility, when compacted above 150 MPa (Figure 3.8 and Figure 3.9). Inclusion of different grades of MgSt also did not show any differences in the compressibility of the tablets (Figure 3.10). *in-vitro* dissolution studies showed similar drug release profile for tablets with Alfa Aesar, Ligamed MF-2-V and Ligamed MF-2-V-BI. However, tablets with Ligamed MF-3-V which has greater surface area and more crystalline that the other MgSt samples showed a slightly slower release (Figure 3.11).

MgSt is an impure material manufactured using variable raw materials, which can influence its behaviour in tablet formulations (Billany, 1982). Commercial MgSts are mixtures of di- and mono-hydrate forms, along with varying amounts of magnesium palmitate, a known impurity, which also exists in the above two forms. The hydrophobicity of MgSt can vary from batch to batch and from grade to grade due to the different levels of water soluble surface active impurities such as sodium stearate (Louw, 2003). Batches containing very low concentrations of these impurities have been shown to retard the dissolution of a drug to a greater extent than batches containing higher levels of other impurities (Louw, 2003). Presence of excess impurities in MgSt is likely to be a significant factor affecting die-wall lubrication, because of the effect of impurities on melting point and crystal lattice of the material (Swaminathan and Kildsig, 2001). The focus of this work was to study the effect of solid state, particulate and bulk properties of MgSt samples on tablet formulations. Therefore, the different types of impurities and their effects on MgSt properties and tablet formulations were not within the scope of this thesis, but an important consideration with regard to MgSt variability.

Different types of loss in weight feeders are available to feed powders with varied degree of flowability. Some examples of feeders are K-Tron MT12, K-Tron KT 35 and K-Tron 20 (Blackshields and Crean, 2018). K-Tron MT12 feeder was choosed based on the study performed by Engisch and Muzzio (Engisch and Muzzio, 2014). The variability of MgSt affected the continuous feeding behaviour. Bulk density of the MgSt samples, dictated the FF achieved, for samples during feeding through MT12 feeder (Figure 4.5). Ligamed MF-2-V and MF-3-V with very similar properties

showed higher feed rate variability, whereas Alfa Aesar with lowest surface area and Ligamed MF-3-V with highest surface area, showed least feed rate variability at both feed rates (Figure 4.6). All samples when fed at lower feed rates showed higher feed rate variability (greater RSD) compared to samples fed at higher feed rate. A study by Kato et al. showed that tablet quality properties become more affected by the effects of over blending, if the D50 of the MgSt is 10μ m or less, particularly 5μm or less (Kato et al., 2005). Among the samples used in this study, D50 of Ligamed MF-2-V when fed at lower feed rate of 0.15 kg/hr showed more reduction in particle size, which when further included in blends, showed a delayed drug release profile (Figure 4.12). As particle size of the samples reduced due to feeding, these samples when included in tablet blends, showed a delayed release. This delay in release was more prominent in tablets with fed MgSt of Alfa Aesar and Ligamed MF-2-V. Ligamed MF-3-V with high crystallinity and was least effected by feeding and when fed samples were included in formulations a very slight delay in drug release was noticed compared to other tablets with other MgSt samples (Figure 4.12). Inclusion of unfed and fed lubricants did not show any real differences in compressibility and tabletability of the formulations studied (Figure 4.9 and Figure 4.11).

7.2 Applicability of BARDS to study lubricated blends and tablets

Many studies have been performed to identify the MgSt in the blends and tablets using different indirect techniques such as, SEM (Roblot-Treupel and Puisieux, 1986), EDX has been (Hussain et al., 1988), N-IR (Abe and Otsuka, 2012), SIMS (Hussain et al., 1990), LIBS - (St-Onge et al., 2005). Direct techniques such as Raman spectroscopy is widely used, which enables the direct detection of MgSt with in blends and tablets by measuring the CH_2- groups within MgSt (Aguirre-Mendez and Romanach, 2007; Lakio et al., 2013). Numerous studies have been made using Raman spectroscopy to map MgSt within blends and tablets (Henson and Zhang, 2006; Vajna et al., 2010; Widjaja and Seah, 2008; Zhang et al., 2005). In this thesis, for the first time we used BARDS to identify the effects of MgSt lubrication within blends and tablets.

Previous studies reported the applicability of BARDS in studying the milk powder concentrates and enteric coated drug spheres (Evans-Hurson et al., 2016; Fitzpatrick et al., 2014; Vos et al., 2016). For the first time, this thesis investigated the applicability of BARDS to study the commonly used pharmaceutical excipients, degree of lubrication within blends and tablets. BARDS clearly discriminated the differences between unlubricated and lubricated blends (Figure 5.3). Unlubricated blends showed faster gas elimination rate compared to lubricated blends (Table 5.2). These unlubricated and lubricated blends were fed through loss in weight feeder at different feed rates to generate the blends with different degrees of lubrication. As the feed rate increased RSD decreased for both blends and lubricated blends showed lower RSD compared to unlubricated blends. BARDS

analysis of these blends showed clear differences with slow gas elimination rate constant between the lubricated blends fed at increasing feed rates (Table 5.3). This indicated the over lubrication of lubricated blend, as the feed rate increased. This was further confirmed by analysing the tabletability profiles of these blends. Unlubricated blend fed at different feed rates showed similar tabletability and lubricated blend showed decrease in tabletability as the feed rate increased indicating the increase in lubrication by MgSt (Figure 5.8).

The results of chapter 6 show that the BARDS was also able to differentiate tablets that are produced at a range of compression forces and tablets with and without lubricant. A significant change in the acoustic response was observed for the tablets produced above the yield pressure for both formulations (Figure 6.6). The dissolution rate of all tablets resulted in metoclompramide dissolution at the 10 min time point (Supplementary information - Figure S4). Therefore, for the formulations studied the dissolution rate is not limited by the disintegration process or sensitive to lubrication effects as would be observed for more poorly water-soluble compounds (Choiri and Maret, 2015). The results generated in chapter 5 and 6 highlight the ability of BARDS as a novel technique to identify over or under lubricated blends and tablets produced at different compression forces.

Compared to other techniques, BARDS is relatively simple and the samples can be analysed in aqueous media or suitable dissolution media for specific formulation. BARDS could assist in predicting dissolution behavior of specific batches. Frequency time and gas-volume time profiles signify the qualitative information about the degree of lubrication within blends. Gas elimination rate constant, can be used to

determine degree of lubrication, within blends and tablets quantitatively. This demonstrates the potentiality of BARDS as an at-line PAT screening tool during development and routine pharmaceutical production for enhanced quality control and finished product quality.

7.3 Strengths and Limitations

7.3.1 Strengths

- Intensive material characterisation was performed to assess the feeding behaviour of MgSt samples. Fed MgSt samples were further characterised, and differences were observed in particle size, which affected the *in-vitro* performance of the selected formulation.
- The work presented demonstrated the ability of BARDS to detect the differences in wetting behaviour of commonly used excipients (MCC, MgSt), a model drug (metoclopramide hydrochloride), blends and tablets with and without lubricant.

7.3.2 Limitations

- Only one type of feeder K-Tron MT12 was investigated in this study. The results of this study in chapter - 3 and chapter - 4 were limited to only four grades of MgSt. A larger sample set would be required to fully explore the impact of MgSt variability with respect to lubricant feeding.
- The *in-vitro* drug release not solely depends on the particle size of MgSt samples. A further study is required to investigate the effect of solid state properties on *in-vitro* drug release profiles.

- ❖ BARDS results in chapter – 5 and chapter – 6 were limited to one type of formulation and the should be assessed in relation to well established wetting techniques like Washburn capillary and PAT techniques like N-IR, Raman etc.

7.4 Recommendations for future work

Based on the findings of this thesis following work is suggested.

- ➢ The formulation used in this study was a simple formulation with 89.5% MCC PH200 which is a plastic component, 10% API and 0.5% MgSt. It would be interesting to see the effect of different grades of unfed and fed MgSt on formulation with elastic, brittle and viscoelastic component within the formulation.
- ➢ MgSt when fed through K-Tron MT12 feeder showed reduction in particle size of MgSt samples. Inclusion of these MgSt showed delay drug release profile of paracetamol formulation. Future work would be interesting to see the effect of this fed MgSt on drug release profiles of poorly water-soluble drugs, granules and formulations with differing release profiles.
- ➢ It would be of interest to study the effect of different grades of MgSt and other powder lubricants on acoustic response and to further explore the applicability of BARDS in pharmaceutical field.

7.5 Conclusions

- It was established that, MgSt samples analysed in this study varied in particulate, bulk and molecular properties, with no effect on tabletability, compressibility and drug release profile of the formulations used.
- Variability of samples impacted their feeding performance. Ligamed MF-2-V and MF-2-V-BI with similar properties, showed greater feed rate variability compared to Alfa Aesar with lower surface area and Ligamed MF-3-V with higher surface area.
- Particle size of the samples was affected due to feeding. No major effect of these fed lubricants was observed on tabletability, compressibility and compactibility. However, *in-vitro* analysis of tablets showed delay in drug release, when fed lubricants were included in blends.
- Novel analytical technique, BARDS was found to be successful in discriminating the differences between unlubricated and lubricated blends and tablets produced at different compression forces.

Bibliography

8. Bibliography

Abe, H., Otsuka, M., (2012). Effects of lubricant-mixing time on prolongation of dissolution time and its prediction by measuring near infrared spectra from tablets. Drug Dev. Ind. Pharm. 38(4), 412–419. https://doi.org/10.3109/03639045.2011.608679

Aguirre-Mendez, C., Romanach, R.J., (2007). A Raman spectroscopic method to monitor magnesium stearate in blends and tablets. Pharm. Technol.

Ahmed, M.R., McSweeney, S., Krüse, J., Vos, B., Fitzpatrick, D., 2018. Contactless, probeless and non-titrimetric determination of acid-base reactions using broadband acoustic resonance dissolution spectroscopy (BARDS). Analyst. 143(4), 956–962. https://doi.org/10.1039/c7an01447c

Alfarsi, A., Dillon, A., McSweeney, S., Krüse, J., Griffin, B., Devine, K., Sherry, P., Henken, S., Fitzpatrick, S., Fitzpatrick, D., (2018). Broadband Acoustic Resonance Dissolution Spectroscopy (BARDS): A rapid test for enteric coating thickness and integrity of controlled release pellet formulations. Int. J. Pharm. 544 (1), 31–38. https://doi.org/10.1016/j.ijpharm.2018.04.018

Alghunaim, A., Kirdponpattara, S., Newby, B.Z., (2016). Techniques for determining contact angle and wettability of powders. Powder Technol. 287, 201–215. https://doi.org/10.1016/j.powtec.2015.10.002

Aulton, M.E., Taylor, K. M. G., (2007). Aulton's Pharmaceutics: The Design and Manufacture of Medicines. Third edition.

Barra, J., Somma, R., (1996). Influence of the physicochemical variability of magnesium stearate on its lubricant properties: Possible solutions. Drug Dev. Ind. Pharm. 22(11), 1105–1120. https://doi.org/10.3109/03639049609065947

Billany, M.R., Richards, J.H., 1982. Batch variation of magnesium stearate and its effect on the dissolution rate of salicylic acid from solid dosage forms. Drug Dev. Ind. Pharm. 8, 497–511. https://doi.org/10.3109/03639048209022117

Blackshields, C., Crean, A., (2018). Continuous powder feeding for pharmaceutical solid dosage form manufacture: a short review. Pharm. Dev. Technol. 23(6), 554–560. https://doi.org/10.1080/10837450.2017.1339197

Blackwood, D., (2017). ISPE Annual Spring Conference. New Jersey, USA

Bolhuis, G.K., De Jong, S.W., Lerk, C.F., Dettmers, H., Pharbita, B. V., (1987). The effect of magnesium stearate admixing in different types of laboratory and industrial mixers on tablet crushing strength. Drug Dev. Ind. Pharm. 13(9-11), 1547–1567. https://doi.org/10.3109/03639048709068680

Borbás, E., Sinkó, B., Tsinman, O., Tsinman, K., Kiserdei, É., Démuth, B., Balogh, A., Bodák, B., Domokos, A., Dargó, G., Balogh, G.T., Nagy, Z.K., (2016). Investigation and mathematical description of the real driving force of passive transport of drug molecules from supersaturated solutions. Mol. Pharm. 13(11), 3816–3826. https://doi.org/10.1021/acs.molpharmaceut.6b00613

Brunauer, S., Emmett, P.H., Teller, E., (1938). Adsorption of Gases in Multi molecular Layers. *60*, 309–319. https://doi.org/10.1021/ja01269a023

Cartwright, J.J., Robertson, J., D'Haene, D., Burke, M.D., Hennenkamp, J.R., (2013). Twin screw wet granulation: Loss in weight feeding of a poorly flowing active pharmaceutical ingredient. Powder Technol. 238, 116–121. https://doi.org/10.1016/j.powtec.2012.04.034

Celik, M., (2011). Pharmaceutical Powder Compaction Technology, 2nd edition. Informa Healthcare USA, Inc.

Chen, Z., Lovett, D., Morris, J., (2011). Process analytical technologies and real time process control a review of some spectroscopic issues and challenges. J. Process Control. 21(10), 1467–1482. https://doi.org/10.1016/j.jprocont.2011.06.024

Choiri, S., Maret, U.S., 2015. The Influence of Magnesium Stearate, Purified Talc And Combination Of Both On Ternary/Quaternary Interactive Mixture Of Freely And Poorly Water- Soluble Drug. Int. J. Pharm. Pharm. Sci. 7, 397–402.

Crawford, F.S., (1982). The hot chocolate effect. Am. J. Phys. 50, 398–404. https://doi.org/10.1119/1.13080

Crowley, M.E., Crean, A., (2015). Quality by design in an evolving manufacturing sector. J Parent Pharm Sci. 20(2), 63–69.

Dansereau, R., Peck, G.E., (1987). The Effect of the Variability in the Physical and Chemical Properties of Magnesium Stearate on the Properties of Compressed Tablets. Drug Development and Industrial Pharmacy 13(6), 975–999. https://doi.org/10.3109/03639048709068365

Dave, V.S., Saoji, S.D., Raut, N.A., Haware, R. V., (2015). Excipient Variability and Its Impact on Dosage Form Functionality. J. Pharm. Sci. 104(3), 906–915. https://doi.org/10.1002/jps.24299

De Villiers, M., (2004). Oral Conventional Solid Dosage Forms, Theory and Practice of Contemporary Pharmaceutics. https://doi.org/10.1201/9780203644478.ch10

Delacourte, A., Predella, P., Leterme, P., Provasi, D., Colombo, P., Conte, U., Catellani, P.L., Guyot, J.C., (1993). A method for quantitative evaluation of the effectiveness of the lubricants used in tablet technology. Drug Dev. Ind. Pharm. 19(9), 1047–1060. https://doi.org/10.3109/03639049309063000

Duong, N., Arratia, P., Muzzio, F., Lange, A., Reynolds, S., Arratia, P., Muzzio, F., Lange, A., (2017). A Homogeneity Study Using NIR Spectroscopy : Tracking Magnesium Stearate in Bohle Bin-Blender. Drug Dev. Ind. Pharm. 29(6), 679-687. https://doi.org/10.1081/DDC-120021317

Engelund, E.T., Klamer, M., Venås, T.M., (2010). Acquisition of sorption isotherms for modified woods by the use of dynamic vapour sorption instrumentation. Principles and Practice. 41st Annual meeting of Int. Res. Gr. Wood Prot. 1–10.

Engisch, W.E., Muzzio, F.J., (2015). Feedrate deviations caused by hopper refill of LIW feeders. Pow. Tech. 283, 389–400.
https://doi.org/10.1016/j.powtec.2015.06.001

Engisch, W.E., Muzzio, F.J., (2014). Loss-in-Weight Feeding Trials Case Study: Pharmaceutical Formulation. J. Pharm. Innov. 10(1), 56–75. https://doi.org/10.1007/s12247-014-9206-1

Engisch, W.E., Muzzio, F.J., (2012). Method for characterization of loss-in-weight feeder equipment. Pow. Tech. 228, 395–403. https://doi.org/10.1016/j.powtec.2012.05.058

Ervasti, T., Simonaho, S.P., Ketolainen, J., Forsberg, P., Fransson, M., Wikström, H., Folestad, S., Lakio, S., Tajarobi, P., Abrahmsén-Alami, S., (2015). Continuous manufacturing of extended release tablets via powder mixing and direct compression. Int. J. Pharm. 495(1), 290–301. https://doi.org/10.1016/j.ijpharm.2015.08.077

Evans-Hurson, R., McSweeney, S., Vos, B., Krüse, J., Keating, J.J., Fitzpatrick, D., (2016). pH dependence of the dissolution rate of enteric- coated drug spheres determined by broadband acoustic resonance dissolution spectroscopy (BARDS). Dissolution Technol. 23(1), 24–31. https://doi.org/10.14227/DT230116P24

Ewald, P.P., (1962). The Principles of X-ray Diffraction. Fifty Years X-Ray Diffr. 82–101. https://doi.org/10.1007/978-1-4615-9961-6_6

Fitzpatrick, D., Evans-Hurson, R., Fu, Y., Burke, T., Krüse, J., Vos, B., McSweeney, S.G., Casaubieilh, P., Keating, J.J., (2014). Rapid profiling of enteric coated drug delivery spheres via Broadband Acoustic Resonance Dissolution Spectroscopy (BARDS). Analyst 139(5), 1000–1006. https://doi.org/10.1039/c3an01809a

Fitzpatrick, D., Evans-Hurson, R., Krüse, J., Vos, B., McSweeney, S., Casaubieilh, P., O'Gorman, É., (2013). The relationship between dissolution, gas oversaturation and outgassing of solutions determined by Broadband Acoustic Resonance Dissolution Spectroscopy. Analyst 138(17), 5005-5010. https://doi.org/10.1039/c3an36838f

Fitzpatrick, D., Krüse, J., Vos, B., Foley, O., Gleeson, D., Ogorman, E., Okeefe, R., (2012a). Principles and applications of broadband acoustic resonance dissolution

spectroscopy (BARDS): A sound approach for the analysis of compounds. Anal. Chem. 84(5), 2202–2210. https://doi.org/10.1021/ac202509s

Fitzpatrick, D., Scanlon, E., Krüse, J., Vos, B., Evans-Hurson, R., Fitzpatrick, E., McSweeney, S., (2012b). Blend uniformity analysis of pharmaceutical products by Broadband Acoustic Resonance Dissolution Spectroscopy (BARDS). Int. J. Pharm. 438(1-2), 134–9. https://doi.org/10.1016/j.ijpharm.2012.07.073

Fonteyne, M., Vercruysse, J., De Leersnyder, F., Van Snick, B., Vervaet, C., Remon, J.P., De Beer, T., (2015). Process Analytical Technology for continuous manufacturing of solid-dosage forms. TrAC Trends Anal. Chem. 67, 159–166. https://doi.org/10.1016/j.trac.2015.01.011

Gabbott, P., (2008). Principles and applications of thermal analysis. Blackwell Publishing Ltd. Oxford.

Garg, N., Pandey, P., Kaushik, D., Dureja, H., (2015). Development of novel multifunction directly compressible co-processed excipient by melt granulation technique. Int. J. Pharm. Investig. 5(4), 266-274.
https://doi.org/10.4103/2230973X.167692

Gohel, M.C., Jogani, P.D., (2005). A review of co-processed directly compressible excipients. J. Pharm. Pharm. Sci. 16;8(1):76-93.

Gregg, S.J., Sing, K.S.W., Salzberg, H.W., (1967). Adsorption Surface Area and Porosity. J. Electrochem. Soc. 114(11), 279C. https://doi.org/10.1149/1.2426447

Guillory, J.K., (2009). Developing solid oral dosage forms. Pharmaceutical theory and practice. Academic Press. United Kingdom.

Gupta, A., Hamad, M.L., Tawakkul, M., Sayeed, V. A, Khan, M. A, (2009a). Difference in the lubrication efficiency of bovine and vegetable-derived magnesium stearate during tabletting. AAPS PharmSciTech. 10(2), 500–4.
https://doi.org/10.1208/s12249-009-9229-y

Gupta, A., Hunt, R.L., Shah, R.B., Sayeed, V.A., Khan, M.A., (2009b). Disintegration of Highly Soluble Immediate Release Tablets: A Surrogate for Dissolution. AAPS PharmSciTech. 10(2), 495–499. https://doi.org/10.1208/s12249-009-9227-0

Hamad, M.L., Gupta, A., Shah, R.B., Lyon, R.C., Sayeed, V.A., Khan, M.A., (2008). Functionality of magnesium stearate derived from bovine and vegetable sources: Dry granulated tablets. J. Pharm. Sci. 97(12), 5328–5340. https://doi.org/10.1002/jps.21381

Haritha, B., (2017). A Review on Evaluation of Tablets. J Formul Sci Bioavailab 1, 1–5.

Hattori, Y., Otsuka, M., (2014). Near infrared spectroscopic study of the hydration/swelling process of microcrystalline cellulose, starch and carboxymethylcellulose. J. Near Infrared Spectrosc. 22(3), 199-204. https://doi.org/10.1255/jnirs.1111

Haware, R. V, Shivagari, R., Johnson, P.R., Staton, S., Stagner, W.C., Gupta, M.R., (2014). Application of multivariate methods to evaluate the functionality of bovine- and vegetable-derived magnesium stearate. J. Pharm. Sci. 103(5), 1466–1477. https://doi.org/10.1002/jps.23920

Heckel, R.W., (1961). Density-Pressure Relationships in Powder Compaction. Trans Met. Soc. AIME. 221, 671–675.

Henson, M.J., Zhang, L., (2006). Drug Characterization in Low Dosage Pharmaceutical Tablets Using Raman Microscopic Mapping. Appl. Spectrosc. 60(11), 1247–1255. https://doi.org/10.1366/000370206778998987

Hiestand, E.N., Wells, J.E., Peot, C.B., Ochs, J.F., (1977). Physical Processes of Tableting. J. Pharm. Sci. 66(4), 510–519. https://doi.org/10.1002/JPS.2600660413

Hinz, D.C., (2006). Process analytical technologies in the pharmaceutical industry: The FDA's PAT initiative. Anal. Bioanal. Chem. 384(5), 1036–1042. https://doi.org/10.1007/s00216-005-3394-y

Hirschfelder, A.D., (1930). The United States pharmacopeial convention. J. Am. Med. Assoc. 95(30), 220. https://doi.org/10.1001/jama.1930.02720030050030

Hopkins, M., (2006). LOSS in weight feeder systems. Meas. Control. 39(8), 237-240 https://doi.org/10.1177/002029400603900801

Howick, K., Alam, R., Chruscicka, B., Kandil, D., Fitzpatrick, D., Ryan, A.M., Cryan, J.F., Schellekens, H., Griffin, B.T., (2018). Sustained-release multi particulates for oral delivery of a novel peptidic ghrelin agonist: Formulation design and in vitro characterization. Int. J. Pharm. 536(1), 63–72. https://doi.org/10.1016/J.IJPHARM.2017.11.051

Hussain, M.S.H., York, P., Timmins, P., (1988). A study of the formation of magnesium stearate film on sodium chloride using energy-dispersive X-ray analysis. Int. J. Pharm. 42(1-3), 89–95. https://doi.org/10.1016/0378-5173(88)90164-0

Hussain, M.S.H., York, P., Timmins, P., Humphrey, P., (1990). Secondary ion mass spectrometry (SIMS) evaluation of magnesium stearate distribution and its effects on the physico-technical properties of sodium chloride tablets. Powder Technol. 60(1), 39–45. https://doi.org/10.1016/0032-5910(90)80102-5

Ilkka, J., Paronen, P., (1993). Prediction of the compression behaviour of powder mixtures by the Heckel equation. Int. J. Pharm. 94(1-3), 181–187. https://doi.org/10.1016/0378-5173(93)90022-8

Iranloye, T.A., Parrott, E.L., (1978). Effects of compression force, particle size, and lubricants on dissolution rate. J. Pharm. Sci. 67(4), 535–9. https://doi.org/10.1002/jps.2600670424.

Jahn, T., Steffens, K.J., (2005). Press Chamber Coating as External Lubrication for High Speed Rotary Presses: Lubricant Spray Rate Optimization. Drug Dev. Ind. Pharm. 31(10), 951–957. https://doi.org/10.1080/03639040500306161

Järvinen, K., Hoehe, W., Järvinen, M., Poutiainen, S., Juuti, M., Borchert, S., (2013). In-line monitoring of the drug content of powder mixtures and tablets by near-

infrared spectroscopy during the continuous direct compression tableting process. Eur. J. Pharm. Sci. 48(4-5), 680–688. https://doi.org/10.1016/j.ejps.2012.12.032

Jarvinen, M., Paaso, J., Paavola, M., Leiviskä, K., Juuti, M., Muzzio, F., Järvinen, K., (2013). Continuous direct tablet compression: effects of impeller rotation rate, total feed rate and drug content on the tablet properties and drug release. Drug Dev. Ind. Pharm. 39(11), 1802–8. https://doi.org/10.3109/03639045.2012.738681

Jenike, A.W., (1964). Storage and flow of solids. Bulletin No. 123; 53(26). Utah Univ., Salt Lake City (USA), Salt Lake City. https://doi.org/10.2172/5240257

Ji, J., Fitzpatrick, J., Cronin, K., Crean, A., Miao, S., (2016). Assessment of measurement characteristics for rehydration of milk protein based powders. Food Hydrocolloids. 54(Part A), 151-161. https://doi.org/10.1016/j.foodhyd.2015.09.027

Jivraj, I., Martini, L., Thomson, C., (2000). An overview of the different excipients useful for the direct compression of tablets. Pharm. Sci. Technolo. Today. 3(2), 58–63. https://doi.org/10.1016/S1461-5347(99)00237-0

Johansson, M.E., Nicklasson, M., (1986). Investigation of the film formation of magnesium stearate by applying a flow-through dissolution technique. J. Pharm. Pharmacol. 38(!), 51–54. https://doi.org/10.1111/j.2042-7158.1986.tb04466.x

Joiris, E., Martino, P. Di, Berneron, C., Guyot-Hermann, A., Guyot, J., (1998). Compression Behavior of Orthorhombic Paracetamol. Pharm. Res. 15(7), 1122–1130. https://doi.org/10.1023/A:1011954800246

Kararli, T.T., Needham, T.E., Seul, C.J., Finnegan, P.M., (1989). Solid-State Interaction of Magnesium Oxide and Ibuprofen to Form a Salt. Pharm. Res. An Off. J. Am. Assoc. Pharm. Sci. 6(9), 804–808. https://doi.org/10.1023/A:1015983732667

Katdare, A. (Ed.), Chaubal, M. (Ed.). (2006). Excipient Development for Pharmaceutical, Biotechnology, and Drug Delivery Systems. Boca Raton: CRC Press.

Kato, H., Kimura, K., Izumi, S., Nakamichi, K., Danjo, K., Sunada, H., (2005). The effect of magnesium stearate particle size on tablet properties and tableting

characteristics of granules prepared with standard formulation. J. Drug Deliv. Sci. Technol. 15(6), 475–480. https://doi.org/10.1016/S1773-2247(05)50091-1

Katz, J.M., Buckner, I.S., (2013). Characterization of strain rate sensitivity in pharmaceutical materials using indentation creep analysis. Int. J. Pharm. 4421-2), 13–19. https://doi.org/10.1016/J.IJPHARM.2012.09.006

Khinast, J., (2016). Continuous Manufacturing Critical Steps and Possible Solutions. 10th PBP world conference, Glasgow, UK.

Kikuta, J.I., Kitamori, N., (1994). Effect of mixing time on the lubricating properties of magnesium stearate and the final characteristics of the compressed tablets. Drug Dev. Ind. Pharm. 20(3), 343–355. https://doi.org/10.3109/03639049409050187

Lakio, S., Vajna, B., Farkas, I., Salokangas, H., Marosi, G., Yliruusi, J., (2013). Challenges in detecting magnesium stearate distribution in tablets. AAPS PharmSciTech. 14(1), 435–44. https://doi.org/10.1208/s12249-013-9927-3

Leane, M., Pitt, K., Reynolds, G., (2015). A proposal for a drug product Manufacturing Classification System (MCS) for oral solid dosage forms. Pharm. Dev. Technol. 20(1), 12–21. https://doi.org/10.3109/10837450.2014.954728

Lee, J., (2007). Nanoscopic friction behaviour of pharmaceutical materials. Int. J. Pharm. 340(1-2), 191–197. https://doi.org/10.1016/J.IJPHARM.2007.03.017

Leinonen, U.I., Jalonen, H.U., Vihervaara, P.A., Laine, E.S.U., (1992). Physical and lubrication properties of magnesium stearate. J. Pharm. Sci. 81(12), 1194–1198. https://doi.org/10.1002/jps.2600811214

Lerk, C.F., Bolhuis, G.K., Smedema, S.S., (1977). Interaction of lubricants and colloidal silica during mixing with excipients. I. Its effect on tabletting. Pharm. Acta Helv. 52(3), 33–39. https://doi.org/10.3390/lubricants2010021

Leuenberger, H., (2001). New trends in the production of pharmaceutical granules: Batch versus continuous processing. Eur. J. Pharm. Biopharm. 52(3), 289–296. https://doi.org/10.1016/S0939-6411(01)00199-0

Li, J., Wu, Y., (2014). Lubricants in Pharmaceutical Solid Dosage Forms. Lubricants. 2(1), 21–43. https://doi.org/10.3390/lubricants2010021

Li, Z., Zhao, L., Lin, X., Shen, L., Feng, Y., (2017). Direct compaction: An update of materials, trouble-shooting, and application. Int. J. Pharm. 529(1-2), 543–556. https://doi.org/10.1016/J.IJPHARM.2017.07.035

Lieberman, H.A., Schwartz, J.B., (1989). Pharmaceutical dosage forms--tablets, second. Ed. Marcel Dekker, INC., New York.

Liew, C. V., Karande, A.D., Heng, P.W.S., (2010). In-line quantification of drug and excipients in cohesive powder blends by near infrared spectroscopy. Int. J. Pharm. 386(1-2), 138–148. https://doi.org/10.1016/j.ijpharm.2009.11.011

Lindberg, N.O., (1970). Preparation of effervescent tablets containing nicotinic acid and sodium bicarbonate. Acta Pharm. Suec. 7(1), 23–8.

Louw, R., 2003. Evaluation and comparison of magnesium stearate and sodium stearyl fumarate (Pruv®) as lubricants in directly compressible tablet formulations: Their effect on tablet properties and drug dissolution (MSc Thesis)

Lowenthal, W., (1972). Disintegration of tablets. J. Pharm. Sci. 61(11), 1695–1711. https://doi.org/10.1002/jps.2600611102

Luangtana-Anan, M., Fell, J.T., (1990). Bonding mechanisms in tabletting, International Journal of Pharmaceutics. 60(3), 197-202. https://doi.org/10.1016/0378-5173(90)90073-D

Mangal, S., Meiser, F., Morton, D., Larson, I., (2015). Particle Engineering of Excipients for Direct Compression: Understanding the Role of Material Properties. Curr. Pharm. Des. 21(40), 5877–89. https://doi.org/10.2174/1381612821666151008125117

Markl, D., Zeitler, J.A., (2017). A Review of Disintegration Mechanisms and Measurement Techniques. Pharm. Res. 34(5), 890–917. https://doi.org/10.1007/s11095-017-2129-z

Marshall, K., (1986). Compression and Consolidation of Powdered Solids, in: Lachman L, Liberman HA, K.J. (Ed.), The Theory and Practice of Industrial Pharmacy. Varghese Publishing, Bombay, pp. 66–99.

Mascia, S., Heider, P.L., Zhang, H., Lakerveld, R., Benyahia, B., Barton, P.I., Braatz, R.D., Cooney, C.L., Evans, J.M.B., Jamison, T.F., Jensen, K.F., Myerson, A.S., Trout, B.L., (2013). End-to-End Continuous Manufacturing of Pharmaceuticals: Integrated Synthesis, Purification, and Final Dosage Formation. Angew. Chemie Int. Ed. 52(47), 12359–12363. https://doi.org/10.1002/anie.201305429

Metin, Ç., (1994). Compaction of Multiparticulate Oral Dosage Forms, in: Ghebre-Sellassie I (Ed.), Multiparticulate Oral Drug Delivery. New York, pp. 181–215. https://doi.org/doi:10.1201/b14855-10\r10.1201/b14855-10

Miller, T.A., York, P., Coghill, J., Jones, T.M., (1985). Magnesium Stearate Lubricant Character: Processing Effects. J. Pharm. Pharmacol. 37(S12), 31P–31P. https://doi.org/10.1111/j.2042-7158.1985.tb14103.x

Mirani, A.G., Patankar, S.P., Borole, V.S., Pawar, A.S., Kadam, V.J., (2011). Direct compression high functionality excipient using coprocessing technique: A brief review. Curr. Drug Deliv. 8(4), 426–435. https://doi.org/10.2174/156720111795767960

Mitrevej, K.T., Augsburger, L.L., (1982). Adhesion of tablets in a rotary tablet press II. Effects of blending time, running time, and lubricant concentration. Drug Dev. Ind. Pharm. 8(2), 237–282. https://doi.org/10.3109/03639048209022100

Moreton, B.R.C., (2006). Functionality and Performance of Excipients, Pharmaceutical Technology. Volume 2006 Supplement, Issue 5

Morin, G., Briens, L., (2013). The Effect of Lubricants on Powder Flowability for Pharmaceutical Application. AAPS PharmSciTech. 14(3), 1158–1168. https://doi.org/10.1208/s12249-013-0007-5

Nakagawa, H., Kano, M., Hasebe, S., Suzuki, T., Wakiyama, N., (2013). Real-time monitoring of lubrication properties of magnesium stearate using NIR spectrometer

and thermal effusivity sensor. Int. J. Pharm. 441(1-2), 402–413. https://doi.org/10.1016/j.ijpharm.2012.11.014

Narang, A.S., Rao, V.M., Raghavan, K.S., (2009). Excipient Compatibility, in: Yihong Qiu, Yisheng Chen, G.G.Z.Z. (Ed.), Developing Solid Oral Dosage Forms. pp. 125–145. https://doi.org/10.1016/B978-0-444-53242-8.00006-0

Nogami, H., Hasegawa, J., Miyamoto, M., (1967). Studies on Powdered Preparations. Disintegration of the Aspirin Tablets containing Starches as Disintegrating Agent. Chem. Pharm. Bull. (Tokyo). 15(3), 279–289. https://doi.org/10.1248/cpb.15.279

Nyström, C., Alderborn, Gör., Duberg, M., Karehill, P.-G., (1993). Bonding Surface area and Bonding Mechanism-Two Important Factors fir the Understanding of Powder Comparability. Drug Dev. Ind. Pharm. 19(17-18), 2143–2196. https://doi.org/10.3109/03639049309047189

Pabari, R., Ramtoola, Z., (2012). Effect of a disintegration mechanism on wetting, water absorption, and disintegration time of or dispersible tablets. J. Young Pharm. 4(3), 157–63. https://doi.org/10.4103/0975-1483.100021

Palmer, E., (2015). GSK doubles down on Singapore continuous processing plant Fierce Pharma. https://www.fiercepharma.com/partnering/gsk-doubles-down-on-singapore-continuous-processing-plant (accessed on 28/7/2018).

Patel, S., Kaushal, A.M., Bansal, A.K., (2006). Compression physics in the formulation development of tablets. Crit. Rev. Ther. Drug Carrier Syst. 23(1), 1–65. https://doi.org/10.1615/CritRevTherDrugCarrierSyst.v23.i1.10

Peddapatla, R.V.G., Ahmed, M.R., Black shields, C.A., Sousa-Gallagher, M.J., McSweeney, S., Kruse, J., Crean, A.M., Fitzpatrick, D., (2018). Broadband Acoustic Resonance Dissolution Spectroscopy (BARDS): A Novel Approach to Investigate the Wettability of Pharmaceutical Powder Blends. Mol. Pharm. 15(1), 31–39. https://doi.org/10.1021/acs.molpharmaceut.7b00658

Pepin, X., Blanchon, S., Couarraze, G., (1999). Powder dynamic contact angle data in the pharmaceutical industry. Pharm. Sci. Technol. Today. 2(3), 111–118. https://doi.org/10.1016/S1461-5347(99)00129-7

Pernenkil, L., Cooney, C.L., (2006). A review on the continuous blending of powders. Chem. Eng. Sci. 61(2), 720–742. https://doi.org/10.1016/j.ces.2005.06.016

Phadke, D.S., Collier, J.L., (1994). Effect of degassing temperature on the specific surface area and other physical properties of magnesium stearate. Drug Dev. Ind. Pharm. 20(5), 853–858. https://doi.org/10.3109/03639049409038335

Plumb, K., (2005). Continuous Processing in the Pharmaceutical Industry: Changing the Mind Set. Chem. Eng. Res. Des. 83(6), 730–738. https://doi.org/10.1205/CHERD.04359

Rajala, R., Laine, E., (1995). The effect of moisture on the structure of magnesium stearate. Thermochim. Acta. 248(2), 177–188. https://doi.org/10.1016/0040-6031(94)01950-L

Rajpurohit, H., Sharma, P., Sharma, S., Purohit, S., Bhandari, A., (2011). Hordeum vulgare hull in the design of fast disintegrating tablets. J. Young Pharm. 3(3), 211–5. https://doi.org/10.4103/0975-1483.83763

Rantanen, J., Khinast, J., (2015). The Future of Pharmaceutical Manufacturing Sciences. J. Pharm. Sci. 104(11), 3612–3638. https://doi.org/10.1002/jps.24594

Rao, K.P., Chawla, G., Kaushal, A.M., Bansal, A.K., (2005). Impact of Solid-State Properties on Lubrication Efficacy of Magnesium Stearate. Pharm. Dev. Technol. 10(3), 423–437. https://doi.org/10.1081/pdt-200054462

Reimer, L., (2000). Scanning Electron Microscopy: Physics of Image Formation and Microanalysis. Meas. Sci. Technol. 11, 1826–1826. https://doi.org/10.1088/0957-0233/11/12/703

Roberts, M., Ford, J.L., Rowe, P.H., Dyas, A.M., MacLeod, G.S., Fell, J.T., Smith, G.W., (2004). Effect of lubricant type and concentration on the punch tip adherence of

model ibuprofen formulations. J. Pharm. Pharmacol. 56(3), 299–305. https://doi.org/10.1211/0022357022827

Roblot-Treupel, L., Puisieux, F., (1986). Distribution of magnesium stearate on the surface of lubricated particles. Int. J. Pharm. 31(1-2), 131–136. https://doi.org/10.1016/0378-5173(86)90222-X

Rogers, A., Hashemi, A., Ierapetritou, M., (2013). Modelling of Particulate Processes for the Continuous Manufacture of Solid-Based Pharmaceutical Dosage Forms. Processes. 1(2), 67–127. https://doi.org/10.3390/pr1020067

Shabana, M.D., (2016). A Review on the Quality Control Analysis of Oral Dosage Form : Quality. Res. Rev. Pharm. Pharm. Sci. 5(2), 108–114.

Shah, A.C., Mlodozeniec, A.R., (1977). Mechanism of surface lubrication: Influence of duration of lubricant-excipient mixing on processing characteristics of powders and properties of compressed tablets. J. Pharm. Sci. 66(10), 1377–1382. https://doi.org/10.1002/jps.2600661006

Shah, R.B., Tawakkul, M.A., Khan, M.A., (2008). Comparative evaluation of flow for pharmaceutical powders and granules. AAPS PharmSciTech. 9(1), 250–8. https://doi.org/10.1208/s12249-008-9046-8

Sharpe, S. a., Celik, M., Newman, A.W., Brittain, H.G., (1997). Physical characterization of the polymorphic variations of magnesium stearate and magnesium palmitate hydrate species. Struct. Chem. 8(1), 73–84. https://doi.org/10.1007/BF02272348

Simonaho, S., Ketolainen, J., Ervasti, T., Toiviainen, M. and Korhonen, O. (2016). Continuous manufacturing of tablets with PROMIS-line — Introduction and case studies from continuous feeding, blending and tableting. European Journal of Pharmaceutical Sciences, 90, pp.38-46. https://doi.org/10.1016/j.ejps.2016.02.006

Singh, R., Román-Ospino, A.D., Romañach, R.J., Ierapetritou, M., Ramachandran, R., (2015). Real time monitoring of powder blend bulk density for coupled feed-forward/feed-back control of a continuous direct compaction tablet manufacturing

process. Int. J. Pharm. 495(1), 612–625.
https://doi.org/10.1016/j.ijpharm.2015.09.029

St-Onge, L., Archambault, J.-F., Kwong, E., Sabsabi, M., Vadas, E.B., (2005). Rapid quantitative analysis of magnesium stearate in tablets using laser-induced breakdown spectroscopy. J. Pharm. Pharm. Sci. 8(2), 272–88.
10.1016/j.jpba.2009.01.004

Stosik, A.G., Junginger, H.E., Kopp, S., Midha, K.K., Shah, V.P., Stavchansky, S., Dressman, J.B., Barends, D.M., (2008). Bio waiver monographs for immediate release solid oral dosage forms: Metoclopramide hydrochloride. J. Pharm. Sci. 97(9), 3700–3708. https://doi.org/10.1002/jps.21276

Sun, C., Grant, D.J.., (2000). Influence of Crystal Structure on the Tableting Properties of Sulfamerazine Polymorphs. Pharm. Res. 18(3), 274–280. https://doi.org/10.1002/ejoc.200901492

Swaminathan, V., Kildsig, D.O., (2001). An examination of the moisture sorption characteristics of commercial magnesium stearate. AAPS PharmSciTech. 2(4), 28. https://doi.org/10.1208/pt020428

Tamari, S., (2004). Optimum design of the constant-volume gas pycnometer for determining the volume of solid particles. Meas. Sci. Technol. 15(3), 549–558. https://doi.org/10.1088/0957-0233/15/3/007

The United States Pharmacopeia USP 26 : the National Formulary NF 21, (2003). Rockville, MD : United States Pharmacopeial Convention, 2002.

Tortora, G.J., Derrickson, B.H., 2011. Principles of Anatomy and Physiology (Tortora, Principles of Anatomy and Physiology).

Tye, C.K., Sun, C., Amidon, G.E., (2005). Evaluation of the effects of tableting speed on the relationships between compaction pressures, tablet tensile strength, and tablet solid fraction. J. Pharm. Sci. 94(3), 465–472.
https://doi.org/10.1002/jps.20262

Uzunović, A., Vranić, E., (2007). Effect of magnesium stearate concentration on dissolution properties of ranitidine hydrochloride coated tablets. Bosn. J. Basic Med. Sci. 7(3), 279–283. https://doi.org/10.17305/bjbms.2007.3060

Vajna, B., Farkas, I., Szabó, A., Zsigmond, Z., Marosi, G., (2010). Raman microscopic evaluation of technology dependent structural differences in tablets containing imipramine model drug. J. Pharm. Biomed. Anal. 51(1), 30–38. https://doi.org/10.1016/J.JPBA.2009.07.030

Vanarase, A.U., Alcalà, M., Jerez Rozo, J.I., Muzzio, F.J., Romañach, R.J., (2010). Real-time monitoring of drug concentration in a continuous powder mixing process using NIR spectroscopy. Chem. Eng. Sci. 65(21), 5728–5733. https://doi.org/10.1016/j.ces.2010.01.036

Vanarase, A.U., Muzzio, F.J., (2011). Effect of operating conditions and design parameters in a continuous powder mixer. Powder Technol. 208(1), 26–36. https://doi.org/10.1016/j.powtec.2010.11.038

Vanhoorne, V., Peeters, E., Van Snick, B., Remon, J.P., Vervaet, C., (2014). Crystal coating via spray drying to improve powder tabletability. Eur. J. Pharm. Biopharm. 88(3), 939–944. https://doi.org/10.1016/J.EJPB.2014.10.018

Vezin, W.R., Khan, K.A., Pang, H.M., (1983). Adjustment of precompression force to reduce mixing-time dependence of tablet tensile strength. J. Pharm. Pharmacol. 35(9), 555–558. https://doi.org/10.1111/j.2042-7158.1983.tb04332.x

Vos, B., Crowley, S. V., O'Sullivan, J., Evans-Hurson, R., McSweeney, S., Krüse, J., Rizwan Ahmed, M., Fitzpatrick, D., O'Mahony, J.A., (2016). New insights into the mechanism of rehydration of milk protein concentrate powders determined by Broadband Acoustic Resonance Dissolution Spectroscopy (BARDS). Food Hydrocoll. 61, 933–945. https://doi.org/10.1016/j.foodhyd.2016.04.031

Wada, Y., Matsubara, T., (1994). Pseudo polymorphism and lubricating properties of magnesium stearate. Powder Technol. 78(2), 109–114. https://doi.org/10.1016/0032-5910(93)02782-6

Wang, J., Wen, H., Desai, D., (2010). Lubrication in tablet formulations. Eur. J. Pharm. Biopharm. 75(1), 1–15. https://doi.org/10.1016/j.ejpb.2010.01.007

Watson, E.S., O'Neill, M.J.,Justin, J.,Brenner, N. (1964). A Differential Scanning Calorimeter for Quantitative Differential Thermal Analysis. Anal. Chem. 36(7), 1233-1238. https://doi.org/10.1021/ac60213a019

Widjaja, E., Seah, R.K.H., (2008). Application of Raman microscopy and band-target entropy minimization to identify minor components in model pharmaceutical tablets. J. Pharm. Biomed. Anal. 46(2), 274–281. https://doi.org/10.1016/J.JPBA.2007.09.023

Wood, A.B., (1930). A textbook of sound 1st ed.; MacMillan: New York

Zhang, L., Henson, M.J., Sekulic, S.S., (2005). Multivariate data analysis for Raman imaging of a model pharmaceutical tablet. Anal. Chim. Acta. 545(2), 262–278. https://doi.org/10.1016/J.ACA.2005.04.080

Supplementary Information

Table S1 - Tukey's multiple comparison tests for dissolution profiles of paracetamol tablets prepared without lubricant and tablets with different MgSt samples.

Comparison	Summary
No Lubricant vs Alfa Aesar	***
No lubricant vs Ligamed MF-2-V	***
No lubricant vs Ligamed MF-2-V-BI	***
No lubricant vs Ligamed MF-3-V	***
API/MCC/AA Unfed vs Ligamed MF-2-V	ns
Alfa Aesar vs Ligamed MF-2-V-BI	ns
Alfa Aesar vs Ligamed MF-3-V	ns
Ligamed MF-2-V vs Ligamed MF-2-V-BI	ns
Ligamed MF-2-V vs Ligamed MF-3-V	ns
API/MCC/MF2VBI Unfed vs Ligamed MF-3-V	ns

*Where, * represents P≤0.05, ** represents P≤0.01, *** represents P≤0.001, **** represents P≤0.0001 and ns Not significant*

Table S2 - ANOVA – Comparison of Alfa Aesar across different feed rates.

Not compared, Repeated comparison

Alfa Aesar				Feed Rate (kg/hr)								
				Unfed			0.15kg/hr			0.25 kg/hr		
			Pressure (Bar)	1.5	2.0	3.0	1.5	2.0	3.0	1.5	2.0	3.0
D10	Feed Rate (kg/hr)	Unfed	1.5		****	***	**	****	****	ns	****	****
			2.0	****		****	**	ns	****	***	ns	****
			3.0	***	****		****	****	ns	****	****	ns
		0.15	1.5	**	**	****		****	****	ns	***	****
			2.0	****	ns	****	****		****	****	ns	****
			3.0	****	****	ns	****	****		****	****	ns
		0.25	1.5	ns	***	****	ns	****	****		****	****
			2.0	****	ns	****	***	ns	****	****		****
			3.0	****	****	ns	****	****	ns	****	****	
D50	Feed Rate (kg/hr)	Unfed	1.5		***	****	ns	****	****	ns	*	****
			2.0	***		****	ns	ns	***	ns	ns	ns
			3.0	****	****		****	**	ns	****	****	**
		0.15	1.5	ns	ns	****		**	****	ns	ns	**
			2.0	****	ns	**	**		ns	**	ns	ns
			3.0	****	***	ns	****	ns		****	****	ns
		0.25	1.5	ns	ns	****	ns	**	****		ns	**
			2.0	*	ns	****	ns	ns	****	ns		**
			3.0	****	ns	**	**	ns	ns	**	**	
D90	Feed Rate (kg/hr)	Unfed	1.5		*	****	****	****	****	***	****	****
			2.0	*		****	ns	*	****	ns	ns	***
			3.0	****	****		**	ns	ns	***	***	ns
		0.15	1.5	****		**		ns	***	ns	ns	ns
			2.0	****	*	ns	ns		ns	ns	ns	ns
			3.0	****	****	ns	***	ns		***	**	ns
		0.25	1.5	***	ns	***	ns	ns	***		ns	*
			2.0	****	ns	***	ns	ns	**	ns		ns
			3.0	****	***	ns	ns	ns	ns	*	ns	

*Where, * represents P≤0.05, ** represents P≤0.01, *** represents P≤0.001, **** represents P≤0.0001 and ns Not significant*

Table S3 - ANOVA – Comparison of Ligamed MF-2-V across different feed rates.

Not compared, Repeated comparison

Ligamed MF-2-V				Feed Rate (kg/hr)								
				Unfed			0.15kg/hr			0.25 kg/hr		
			Pressure (Bar)	1.5	2.0	3.0	1.5	2.0	3.0	1.5	2.0	3.0
D10	Feed Rate (kg/hr)	Unfed	1.5		****	****	****	****	****	ns	****	****
			2.0	****		****	*	****	****	****	**	****
			3.0	****	****		****	****	***	****	****	ns
		0.15	1.5	****	*	****		****	****	**	****	****
			2.0	****	****	****	****		****	ns	****	****
			3.0	****	****	***	****	****		****	****	*
		0.25	1.5	ns	****	****	**	ns	****		****	****
			2.0	****	**	****	****	****	****	****		****
			3.0	****	****	ns	****	****	*	****	****	
D50	Feed Rate (kg/hr)	Unfed	1.5		****	****	*	****	****	**	****	****
			2.0	****		****	*	****	****	ns	****	****
			3.0	****	****		****	**	***	****	**	*
		0.15	1.5	*	*	****		****	****	ns	****	****
			2.0	****	****	**	****		****	****	ns	****
			3.0	****	****	***	****	****		****	****	ns
		0.25	1.5	**	ns	****	ns	****	****		****	****
			2.0	****	****	**	****	ns	****	****		****
			3.0	****	****	*	****	****	ns	****	****	
D90	Feed Rate (kg/hr)	Unfed	1.5		ns	**	****	****	****	****	****	****
			2.0	ns		ns	**	****	****	*	****	****
			3.0	**	ns		ns	****	****	ns	***	****
		0.15	1.5	****	**	ns		***	****	ns	**	****
			2.0	****	****	****	***		***	***	ns	*
			3.0	****	****	****	****	***		****	****	ns
		0.25	1.5	****	*	ns	ns	***	****		**	****
			2.0	****	****	***	**	ns	****	**		**
			3.0	****	****	****	****	*	ns	****	**	

*Where, * represents P≤0.05, ** represents P≤0.01, *** represents P≤0.001, **** represents P≤0.0001 and ns Not significant*

Table S4 - ANOVA – Comparision of Ligamed MF-2-V-BI across different feed rates

Not compared, Repeated comparison

Ligamed MF-2-V-BI				Feed Rate (kg/hr)								
				Unfed			0.15kg/hr			0.25 kg/hr		
			Pressure (Bar)	1.5	2.0	3.0	1.5	2.0	3.0	1.5	2.0	3.0
D10	Feed Rate (kg/hr)	Unfed	1.5		ns	****	*	****	****	ns	****	****
			2.0	ns		****	ns	****	****	ns	****	****
			3.0	****	****		****	****	****	****	****	**
		0.15	1.5	*	ns	****		****	****	*	****	****
			2.0	****	****	****	****		****	****	ns	****
			3.0	****	****	****	****	****		****	****	ns
		0.25	1.5	ns	ns	****	*	****	****		****	****
			2.0	****	****	****	****	ns	****	****		****
			3.0	****	****	**	****	****	ns	****	****	
D50	Feed Rate (kg/hr)	Unfed	1.5		ns	****	ns	****	****	ns	****	****
			2.0	ns		****	*	****	****	ns	****	****
			3.0	****	****		****	ns	****	****	ns	****
		0.15	1.5	ns	*	****		****	****	ns	****	****
			2.0	****	****	ns	****		****	****	ns	****
			3.0	****	****	****	****	****		****	****	ns
		0.25	1.5	ns	ns	****	ns	****	****		****	****
			2.0	****	****	ns	****	ns	****	****		****
			3.0	****	****	****	****	****	ns	****	****	
D90	Feed Rate (kg/hr)	Unfed	1.5		*	ns	*	****	****	ns	****	****
			2.0	*		**	****	****	****	***	****	****
			3.0	ns	**		ns	****	****	ns	****	****
		0.15	1.5	*	****	ns		*	****	ns	ns	****
			2.0	****	****	****	*		ns	****	ns	ns
			3.0	****	****	****	****	ns		****	*	ns
		0.25	1.5	ns	***	ns	ns	****	****		**	****
			2.0	****	****	****	ns	ns	*	**		ns
			3.0	****	****	****	****	ns	ns	****	ns	

*Where, * represents P≤0.05, ** represents P≤0.01, *** represents P≤0.001, **** represents P≤0.0001 and ns Not significant*

Table S5 - ANOVA – Comparision of Ligamed MF-3-V across different feed rates.

Not compared, Repeated comparison

Ligamed MF-3-V				Feed Rate (kg/hr)								
				Unfed			0.15kg/hr			0.25 kg/hr		
			Pressure (Bar)	1.5	2.0	3.0	1.5	2.0	3.0	1.5	2.0	3.0
D10	Feed Rate (kg/hr)	Unfed	1.5		****	****	ns	****	****	ns	****	****
			2.0	****		****	****	ns	****	****	****	****
			3.0	****	****		****	****	ns	****	****	ns
		0.15	1.5	ns	****	****		****	****	ns	****	****
			2.0	****	ns	****	****		****	****	*	****
			3.0	****	****	ns	****	****		****	****	ns
		0.25	1.5	ns	****	****	ns	****	****		****	****
			2.0	****	****	****	****	*	****	****		****
			3.0	****	****	ns	****	****	ns	****	****	
D50	Feed Rate (kg/hr)	Unfed	1.5		****	****	****	****	****	****	****	****
			2.0	****		****	ns	****	****	****	****	****
			3.0	****	****		****	****	**	****	****	ns
		0.15	1.5	****	ns	****		****	****	**	****	****
			2.0	****	****	****	****		****	****	ns	****
			3.0	****	****	**	****	****		****	****	ns
		0.25	1.5	****	****	****	**	****	****		****	****
			2.0	****	****	****	****	ns	****	****		****
			3.0	****	****	ns	****	****	ns	****	****	
D90	Feed Rate (kg/hr)	Unfed	1.5		ns	****	****	****	****	****	****	****
			2.0	ns		****	****	****	****	****	****	***
			3.0	****	****		*	ns	****	**	ns	****
		0.15	1.5	****	****	*		****	****	ns	****	****
			2.0	****	****	ns	****		****	****	ns	***
			3.0	****	****	****	****	****		****	****	ns
		0.25	1.5	****	****	**	ns	****	****		****	****
			2.0	****	****	ns	****	ns	****	****		****
			3.0	****	***	****	****	***	ns	****	****	

*Where, * represents P≤0.05, ** represents P≤0.01, *** represents P≤0.001, **** represents P≤0.0001 and ns Not significant*

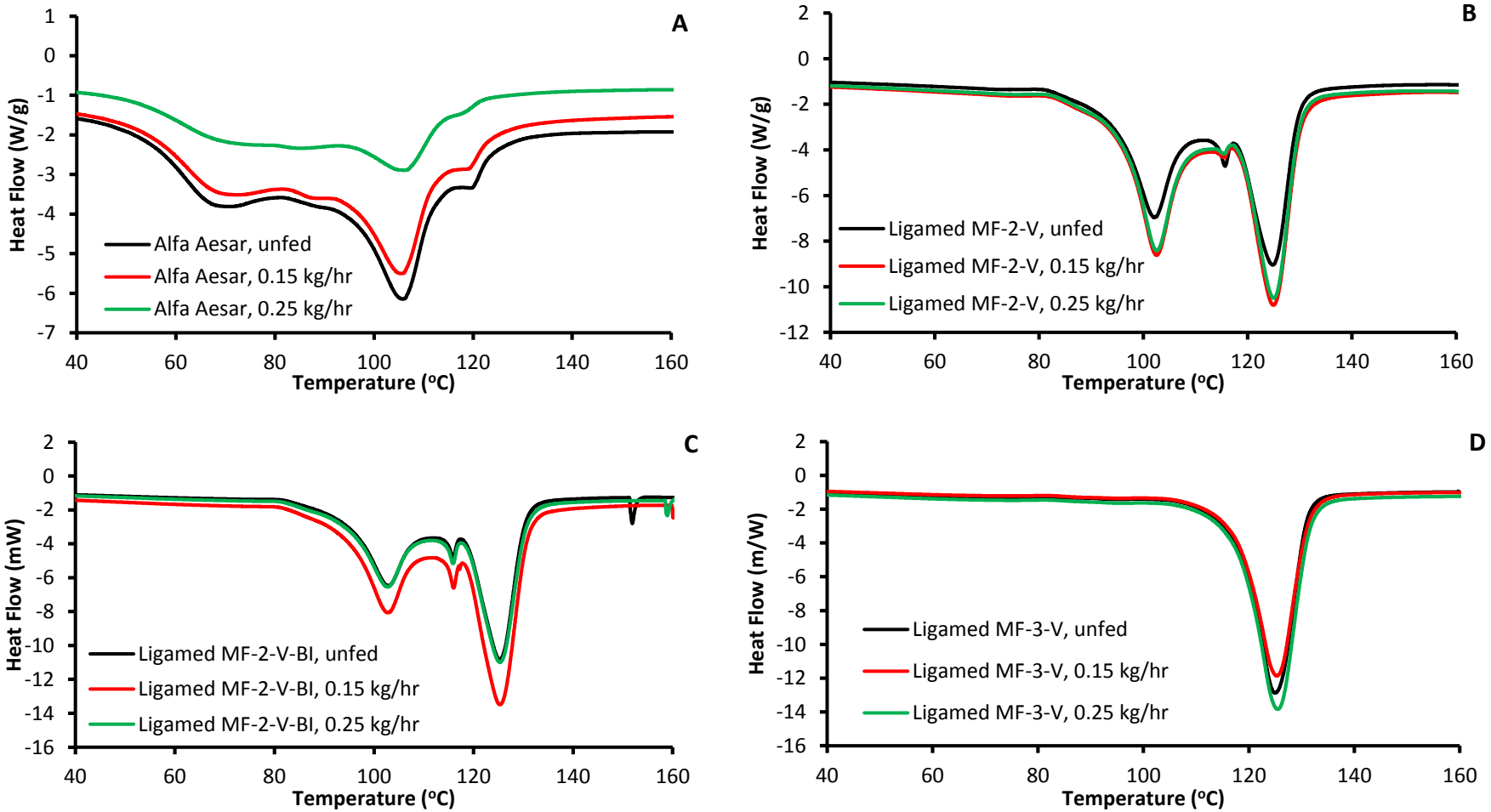


Figure S1 – DSC thermograms of unfed and fed lubricants through K-Tron MT12 feeder.

(A) Alfa Aesar, (B) Ligamed MF-2-V, (C) Ligamed MF-2-V-BI, (D) Ligamed MF-3-V.

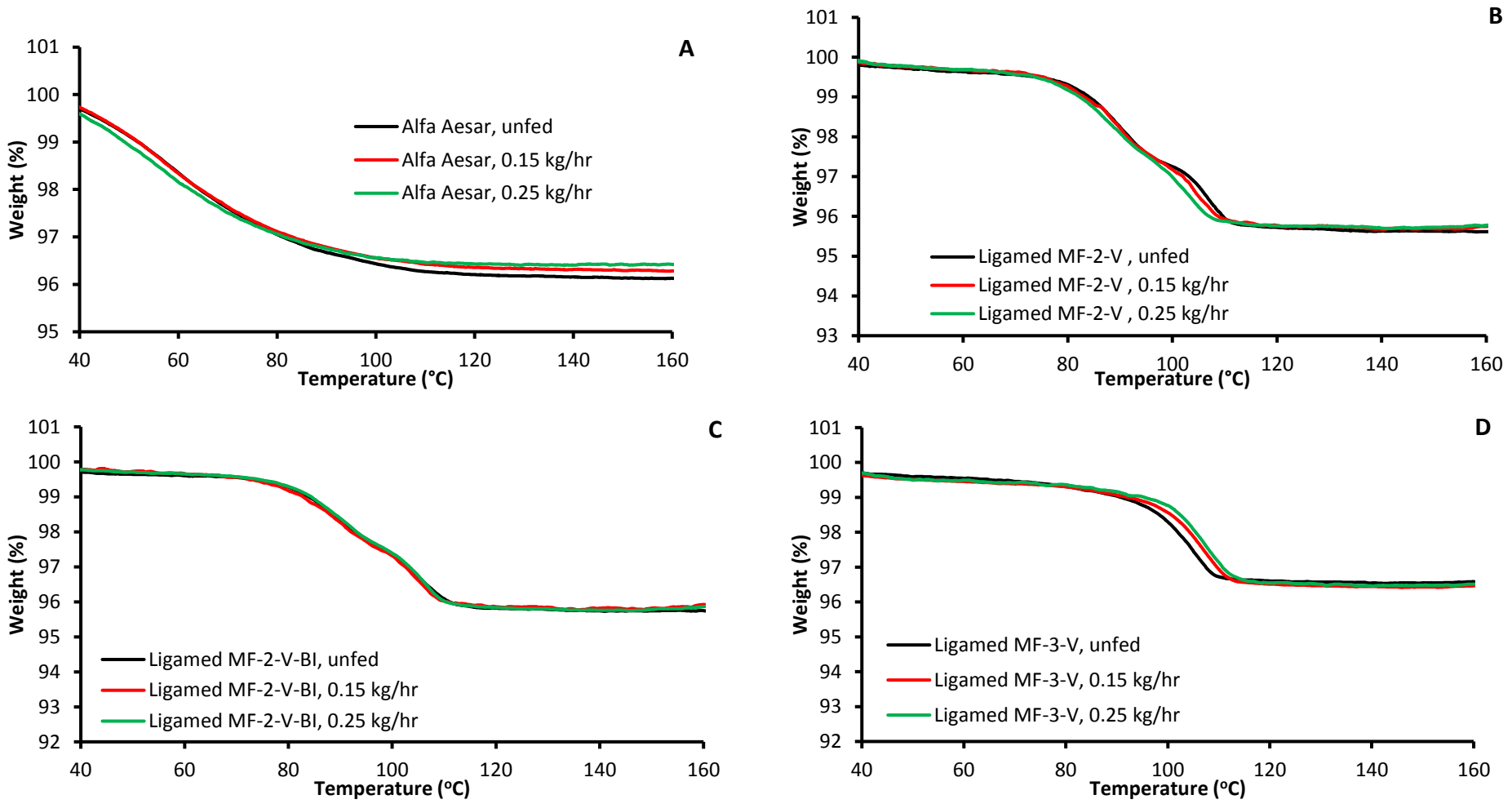


Figure S2 – TGA thermograms of unfed and fed lubricants through K-Tron MT12 feeder.

(A) Alfa Aesar, (B) Ligamed MF-2-V, (C) Ligamed MF-2-V-BI, (D) Ligamed MF-3-V.

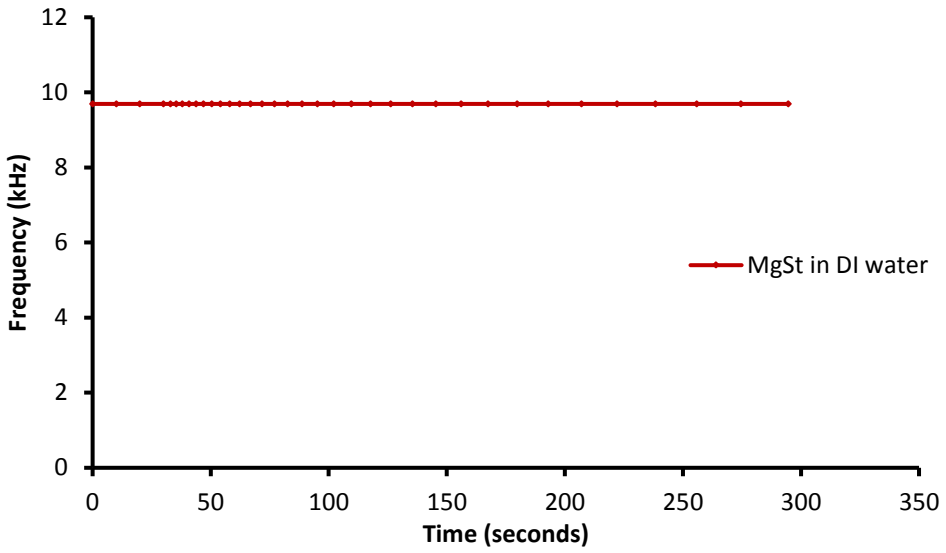


Figure S3 – BARDS acoustic response of MgSt in 25 mL of deionised water at room temperature.

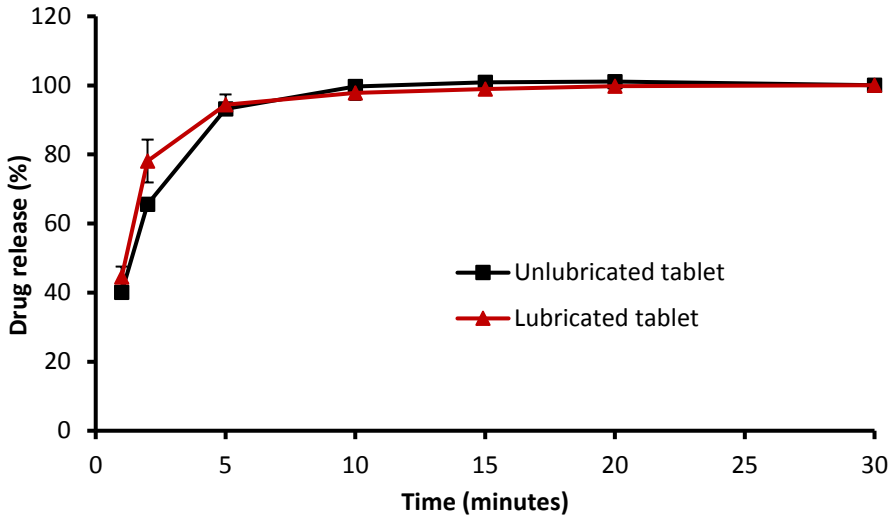


Figure S4 – Dissolution profiles of tablets from unlubricated and lubricated blends fed at three feed rates compacted produced at 3 MPa and tested in water at 37^{o}C. Average values shown n=3, y error bars indicate standard deviation.